Characterization of xenobiotic substrates and inhibitors of CYP26A1, CYP26B1 and CYP26C1 using computational modeling and in vitro analyses

Robert Foti

Université de Nice-Sophia Antipolis

Thèse

pour obtenir le grade de
DOCTEUR DE L'UNIVERSITE NICE SOPHIA ANTIPOLIS
Spécialité : Interactions Moléculaires et Cellulaires
Ecole Doctorale : Sciences de la Vie et de la Santé (SVS)

Caractérisation des substrats xénobiotiques et des inhibiteurs des cytochromes CYP26A1, CYP26B1 et CYP26C1 par modélisation moléculaire et études in vitro

présentée et soutenue publiquement
par

Robert S. Foti

Le 4 Juillet 2016

Membres du jury

Dr. Danièle Werck-Reichhart	Rapporteur
Dr. Philippe Roche	Rapporteur
Pr. Serge Antonczak	Examinateur
Dr. Philippe Breton	Examinateur
Pr. Philippe Diaz	Examinateur
Dr. Dominique Douguet	Directrice de thèse

1. Table of Contents

2. Acknowledgements

Foremost, I would like to express my sincerest gratitude to Dr. Dominique Douguet and Dr. Philippe Diaz, whose guidance and willingness to think creatively allowed for a unique Ph.D. experience. I especially want to thank Dr. Nina Isoherranen, a true friend, colleague and mentor, for providing a continual source of personal encouragement and intellectual critique for as long as I've known her. I would also like to thank Dr. Larry Wienkers for stressing the importance of first-principle, hypothesis driven science and for enabling this opportunity to become a reality.

I am indebted to a multitude of professional and academic colleagues who have contributed directly or indirectly to this research over the years. Whether through generation of new reagents, assistance in designing experimental protocols or engaging in much needed coffee-chats, you have all played a key role in getting me to where I am today and for that, I thank you.

Finally, there are not enough words in the English and French languages combined to adequately describe my appreciation for the loving support, understanding and patience shown by my wife, Dr. Sally Moores, and my son, Liam Moores Foti, as I embarked on this long journey. I thank you with all of my heart for giving me the ability to pursue a dream and it is you to whom I dedicate this thesis.

3. Funding Sources

This research was supported in part by Amgen Inc. (Thousand Oaks, CA), l'Institut National de la Santé et de la Recherche Médicale (INSERM), the Centre National de la Recherche Scientifique (CNRS), by the National Institutes of Health National Institute of General Medical Sciences [Grants R01-GM081569, R01-GM111772], by the National Institutes of Health National Institute of Aging [Grant R41AG046987] and by a RRIA award from the Michael J. Fox Foundation for Parkinson's Research.

4. List of Tables

5. List of Figures

6. List of Abbreviations

ADME	Absorption, distribution, metabolism, excretion
at-RA	all trans-retinoic acid
Cl_{int}	In vitro intrinsic clearance
C_{max}	Maximum drug concentration
$C_{max,u}$	Maximum unbound drug concentration
CYP	Cytochrome P450
FMO	Flavin containing monooxygenase
$K_{s,u}$	Unbound spectral binding constant
LC-MS/MS	Liquid chromatography-tandem mass spectrometry
NADPH	Nicotinamide adenine dinucleotide phosphate, reduced
PCR	Polymerase chain reaction
RAMBA	Retinoic Acid Metabolism Blocking Agent
RAR	Retinoic acid receptor
RMSD	Root-mean-square deviation
RXR	Retinoid X receptor
SNP	Single nucleotide polymorphism

Sous-titre de la thèse Rôle des CYP26s dans la métabolisation des medicaments

Mots-clés CYP26A1, CYP26B1, CYP26C1, modélisation par homologie, acide rétinoïque, acide tazaroténique, adapalène, interactions protéine-ligand

En l'absence de structures tridimensionnelles expérimentales des cytochromes P450 CYP26A1, CYP26B1 et CYP26C1, la caractérisation de leur substrats et ligands s'est basée sur l'analyse des modèles structuraux obtenus par modélisation par homologie avec la structure expérimentale du cytochrome P450 CYP120. La justesse des modèles a été validée par l'amarrage de l'acide rétinoïque all-trans dans des configurations compatibles avec les métabolites attendus. L'amarrage d'agonistes et d'antagonistes des récepteurs nucléaires RARs prédirent l'acide tazaroténique (TA) et l'adapalène comme des substrats potentiels. Les expériences in vitro confirmèrent la métabolisation de ces 2 médicaments par les CYP26s. L'analyse de la cinétique de sulfoxidation du TA par CYP26A1 and CYP26B1 a permis d'établir le TA comme la référence contrôle de l'activité de ces enzymes. Puis, la comparaison des modèles des CYP26s avec la structure cristalline de CYP2C8 a permis d'identifier des similarités structurales de leurs inhibiteurs. Une corrélation entre l'inhibition de CYP26A1 et de CYP2C8 par des inhibiteurs connus de CYP2C8 a été démontrée après détermination de leurs IC50 pour CYP26A1 et CYP26B1 en utilisant le TA comme substrat de référence. La mesure de l'inhibition in vitro fut ensuite utilisée pour évaluer la possibilité que les CYP26s soient impliquées dans des interactions médicamenteuses observées pour certaines molécules. Cette thèse caractérise et appuie le rôle encore mal connu des CYP26s dans la métabolisation in vivo de certains xénobiotiques ainsi que l'effet potentiel de leur inhibition qui favoriserait la survenue d'effets indésirables.

7. Chapter I: Introduction to Retinoic Acid Signaling and Cytochrome P450 26

7.1. Introduction.

Cytochrome P450 26A1 (CYP26A1), B1 (CYP26B1) and C1 (CYP26C1) are enzymes belonging to the cytochrome P450 superfamily of drug metabolizing enzymes that catalyze the metabolism of all-trans retinoic acid (*at*-RA) and related structural isomers. Scientific interest in retinoic acid began to increase in the 1970s, while the study of the role of CYP26 in retinoic acid homeostasis began in the late 1990s (Figure 7-1). As no crystal structures for any of the CYP26 isoforms have been solved to date, the majority of the structural characterization efforts for the enzyme subfamily have utilized a computational approach. Further, while the catalysis of *at*-RA and related endogenous substrates has been the core of many robust scientific endeavors, the role of the enzymes in the metabolism of xenobiotic compounds and the inhibition of the enzymes by compounds other than retinoid-like molecules remains an area of considerable scientific focus.

The research presented in this thesis examined the metabolism and inhibition properties of CYP26 by xenobiotic compounds. Homology models were designed for each isoform and initially validated using the known metabolic profile of *at*-RA. Structural comparison of the active sites of the isoforms suggested similar hydrophobic binding regions proximal to the heme iron with differences in the amino acid residues distal to the heme and capable of stabilizing interactions with carboxylate moieties. Active site volumes for CYP26A1, CYP26B1 and CYP26C1 were estimated at 918 $Å^3$, 977 $Å^3$ and 1090 $Å^3$, respectively, suggesting the ability of each of the enzymes to accommodate the molecular volumes of typical xenobiotic ligands. As such, the models were utilized to assess the active site characteristics of each CYP26 isoform that are essential in describing their ligand binding abilities. Based on homology model results, tazarotenic acid, adapalene and other retinoic acid receptor ligands were identified as metabolic substrates of CYP26.

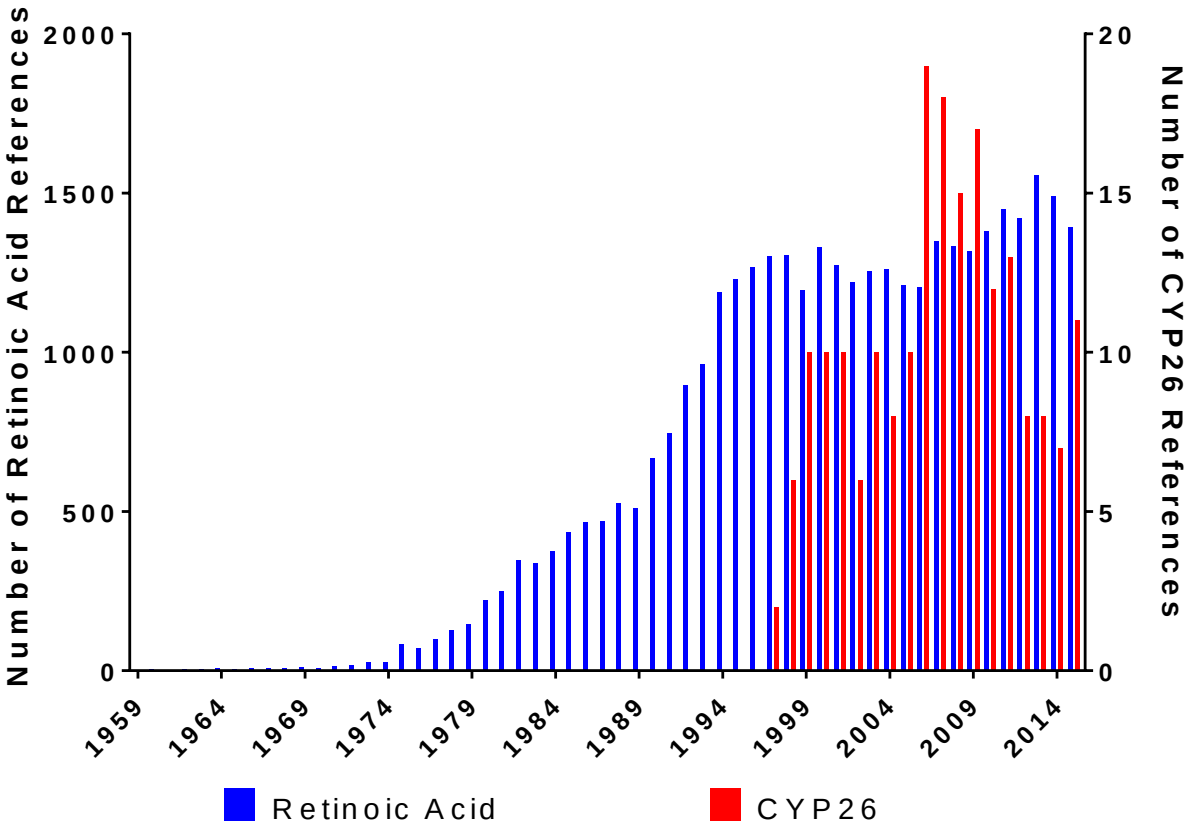

Figure 7-1. Publications related to "Retinoic Acid" or "CYP26" sorted by year.

A comparison of the ligand binding characteristics of CYP26 and CYP2C8 pointed to a potential overlap between the inhibitory pharmacophores of the enzymes. Indeed, when a set of known CYP2C8 inhibitors was screened for their ability to inhibit CYP26A1 or CYP26B1, a correlation was observed between the inhibitory potencies (IC50) for CYP2C8 and CYP26A1 (r^2 = 0.849), with clotrimazole being identified as a very potent inhibitor of both CYP26A1 and CYP26B1. In the process, the use of tazarotenic acid sulfoxidation as a probe reaction for CYP26 activity in recombinantly expressed single enzyme systems was verified. A cursory evaluation of the unbound Cmax concentrations and the IC50 values of the inhibitors in the screening set suggested the possibility for compounds such as clotrimazole or fluconazole to be involved in clinically-relevant drug interactions that involve CYP26.

Collectively, the data presented in this thesis supports a significant role for CYP26 in both the metabolism of xenobiotics as well as xenobiotic drug interactions. To date, one manuscript is in press and has been highlighted on the cover of the Journal of Pharmacology and Experimental Therapeutics (see Chapter II) and a second manuscript is currently under peer review (see Chapter III). Future evaluations of the active site characteristics of CYP26A1, CYP26B1 and CYP26C1 that are integral to defining their substrate binding characteristics will increase the potential of identifying CYP26-selective inhibitors and may ultimately prove useful for the treatment of various disease states while increasing patient safety in regard to modulation of CYP26 activity in vivo.

7.2. Retinoic Acid Signaling.

The homeostatic control of endogenous retinoic acid concentrations is a highly conserved process because of its global role in the cellular lifecycle (Lotan, 1980; Sporn and Roberts, 1984; McCaffery and Drager, 2000; Ross et al., 2000; Clagett-Dame and DeLuca, 2002; Maden, 2002). In humans, retinoic acid exerts its mechanism of action by binding to the retinoic acid and retinoid X receptors, regulating the expression of genes that are directly involved in cellular proliferation, differentiation and apoptotic processes (Figure 7-2) (Levin et al., 1992; Mangelsdorf et al., 1992; Mark et al., 2006; Altucci et al., 2007; di Masi et al., 2015). Ligand-bound retinoic acid and retinoid X receptors form a heterodimeric protein complex which subsequently binds to retinoic acid response element to elicit a physiological response (Giguere et al., 1987; Petkovich et al., 1987; Brand et al., 1988; Duester, 2008; Niederreither and Dolle, 2008). Endogenous ligands for the retinoic acid receptors include all trans-retinoic acid (*at*-RA), 9-cis-RA and 13-cis-RA. Additional evidence suggests that cellular retinoic acid binding proteins (CRABP-I and CRABP-II) are responsible for the facilitation and transport of retinoic acid with its cellular receptors (Fiorella and Napoli, 1991; Giguere, 1994; Noy, 2000).

Physiologically, retinoic acid signaling plays a key role in immune function, brain activity, spermatogenesis, dermatological regulation and organ development (Ransom et al., 2014; Cunningham and Duester, 2015). Significant changes to circulating concentrations of retinoic acid are also known to factor into the onset or alleviation of various disease states (Miller, 1998; Kuenzli and Saurat, 2001; Njar, 2002; Ahmad and Mukhtar, 2004; Njar et al., 2006; Verfaille et al., 2008).

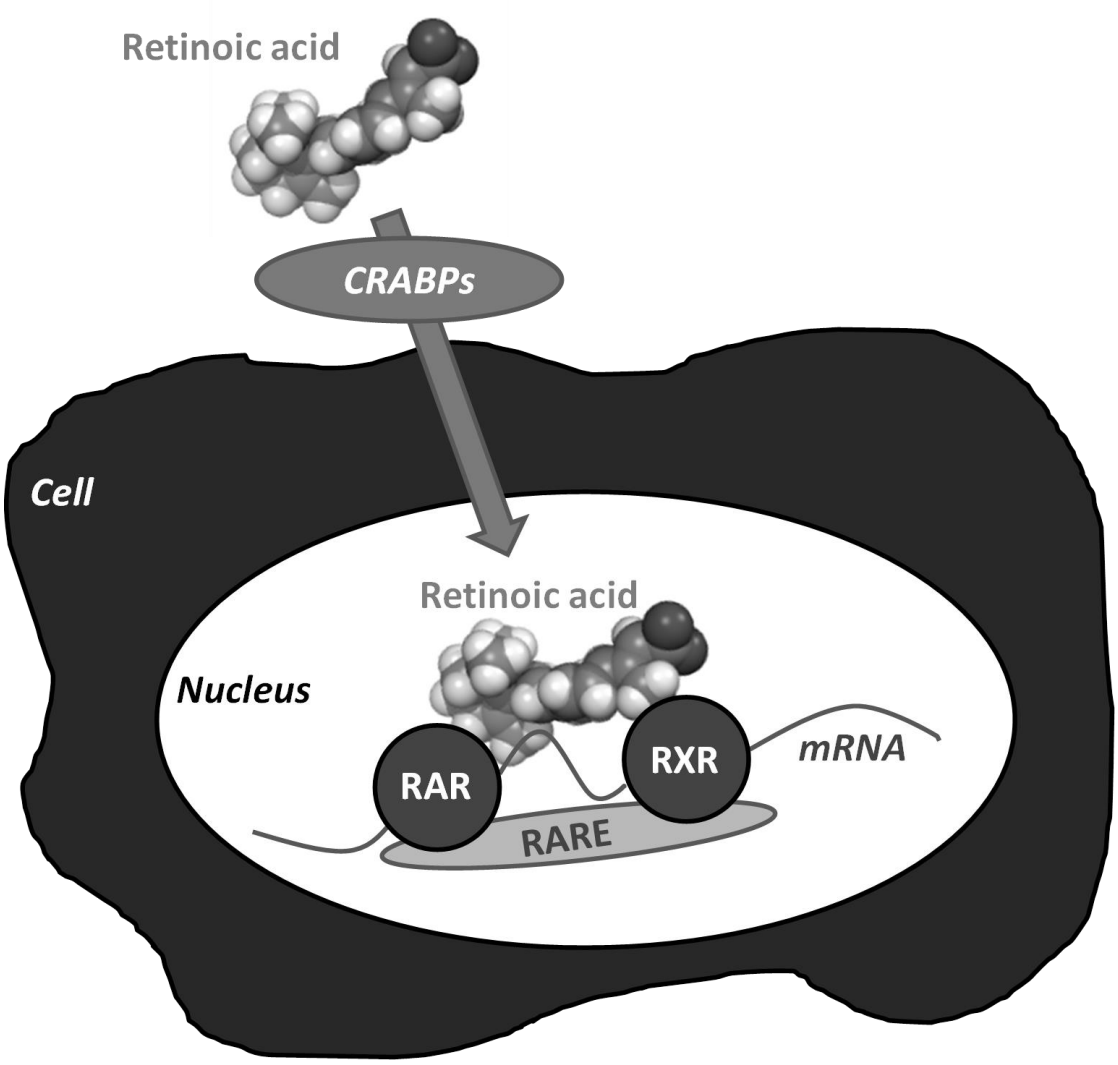

Figure 7-2. Retinoic acid signaling pathway.

7.3. Cytochrome P450.

The cytochrome P450s are a superfamily of heme-containing enzymes that are responsible for the oxidation or reduction of the majority of drugs currently in use (Ortiz de Montellano and De Voss, 2002). The superfamily is comprised of over 57 individual enzymes in humans, though the major isoforms believed to be involved in drug metabolism are generally limited to CYP1A1, CYP1A2, CYP2B6, CYP2C8, CYP2C9, CYP2C19, CYP2D6, CYP2E1, CYP3A4 and CYP3A5 (Guengerich, 2005). Cytochrome P450s are predominantly localized to the endoplasmic reticulum of liver, intestinal, lung, kidney, brain and nasal mucosa cells (Ding and Kaminsky, 2003)**.** Cytochrome P450 isoforms involved in homeostatic processes include CYP4B1, CYP4F2, CYP4F12, CYP17A1, CYP19A1, CYP26 (A1, B1 and C1) and CYP46A1, in addition to many others. They require the transfer of electrons from NADPH for catalytic activity, a process which occurs through interactions with multiple redox partners such as cytochrome P450 reductase and cytochrome b5 (Iyanagi and Mason, 1973; Vermilion and Coon, 1978; Vermilion et al., 1981; Schenkman and Jansson, 1999). An abbreviated reaction cycle is shown in Figure 7-3.

From a protein conformation standpoint, the overall structure of cytochrome P450 isoforms is relatively conserved across the family and appears designed specifically for catalyzing heme-thiolate reactions, interactions with cytochrome P450 reductase and cytochrome b5 and binding of endogenous and exogenous ligands (Poulous and Johnson, 2005). In general, structural conservation across family members increases as one is closer to the heme, and the I-helix of the different P450s is often used as a point of orientation in P450 modeling and crystal structures. Eukaryotic P450s are primarily membrane bound and located in the endoplasmic reticulum, with an N-terminal polypeptide chain responsible for anchoring the protein in the membrane (von Wachenfeldt et al., 1997; Cosme and Johnson, 2000; McDougle et al., 2013).

In addition to being involved in the metabolism of many endogenous and exogenous

ligands, the inhibition of cytochrome P450 isoforms plays an important role in both the regulation of homeostatic functions as well as in clinical drug interactions. Inhibition of cytochrome P450 can be reversible (competitive, noncompetitive or mixed inhibition) or irreversible (mechanism-based inhibition) (Blobaum, 2006; Foti et al., 2010). The mechanism of inhibition can also be characterized by the interactions between the ligand and the heme iron. Of particular note is the type II interaction that is often observed for compounds such as anti-fungal compounds and select retinoids or retinoic acid metabolizing blocking agents, many of which contain an sp^2 hybridized nitrogen capable of coordinating the heme iron. Owing to the tendency of the heme-thiolate bond to stretch depending on the type of ligand interaction and the resulting change in the spin state of the heme iron, such interactions can be characterized through the use of various spectroscopic techniques (Schenkman and Jansson, 2006).

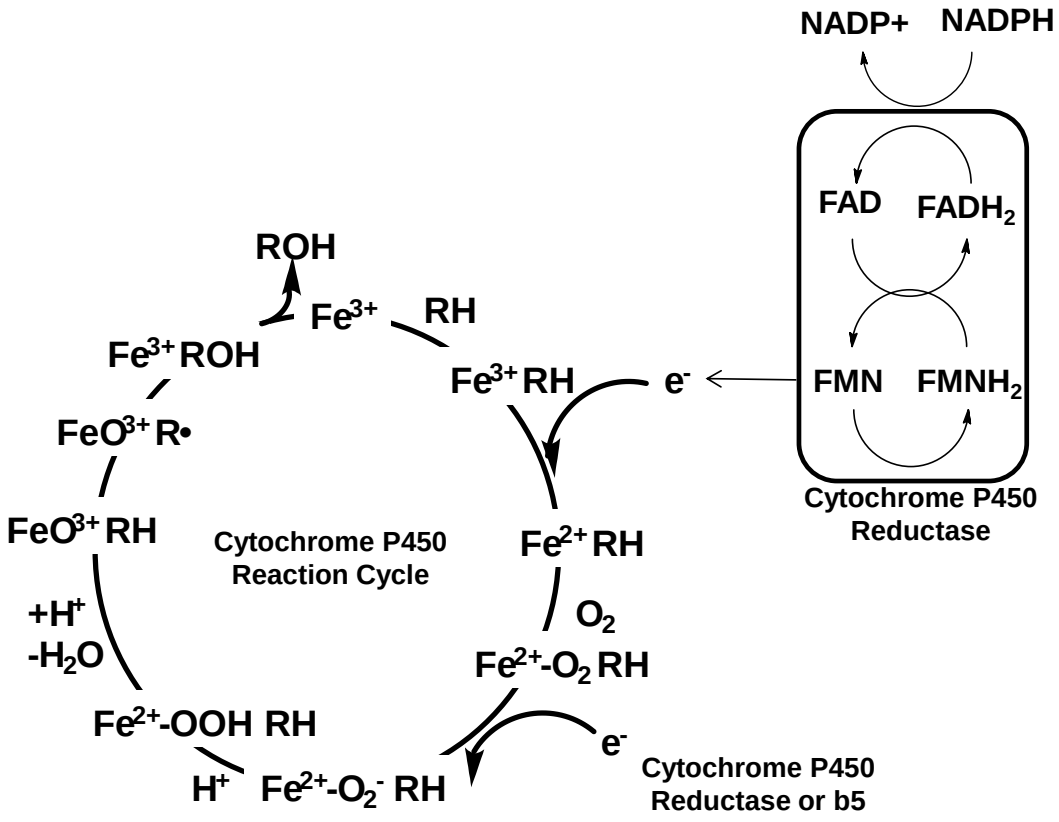

Figure 7-3. Cytochrome P450 reaction cycle.

7.4. Role of CYP26.

Endogenous control of retinoic acid occurs through increasing or decreasing its rate of synthesis, which can take place through the modulation of a number of catalytic processes through which retinol is converted to all-trans-retinoic acid (*at*-RA) or through altering the elimination or metabolism of retinoic acid, which occurs through oxidative metabolism catalyzed by cytochrome P450 enzymes, which are responsible for the oxidative metabolism of both drugs and endogenous substances (Figure 7-4) (Nelson, 2006; Duester, 2008; Niederreither and Dolle, 2008; Zanger and Schwab, 2013). A subfamily within the cytochrome P450s, CYP26 (CYP26A1, CYP26B1 and CYP26C1) is primarily responsible for the oxidative metabolism of retinoic acid (Ray et al., 1997; Lutz et al., 2009; Thatcher and Isoherranen, 2009; Thatcher et al., 2010; Ross and Zolfaghari, 2011). CYP26A1 and CYP26B1 are the two most widely studied isozymes within the CYP26 family, with less known about the homeostatic and pharmacological significance of CYP26C1. Similar to the channeling pathways reported for the retinoic acid and retinoid X receptors, CRABPs are also thought to be involved in the transport of retinoic acid to CYP26 to facilitate metabolism (Nelson et al., 2013b). The expression of both CYP26A1 and CYP26B1 have also been shown to be induced by retinoic acid, representing a major hurdle in the use of retinoic acid as a pharmacological intervention (Muindi et al., 1992; van der Leede et al., 1997; Wang et al., 2002; Wang et al., 2009).

Quantitatively, CYP26 expression in the liver is primarily comprised of CYP26A1, with minimal amounts of hepatic CYP26B1 being present (Xi and Yang, 2008; Thatcher and Isoherranen, 2009; Thatcher et al., 2010; Topletz et al., 2012). The highest levels of CYP26B1 mRNA expression have been identified in the adult brain (White et al., 2000; Thatcher and Isoherranen, 2009; Topletz et al., 2012). Extra-hepatically, both isozymes are ubiquitously expressed, with corresponding mRNA having been identified in skin, kidney, testes and lung (CYP26A1) or skin, lung, testes, placenta, ovaries and intestine (Ray et al., 1997; White et al.,

2000; Wang et al., 2002; Xi and Yang, 2008; Tay et al., 2010; Thatcher et al., 2010; Osanai and Lee, 2011; Topletz et al., 2012; Nelson et al., 2013a).

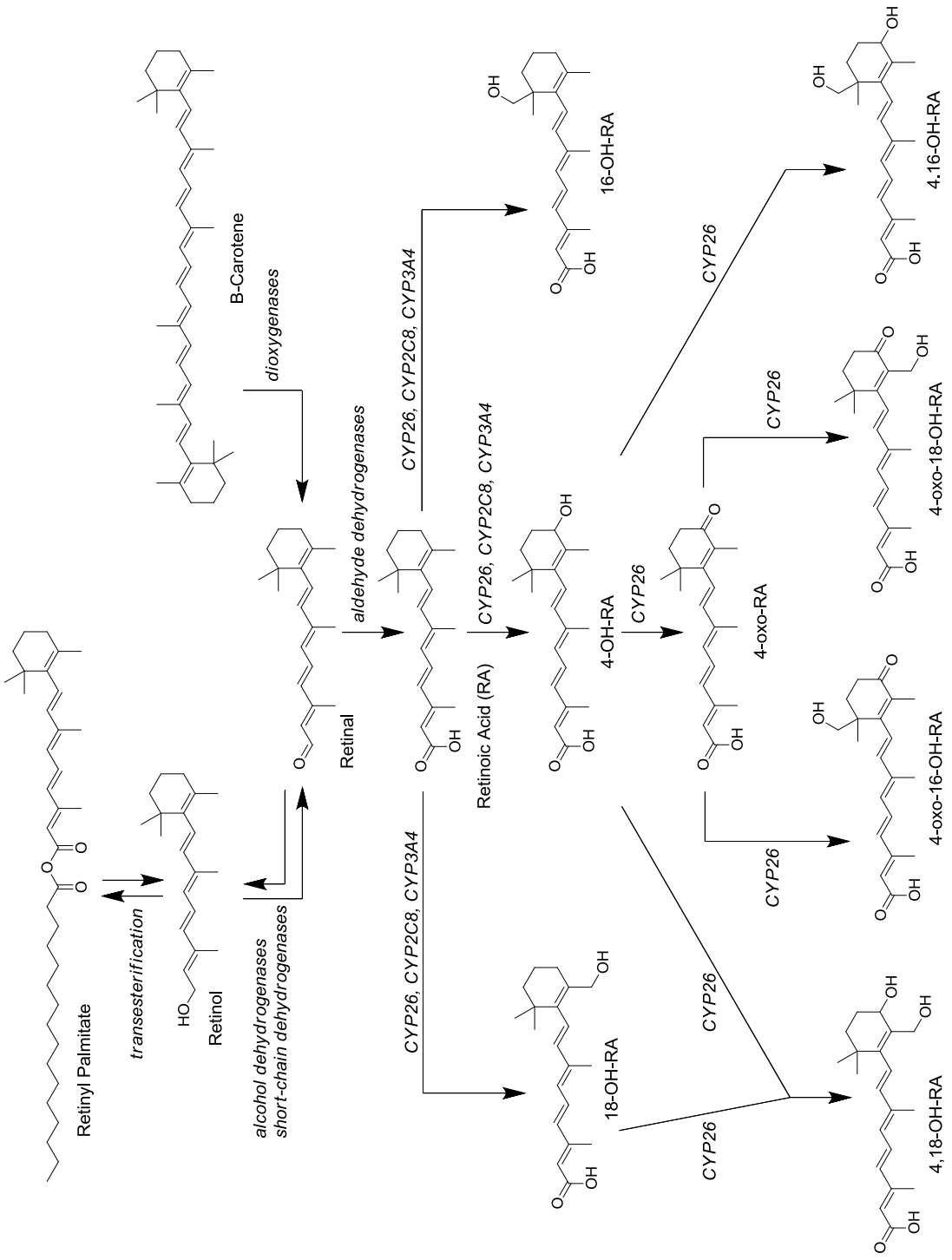

Figure 7-4. Metabolic scheme for the formation and elimination of *at*-RA.

The evolutionary importance of regulating endogenous retinoic acid concentrations is consistent with the functional overlap of CYP26A1 and CYP26B1, though interestingly the two isoforms share only a 42 – 44% sequence homology (Taimi et al., 2004; Topletz et al., 2012). Knowledge of the metabolic ligand profiles of each enzyme is relatively sparse, with in-depth characterizations limited to retinoic acid isomers and structurally-related metabolites (White et al., 1996; Sonneveld et al., 1998; White et al., 2000; Taimi et al., 2004; Thatcher et al., 2010; Ross and Zolfaghari, 2011; Topletz et al., 2012; Topletz et al., 2014). Previous reports indicated that the greatest catalytic efficiency is observed when *all trans*-retinoic acid (*at*-RA) is bound in the active site, though additional evidence suggests that CYP26A1, CYP26B1 and CYP26C1 are also able to catalyze the oxidative metabolism of other retinoic acid stereoisomers and structurally similar conformers. (White et al., 1996; White et al., 2000; Taimi et al., 2004; Ross and Zolfaghari, 2011). CYP26A1 and CYP26B1 are capable of catalyzing multiple steps in the metabolic clearance of *at*-RA (Figure 7-4), with roles in the sequential metabolism of 4-hydroxy-*at*-RA, 4-oxo-*at*-RA and 18-hydroxy-*at*-RA (Lutz et al., 2009; Shimshoni et al., 2012; Topletz et al., 2012; Topletz et al., 2014).

7.5. CYP26 Pharmacology.

Given the role of CYP26A1 and CYP26B1 in the endogenous control of retinoic acid concentrations in vivo, the identification of selective chemical inhibitors of the enzymes has been evaluated as a potential therapeutic approach in both inflammatory and oncological-related disease states (Miller, 1998; Kuenzli and Saurat, 2001; Njar, 2002; Ahmad and Mukhtar, 2004; Njar et al., 2006; Verfaille et al., 2008). Initial attempts to identify inhibitors of CYP26A1 or CYP26B1 resulted in the synthesis and characterization of retinoic acid metabolism blocking agents (RAMBAs). The majority of known RAMBAs share a conserved pharmacophore, with a bridging hydrophobic tether that couples a hydrophobic or aromatic functional group to a

hydrogen bond acceptor, an observation which can be exploited to both characterize the active site binding characteristics of the enzymes as well as to design new inhibitors of the enzymes (Purushottamachar et al., 2012; Sun et al., 2015). Often, the hydrophobic functional group is an azole-type moiety, integrated into the molecule to take advantage of a type II binding mechanism with the heme iron of CYP26A1 or CYP26B1, resulting in inhibition of the enzymes (Njar, 2002; Njar et al., 2006; Gomaa et al., 2008; Gomaa et al., 2011a; Thatcher et al., 2011; Nelson et al., 2013a).

Various structural analogs of retinoic acid, commonly referred to as retinoic acid receptor agonists or antagonists depending on their specific regulatory function, are also being pursued as therapeutic interventions across different therapeutic areas, including oncology, dermatology and regenerative medicine (Charpentier et al., 1995; Gudas and Wagner, 2011; di Masi et al., 2015). Often, the understanding of the adsorption, distribution, metabolism and excretion characteristics of these compounds is limited. However, the identification of these compounds has led to the evaluation of CYP26 as a potential drug target, as many of these compounds also have inhibitory activity against CYP26A1 or CYP26B1 (Thatcher et al., 2011).

7.6. CYP26 Homology Modeling.

Characterization of the three-dimensional structure of a protein and, perhaps more importantly, its ligand binding regions can prove crucial to understanding the biological functions of a given drug target or metabolic enzyme. Though a definitive assessment of a protein's structure generally relies on experimentally-determined structural data, the prediction of the protein's structure through homology modeling can also prove valuable in understanding the structural features which contribute to its ligand binding characteristics and biological mechanism of action (Hillisch et al., 2004; Cavasotto and Phatak, 2009). A homology modeling approach aims to develop a computationally derived three-dimensional model for a protein with

an unknown structure based on its similarity to other proteins with experimentally determined structures (Lesk and Chothia, 1986; Murzin, 2001; John and Sali, 2003; Zhang, 2008). The success of such an approach relies heavily on the degree of similarity between the two proteins as well as the generation of a correct sequence alignment between the two protein sequences (Khan et al., 2016). The data generated through the use of a homology model can be used to identify endogenous substrates or rationally design new xenobiotic ligands for the protein of interest, whose observed binding properties in the active site of the protein can then be used to further refine the model (Hillisch et al., 2004).

The first step in developing a homology model is the selection of a template protein with a known three dimensional structure and high degree of sequence similarity to the target protein with unknown structure using either comparative sequence assessment, multiple sequence assessments such as hidden Markov models and intermediate sequence searches for secondary structure prediction and fold recognition or a threaded template matching approach (Berman et al., 2000; Westbrook et al., 2002; Saxena et al., 2013). In general, a template structure with 30% or greater structural similarity to the target protein can provide the basis for a reliable homology model (Khan et al., 2016). After identification of an appropriate template, the two protein sequences must be aligned in such a manner to provide the greatest degree of sequence alignment, using either dynamic programming algorithms designed to take a relatively insensitive approach to aligning two sequences or a more complex approach where the target sequence is aligned to the protein sequences of multiple related proteins or where position specific information is incorporated into the sequence alignment (Sanchez and Sali, 1997a; Sanchez and Sali, 1997b). The latter approach becomes necessary for two proteins with less than optimal degrees of structural similarity (Xu et al., 1996; John and Sali, 2003).

Upon achievement of an acceptable degree of sequence alignment, a number of computational approaches are available with which to design and optimize the resulting homology model. Perhaps the most widely used approach is model assembly using a subset of

rigid protein sequences that are derived from the overall target sequence (Browne et al., 1969; Blundell et al., 1987; Greer, 1990; Blundell et al., 2006). A common approach to sub-dividing the protein sequence involves individually modeling the core backbone regions of the protein, followed by connecting variable loops and ultimately optimizing the individual amino acid side chains (Saxena et al., 2013). Additional approaches include coordinate reconstruction, where the segmentation of the target protein into hexapeptide segments leads to the ultimate structural assignments, spatial restraint modelling, where geometrical deviations from the template structure using a set of pre-defined spatial restraints are minimized, or loop modeling, used to define flexible regions in a protein structure (generally less than eight amino acid residues) based on known libraries and conformational searching or energy-based approaches (Krieger et al., 2003; Saxena et al., 2013).

Model optimization follows the initial model design. Owing to the dynamic interplay between the predicted structure of the backbone core regions and the geometry of the individual side chains, an iterative approach is often utilized where the effects of energy minimization of the side chains on the backbone and vice-versa are taken into account over multiple cycles until the entire model eventually converges into a global energy minimum (Krieger et al., 2003). In general, the energy minimization step is achieved by using either classical molecular dynamics or quantum force fields, which incorporate the positions of each atomic nucleus as well as the inherent charge distribution and treat the overall protein as a sum of the individual amino acids or a self-parameterizing force field, which build upon the aforementioned force fields by randomly changing a given parameter such as van der Waals radii and reminimizing the model to determine if an improvement in the model was obtained (Liu et al., 2001; Krieger et al., 2002).

The final step in homology modeling is the validation of the model, which identifies errors inherent to all homology models. As homology modeling is an inherently iterative process, errors in model design are easily propagated and can result in serious deficiencies in the final model design. Commonly observed errors include sequence misalignments, incorrectly

assigned geographical sequences of the target protein, unacceptable side-chain conformations and abnormal bond lengths or angles (Morris et al., 1992; Czaplewski et al., 2000; Czaplewski et al., 2003; Krieger et al., 2003; Saxena et al., 2013). Validation of the model can involve the entire model or distinct subdivided regions of the model, with each approach generating scoring functions that evaluate template alignment, protein stereochemistry and protein misfolding, in addition to a plentitude of other parameters (Sippl, 1995; Hooft et al., 1996; Marti-Renom et al., 2000; Hillisch et al., 2004). The scoring functions can generally be divided into either statistical-based or physical-based energy functions (Sippl, 1995; Lazaridis and Karplus, 1999; Al-Lazikani et al., 2001; Xiang, 2006). The former scoring functions incorporate the well-characterized properties of amino acids in a given structure while the latter is based on calculating the conformational free energy of the overall protein structure (Xiang, 2006).

The homology models presented in this body of work were designed and validated using Prime (Schrodinger LLC, New York). Within Prime, structural alignments are calculated using both the overall sequence of the target and template proteins as well as the secondary structure of each protein (Nayeem et al., 2006). Contributions from protein structure, docked ligands, solvent and multiple force fields are combined to build the model using aligned atom positions. Nonaligned sequences between the target and template protein structures are calculated using solvation energies and ab initio approaches (Jacobson et al., 2004). The simulations utilize the commonly used OPLS (Optimized Potential for Liquid Simulations) force field, developed by William Jorgensen (Jorgensen and Tirado-Rives, 1988). The force field incorporates bonds and angles from known x-ray crystal structures, ab initio calculated dihedral angles, calculated partial charges from the equilibrated protein conformation and van der Waals parameters which account for solvent interactions (Weiner et al., 1984; Jorgensen and Tirado-Rives, 1988; Kaminski et al., 1994; Jorgensen et al., 1996; Mackerell, 2004; Jorgensen and Tirado-Rives, 2005).

With respect to the structural characteristics of the cytochrome P450 family of drug metabolizing enzymes, their relatively flexible and lipophilic active sites can often pose a challenge in regard to accurately simulating the binding of a substrate within the active site and subsequently predicting the preferred site of metabolism (Williams et al., 2000; Lewis, 2002; Eksterowicz et al., 2014). As no crystal structures currently exist, multiple CYP26A1 or CYP26B1 homology models are currently available, the majority of which have been used to characterize the ability of CYP26A1 to stereoselectively catalyze the formation of 4-(S)-OH-*at*-RA or to investigate the ligand site interactions of azole-based inhibitors of CYP26A1 or CYP26B1 which are designed to coordinate to the heme iron and whose conformation in the active site can be confirmed through various spectral analyses (Gomaa et al., 2006; Gomaa et al., 2008; Karlsson et al., 2008; Ren et al., 2008; Gomaa et al., 2011a; Gomaa et al., 2011b; Shimshoni et al., 2012; Sun et al., 2015).

8. Aims and Scope.

The use of a homology model approach to identifying xenobiotic molecules which are capable of being metabolized by the CYP26 family of drug metabolizing enzymes is currently undefined and serves as the basis of the work presented in this thesis. Homology models of CYP26A1, CYP26B1 and CYP26C1 were designed and utilized to compare the structural characteristics of each enzyme, especially in regard to active site architecture. The models were validated through docking simulations with *at*-RA and subsequently utilized to identify and characterize tazarotenic acid as the first known xenobiotic substrate of CYP26. Similar to earlier homology models, structural assessment of the models suggested active site similarities with CYP2C8, another cytochrome P450 isozyme capable of metabolizing *at*-RA (see Chapter II). Tazarotenic acid was used as an in vitro probe of CYP26A1 or CYP26B1 activity to determine the inhibitory potency of set of known CYP2C8 inhibitors against CYP26 activity and the models applied to propose binding orientations for the most potent inhibitors (see Chapter

III). Ultimately, in vitro inhibition properties were extrapolated to predicted in vivo outcomes in order to determine the ability of select CYP2C8 inhibitors to cause clinically meaningful drug interactions through inhibition of CYP26 activity. Finally, the role of CYP26A1, CYP26B1 and CYP26C1 in the metabolism of additional retinoic acid agonists or antagonists was evaluated using in vitro experiments and computational modeling (see Chapter IV). The metabolism of adapalene by CYP26 was evaluated and used to determine the ability of the CYP26 enzymes to alter the preferred sites of metabolism in response to sterically-hindering functional groups. Taken in their entirety, the results presented herein provide the basis for a significant role for the CYP26 family of drug metabolizing enzymes both in the metabolism of xenobiotic compounds as well as in the potential for clinical drug interactions through inhibition of CYP26-mediated catalytic pathways.

9. Chapter II: Identification of Tazarotenic Acid as the First Xenobiotic Substrate of Human Retinoic Acid Hydroxylase CYP26A1 and CYP26B1

Accepted for Publication: Journal of Pharmacology and Experimental Therapeutics, 2016.

Highlighted as Cover Art in May 2016 Issue

9.1. Introduction.

Cytochrome P450 26A1 and 26B1 are members of the cytochrome P450 superfamily of heme-containing enzymes that are responsible for the metabolism of retinoic acid (Ray et al., 1997; Guengerich, 2006; Lutz et al., 2009; Thatcher and Isoherranen, 2009; Ross and Zolfaghari, 2011). In addition to metabolizing retinoic acid, both CYP26A1 and CYP26B1 are induced by retinoic acid (Muindi et al., 1992; van der Leede et al., 1997; Wang et al., 2002; Wang et al., 2009). The two enzymes are widely expressed throughout the adult human body, though CYP26A1 is the primary isoform expressed in the adult liver, with little to no hepatic expression of CYP26B1 observed (Xi and Yang, 2008; Thatcher and Isoherranen, 2009; Thatcher et al., 2010; Topletz et al., 2012). CYP26B1 mRNA expression has been reported to be the highest in the adult brain (White et al., 2000; Thatcher and Isoherranen, 2009; Topletz et al., 2012). Additional sites of expression for CYP26A1 mRNA include the skin, testes, kidney, and lung, while CYP26B1 mRNA has been identified in skin, lung, testes, placenta, ovaries and intestine (Xi and Yang, 2008; Osanai and Lee, 2011; Topletz et al., 2012). While CYP26A1 and CYP26B1 share only a 42 – 44% sequence homology with each other, a significant amount of functional redundancy is observed between the two enzymes, indicating the importance of their role in the regulation of endogenous retinoic acid concentrations (Taimi et al., 2004; Topletz et al., 2012). Reports on the catalytic activity of CYP26A1 and CYP26B1 are currently limited to various retinoic acid isomers and structurally-related metabolites (White et al., 1996; Sonneveld et al., 1998; White et al., 2000; Taimi et al., 2004; Thatcher et al., 2010; Ross and Zolfaghari, 2011; Topletz et al., 2012; Topletz et al., 2014). While the enzymes generally exhibit the highest degree of activity with *all trans*-retinoic acid (*at*-RA) as the substrate, they also metabolize other retinoic acid stereoisomers, albeit with much lower activities (White et al., 1996; White et al., 2000; Taimi et al., 2004; Ross and Zolfaghari, 2011). CYP26A1 and CYP26B1 also catalyze the in vitro clearance of the retinoic acid metabolites 4-hydroxy-*at*-RA,

4-oxo-*at*-RA and 18-hydroxy-*at*-RA (Lutz et al., 2009; Shimshoni et al., 2012; Topletz et al., 2012; Topletz et al., 2014).

Retinoic acid signaling and altered retinoic acid concentrations play a significant role in various disease states (Miller, 1998; Kuenzli and Saurat, 2001; Njar, 2002; Ahmad and Mukhtar, 2004; Njar et al., 2006; Verfaille et al., 2008). As a result of the contribution of CYP26A1 and CYP26B1 to retinoic acid metabolism, significant effort has gone into the design and synthesis of inhibitors of CYP26 activity, as increased retinoic acid concentrations have been considered beneficial in many instances. Recent efforts to characterize CYP26 as a drug target have focused on structurally-related analogs of retinoids, retinoic acid metabolism blocking agents (RAMBAs) and retinoic acid receptor agonists, as a number of these compounds have been characterized as inhibitors of CYP26A1 activity in vitro (Thatcher et al., 2011). While inhibitors of CYP26 have been identified, the role of these enzymes in the metabolism of xenobiotic compounds remains unclear. Of special interest are the synthetic retinoic acid receptor agonists that are structurally similar to retinoic acid and have structural moieties which can undergo metabolism by cytochrome P450 enzymes. One such retinoid is tazarotene, an acetylene-containing compound that is administered topically to stable plaque psoriasis or mild acne patients (Tang-Liu et al., 1999). Tazarotene acts as a pro-drug in the skin with its activity being attributed to an active metabolite, tazarotenic acid, which binds with a high affinity to the retinoic acid receptors (Chandraratna, 1996). The active metabolite shares key structural features with *at*-RA and has been reported to be metabolized by a number of drug metabolizing enzymes including CYP2C8, CYP3A4, FMO1 and FMO3 (Madhu et al., 1997; Tang-Liu et al., 1999; Attar et al., 2003; Attar et al., 2005). Whether tazarotenic acid is a substrate of CYP26A1 and CYP26B1 is currently unknown.

In the absence of experimentally-determined structural data, homology modeling is a commonly applied computational technique used to predict protein structure and function (Hillisch et al., 2004; Cavasotto and Phatak, 2009). The approach utilizes the known crystal

structure of a given protein to predict the three-dimensional properties of a second protein with a similar amino acid sequence but unknown structure (Lesk and Chothia, 1986; Murzin, 2001; Zhang, 2008). The hypotheses generated by a homology model can be used to assess target druggability, to aid in the rational design of ligands for the given protein and to predict drug metabolism and toxicity, all of which can then be used to iteratively refine the model (Hillisch et al., 2004). In regard to the cytochrome P450 family of drug metabolizing enzymes, the flexible and hydrophobic nature of their active sites often presents a challenge when attempting to use a homology model to accurately predict the site of metabolism for a given substrate (Williams et al., 2000; Lewis, 2002; Eksterowicz et al., 2014). While it may be possible to correctly predict whether or not a ligand binds as an inhibitor of a cytochrome P450, correctly identifying the site of metabolism for a cytochrome P450 substrate may prove more challenging and can be indicative of the overall quality of the homology model (Arimoto, 2006; Yu et al., 2015). Several homology models have been published for CYP26A1 and CYP26B1 and have been successfully used to rationalize the stereoselective product formation of 4-OH-*at*-RA by CYP26A1 or the binding of triazole- or imidazole-containing inhibitors of CYP26A1 or CYP26B1 within the active site of each enzyme (Gomaa et al., 2006; Gomaa et al., 2008; Karlsson et al., 2008; Gomaa et al., 2011a; Gomaa et al., 2011b; Shimshoni et al., 2012; Sun et al., 2015). There are currently no homology models that compare the structure and function of CYP26A1 and CYP26B1 based on the metabolism of a xenobiotic compound and attempts to crystallize either isoform have been largely unsuccessful.

The aim of this work was to evaluate and characterize the active sites of CYP26A1 and CYP26B1 using homology modeling supported by *at*-RA and xenobiotic metabolism data. Homology models were constructed for each enzyme and compared for structural similarities and differences. *at*-RA and tazarotenic acid were docked into the active site of each enzyme and the predicted sites of metabolism evaluated. Metabolite identification experiments in recombinantly expressed enzyme systems were used to confirm the hypotheses generated by

the homology models. Finally, in vitro experiments were carried out to compare the metabolism of tazarotenic acid across a panel of drug metabolizing enzymes and to determine the kinetic parameters for the formation of metabolites from tazarotenic acid by CYP26A1 and CYP26B1.

9.2. Materials and Methods.

9.2.1. Materials.

Tazarotenic acid and all metabolite standards were obtained from Tocris Chemicals (Bristol, United Kingdom). CYP26A1 was expressed and characterized as previously described (Lutz et al., 2009). All other reagents were obtained as noted below. Solvents were from Sigma-Aldrich (St. Louis, MO) and were of the highest grade available.

9.2.2. Sequence Verification and Expression of CYP26B1.

To express recombinant CYP26B1, the human CYP26B1 cDNA was obtained from OriGene Technologies (Rockville, MD) (catalog number TC120799). Upon sequencing of the obtained clone, two single nucleotide polymorphisms were discovered that differed from the sequence reported in NCBI (Q9NR63). The two SNPs were an A191G conversion resulting in an H>R amino acid change and a G788A conversion resulting in a G>S amino acid change (CYP26B1*1, Figure 9-1). To determine which of the possible SNPs would be reflective of the CYP26B1 sequence in the human population, genomic DNA was extracted from 12 human livers from the University of Washington human liver bank and the two sections of the CYP26B1 gene were sequenced in all 12 donors. In brief, genomic DNA (50 ng) was amplified by PCR using either forward *(*5'-TCTTTGAGGGCTTGGATCTG-3') and reverse *(*5'-GGCAGAGAGGGAAGG-3') primers for the A191G SNP or forward *(*5'-GACAAAGGGGAGAGGTGTCA-3') and reverse *(*5'-GTAGAAATGGCTGGGCACAT-3') primers for the G778A SNP at concentrations of 400 nM. The primers and template DNA together with a

Ready-to-Go bead (puReTaq Ready-to-Go PCR beads, Amersham Biosciences, Piscataway, NJ) were mixed in a final volume of 25 µL and PCR amplification was done as follows: after an initial denaturing step at 94°C for 4 min, amplification was performed for 32 cycles of denaturation (94°C for 30 s), annealing (55°C for 20 s), and extension (72°C for 30 s), followed by a final extension at 72°C for 30 s. PCR products were analyzed by gel electrophoresis, spin column-purified to remove unincorporated nucleotides and primers using the QIAquick® PCR Purification Kit (Qiagen Inc., Hilden, Germany) and sequenced for the forward and reverse direction on an ABI Prism 377Xl DNA Sequencer (Applied Biosystems, Foster City, CA) with the ABI Prism® BigDye™ Terminator Cycle Sequencing Ready Reaction Kit (PerkinElmer, Waltham, MA). After the wild-type sequence was confirmed, the CYP26B1 coding sequence from the original clone was amplified while adding a 6xHis tag with a TEV cleavage site to maintain similarity with the commercially available clone as previously described (Topletz et al., 2012). CYP26B1 protein was expressed using the Bac-to-Bac baculovirus expression system (Life Technologies, Grand Island, NY) in Sf9 cells according to the manufacturer's instructions as described previously (Topletz et al., 2012). Sf-900 II SFM liquid media (Life Technologies, Grand Island, NY) supplemented with 2.5% fetal bovine serum was used and during protein expression ferric citrate (0.2 mM) and δ-aminolevulinic acid (0.3 mM) were added to the media 24 hours post-infection to facilitate heme synthesis. The cells were harvested 48 hours post infection, washed once in PBS with 1 mM PMSF, pelleted and stored at –80˚C. Membrane fractions containing CYP26B1 were prepared by centrifugation as described previously (Topletz et al., 2012) and P450 content determined via CO-difference spectrum.

9.2.3. IC_{50} Determination for Retinoic Acid Receptor Agonists.

Six retinoic acid receptor agonists were assessed for in vitro inhibition of CYP26A1 and CYP26B1 catalyzed 9-*cis*-4-hydroxyretinoic acid formation. Various concentrations of each inhibitor (0 – 100 µM) were incubated with 5 pmol CYP26A1 or CYP26B1, 10 pmol cytochrome

P450 reductase, and 100 nM 9-*cis*-retinoic acid in 100 mM potassium phosphate buffer (pH 7.4). Incubations were initiated by the addition of 1 mM NADPH (final concentration) and quenched after 2 minutes (CYP26A1) or 5 minutes (CYP26B1) with 5 volumes of ethyl acetate containing acitretin as an internal standard. All samples were evaporated to dryness under a gentle stream of N_2, reconstituted in methanol and assayed for 9-*cis*-4-hydroxyretinoic acid concentrations by HPLC-UV as previously described (Thatcher et al., 2011). All IC_{50} determinations were conducted in triplicate.

9.2.4. Homology Modeling.

Homology models of CYP26A1 and CYP26B1 were constructed using Prime (Schrodinger LLC, New York). The amino acid sequence of human CYP26A1 was obtained from the NCBI protein server (GenBank ID: 2688846) and the CYP26B1 amino acid sequence was obtained as described above. CYP120 (crystal structure, pdb 2VE3) was used as the template for both homology models. Compared to CYP120, CYP26A1 had 33% sequence identity and 53% positive sequence coverage while CYP26B1 had 34% sequence identity and 54% positive sequence coverage. The heme prosthetic group was added to each homology model and ligated to Cys442 (CYP26A1) or Cys441 (CYP26B1), followed by energy minimization prior to ligand docking using OPLS_2005 force field constraints as defined within the MacroModel algorithm (Schrodinger LLC, New York). In order to flexibly dock *at*-RA, tazarotenic acid and tazarotenic acid sulfoxide, a ligand grid (12 x 12 x 12 Å) for which the center of mass of each ligand would be constrained to was defined and centered approximately 2 – 3 Å above the heme iron using Glide (Schrodinger LLC, New York). Structural rationalization of each homology model was performed through the evaluation of Ramachandran plots and model assessment of odd bond lengths and angles (Figure 9-2). Determination of model flexibility was assessed by comparison of helical versus loop motifs and by prediction of 2° structure characteristics using PSIPRED (University College London, UK) and SSPro (Schrodinger).

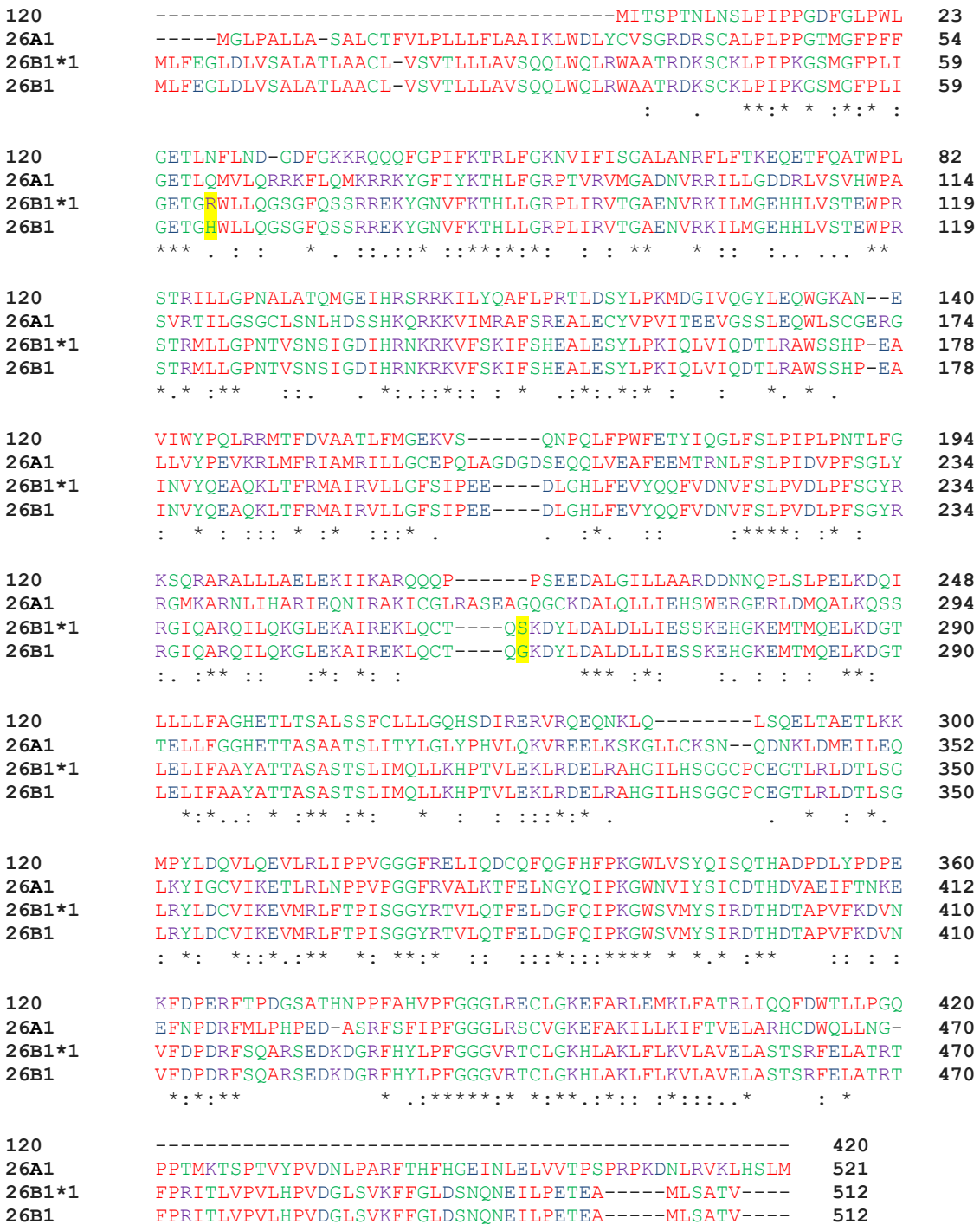

Figure 9-1. Multiple sequence alignment of CYP120, CYP26A1, CYP26B1*1 and CYP26B1 amino acid sequences.

The sequence identity between CYP26A1 and CYP26B1, CYP26B1*1 and CYP120 was 44.47%, 44.26% and 33.26%, respectively. For CYP26B1*1, a 99.61% and 34.69% sequence identity was observed with CYP26B1 and CYP120, respectively. Amino acids are represented in red (small/hydrophobic), blue (acidic), purple (basic) and green (hydroxyl/sulfhydryl/amine). Sequence consensus is indicated by an asterisk (residue is fully conserved across all sequences), a colon (consensus group contains very similar properties) or a period (consensus group contains weakly similar properties).

Ligand structures were also minimized using the OPLS_2005 force field constraints within LigPrep (Schrodinger LLC, New York). GlideScore and eModel scoring algorithms were used to assess the docking poses of the ligands within the active site of each enzyme (Friesner et al., 2004; Friesner et al., 2006). The use of the eModel scoring algorithm allowed for selection of the best docking pose based upon the GlideScore, grid score and ligand score of each docked ligand (Perola et al., 2004). The hydrogen atoms nearest the heme iron for the *at*-RA and tazarotenic acid docking poses with the highest GlideScores and eModel scores were used as the predicted sites of oxidative metabolism for each compound. The volume of the active site within each homology model was estimated using DoGSiteScorer (Volkamer et al., 2012).

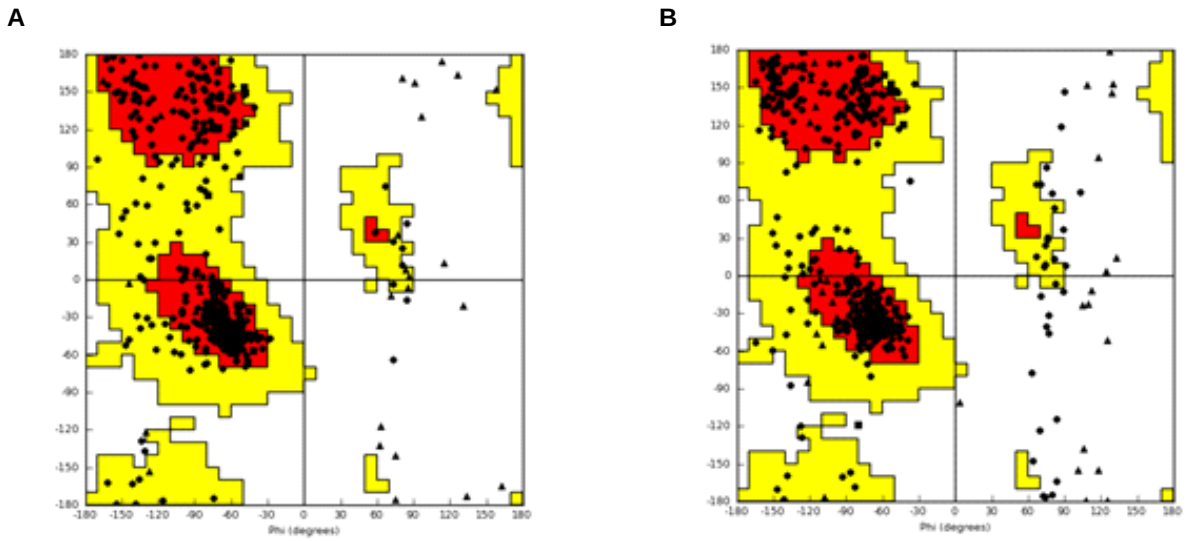

Figure 9-2. CYP26A1 and CYP26B1 Ramachandran Plot.

Analysis of the Phi-Psi angles in the CYP26A1 and CYP26B1 homology model demonstrated 98.9% and 98.3%, respectively, were in the favorable or allowable regions.

9.2.5. Metabolic Profiling.

Due to its relative potency in the CYP26A1 and CYP26B1 inhibition assays, tazarotenic acid was selected for further evaluation. In vitro experiments to elucidate the metabolic pathways of tazarotenic acid in CYP26A1 and CYP26B1 recombinant preparations were carried out using previously optimized conditions of 20 nM recombinant enzyme, 200 nM purified human reductase and tazarotenic acid (10 µM) in 100 mM potassium phosphate buffer (pH 7.4; final volume 100 µL). Incubations were initiated with the addition of 1 mM NADPH (final concentration) and incubated at 37 ºC for 30 minutes. Control incubations were performed in the absence of NADPH. Subsequent incubations to confirm the sequential metabolism of tazarotenic acid by CYP26A1 and CYP26B1 utilized 10 µM tazarotenic acid sulfoxide (final concentration) as the substrate in the incubation. Upon completion, in vitro incubations were extracted into 4 volumes of ethyl acetate, dried under a gentle stream of N_2 at 40 ºC and reconstituted in 100 µL methanol prior to LC-MS/MS analysis and compared to synthetic standards of each metabolite, if available. LC-MS/MS analysis was performed as described below.

9.2.6. Enzyme Kinetics.

In vitro enzyme kinetic parameters were determined for tazarotenic acid metabolite formation using 5 nM CYP26A1 or CYP26B1, 25 nM purified human reductase and 0 – 10 µM tazarotenic acid. Incubations were carried out for 10 minutes at 37 ºC to ensure product linearity with regard to time and protein concentration. Additional experiments to determine the kinetic parameters for the sequential metabolism of tazarotenic acid metabolite sulfoxide used substrate concentrations ranging from 0 – 50 µM. Samples were prepared as described for in vitro metabolic profiling experiments.

9.2.7. Tazarotenic Acid Phenotyping.

To assess the relative contribution of CYP26A1 and CYP26B1 to the in vitro oxidative metabolism of tazarotenic acid, metabolite formation was monitored across a panel of drug metabolizing enzymes. Previously reported studies to characterize the enzymes responsible for the metabolism of tazarotenic acid were conducted at substrate concentrations of 1 – 200 µM (Attar et al., 2003). As total circulating plasma concentrations of tazarotenic acid are approximately 1 – 280 nM following typical doses of tazarotene, current studies were conducted using clinically relevant substrate concentrations. In vitro incubations consisted of 5 nM recombinant enzyme, 50 nM purified human reductase and 100 nM tazarotenic acid (final concentrations) in 100 mM potassium phosphate buffer (pH 7.4). Following a three minute pre-incubation at 37 ºC, reactions were initiated with the addition of 1 mM NADPH (final concentration). For incubations utilizing flavin-containing monooxygenase enzymes, the pre-incubation step consisted of enzyme and NAPDH followed by initiation with substrate due to the known instability of FMOs at 37 ºC in the absence of cofactor (Foti and Fisher, 2004). Incubations (50 µL, final volume) were carried out for 30 minutes at 37 ºC before being quenched with 3 volumes (v/v) of ice-cold acetonitrile containing tolbutamide as an internal standard. Samples were vortexed and centrifuged at 1240 x g for ten minutes before being transferred for LC-MS/MS analysis. Data was expressed as the percent of total metabolite formed across the panel of enzymes for each individual metabolite.

9.2.8. LC-MS/MS Analysis.

Analysis of tazarotenic acid and its metabolites was conducted using LC-MS/MS. The analytical platform was comprised of an Applied Biosystems API4000 fitted with an electrospray ionization source (Applied Biosystems, Foster City, CA). Liquid chromatography and sample introduction was achieved using two LC-20AD binary pumps with an in-line DGU-20A5 solvent degasser

(Shimadzu, Columbia, MD) and a LEAP CTC HTS PAL autosampler (CTC Analytics, Carrboro, NC). An injection volume of 10 µL was used for all analyses. For enzyme kinetic experiments, chromatographic separation was achieved using 0.1% formic acid (v/v) in water (mobile phase A) and 0.1% formic acid in methanol:acetonitrile (1:1; mobile phase B) on a Synergi 2.5 µm Hydro RP 100 Å (50 x 2.0 mm) column (Phenomenex, Torrance, CA). Gradient conditions consisted of 2.5% B (0 – 0.4 minutes), 2.5% B – 95% B (from 0.4 – 1.4 minutes), 95% B (from 1.4 – 2.5 minutes) and re-equilibration at 2.5% B for 0.5 minutes. For metabolite identification experiments, the same mobile phase system was used with a Kinetex 2.6 µm C18 100 Å (100 x 2.1 mm) column (Phenomenex, Torrance, CA). A gradient of 2.5% B (0 – 3 minutes), 2.5% B – 95% B (from 3 – 14 minutes), 95% B (from 14 – 17 minutes) followed by re-equilibration at 2.5% B for 3 minutes was used to achieve chromatographic separation of all analytes. Initial metabolite identification experiments used full scan analysis from 100 – 800 amu followed by analysis of the corresponding product ion spectra for each observed analyte. Subsequent LC-MS/MS analyses utilized multiple reaction monitoring (MRM) for each analyte. MRM transitions (positive ionization mode) were as follows: tazarotenic acid (m/z 324.2 / 294.3), tazarotenic acid sulfoxide and hydroxytazarotenic acid (m/z 340.3 / 280.3), tazarotenic acid sulfone (m/z 356.3 / 276.3) and the internal standard tolbutamide (m/z 271.2 / 91.1). Generic parameters applied to all MS analyses included the curtain gas (12 arbitrary units), CAD gas (medium), ion spray voltage (5000 V), source temperature (500 °C) and ion source gas 1 and gas 2 (30 arbitrary units, each).

9.2.9. Data Analysis.

Mass spectrometry data was evaluated using Analyst (version 1.5; Applied Biosystems, Foster City, CA). Analyte concentrations were determined by comparing peak areas in unknown samples to those obtained from standard curves with analytical standards (dynamic range: 1 –

2000 nM; weighting: 1/x). Parameter fitting for IC_{50} and enzyme kinetic data was performed using Graphpad Prism as described below (version 6.03; Graphpad Software Inc., San Diego, CA).

IC_{50} values for retinoic acid receptor agonists in the 9-*cis*-4-hydroxyretinoic acid assay were determined by nonlinear regression using Equation 1. In the following equation, $100\%*(V_i/V)$ represents the percent activity remaining for a given inhibitor concentration, [*I*], $(V_i/V)_{max}*100\%$ is the maximum observed activity with no inhibitor present, and $(V_i/V)_{min}$ is the remaining enzyme activity at infinitely high concentrations of inhibitor.

Equation 1

$$100\% * \frac{v_i}{v} = \left(\frac{v_i}{v}\right)_{\min} * 100\% + \frac{\left(\left(\frac{v_i}{v}\right)_{\max} - \left(\frac{v_i}{v}\right)_{\min} * 100\%\right)}{\left(1 + 10^{[I] - \log IC50}\right)}$$

Enzyme kinetic parameters (K_m and V_{max}) were estimated through nonlinear regression analysis using the Michaelis-Menten model as shown in Equation 2. In the equation below, K_m denotes half the substrate concentration ([*S*]) at maximal reaction velocity (V_{max}).

Equation 2

$$V = \frac{V_{\max} * [S]}{K_m + [S]}$$

9.3. Results.

9.3.1. Homology Modeling.

Characterization of CYP26B1 from a commercially available clone (OriGene, Rockville, MD) and set of 12 human livers identified two amino acids which differed from the currently accepted amino acid sequence of the enzyme (Figure 9-1). The two sequencing differences were an A191G substitution resulting in an H64R amino acid change and a G778A substitution resulting in a G260S amino acid change. All 12 human donors sequenced had a CYP26B1 sequence identical to the clone obtained from OriGene and did not have the two sequencing differences observed in the previously reported clone of CYP26B1 (UniProtKB Q9NR63). Therefore the sequence with arginine at position 64 and serine in residue 260 was accepted as the wild type sequence of CYP26B1 (CYP26B1*1). The sequence of CYP26B1*1 is shown in Figure 9-1 and was used to build the subsequent CYP26B1 homology model. In order to assess the active sites of CYP26A1 and CYP26B1, homology models of each enzyme were constructed using the crystal structure of CYP120 (pdb 2VE3), which showed the highest degree of sequence similarity with CYP26A1 or CYP26B1 in a BLAST search. Sequence analysis indicated CYP26A1 had a sequence identity of 44.47% with CYP26B1 (Q9NR63), 44.26% with CYP26B1*1 and 33.26% with CYP120 (2VE3). CYP26B1*1 had a 99.61% sequence identity with CYP26B1 (Q9NR63) and a 34.69% sequence identity with CYP120. Superimposition of the CYP26A1 or CYP26B1 homology models with the template structure (CYP120) resulted in RMSD values of 1.038 and 1.168, respectively. Superimposition of the CYP26A1 and CYP26B1 homology models with each other resulted in a RMSD value of 1.651. Similarities in hydrophobic binding residues were observed for CYP26A1 and CYP26B1, with W112, Phe222 and Phe299 occupying analogous positions in the CYP26A1 active site as W117, Phe222 and Phe295 in the CYP26B1 active site (Figure 9-3). A greater divergence was observed for those

Table 9-1. Estimated parameters for CYP26A1 and CYP26B1 homology models.

Parameter	CYP26A1 Model	CYP26B1 Model
Template	CYP120 (pdb 2VE3)	CYP120 (pdb 2VE3)
Template Sequence Identity	33%	34%
Template Positive Sequence Coverage	53%	54%
BLAST Query Coverage	89%	89%
BLAST E-Value	2e-82	6e-91
RMSD vs Template	1.038	1.168
Favorable Bond Angles	86.2%	95.0%
Allowable and Favorable Bond Angles	98.9%	98.3%
I-Helix Residues	M287 – L318	M283 – A304
Active Site Volume	918.01 Å^3	976.86 Å^3
at-RA Docking Score (4-(*S*)-OH)	-9.552	-4.999
at-RA Distance from Heme (4-(*S*)-OH)	3.85 Å	2.99 Å
at-RA Docking Score (4-(*R*)-OH)	N/A	-4.128
at-RA Distance from Heme (4-(*R*)-OH)	N/A	4.06 Å
at-RA Docking Score (16-OH)	-9.552	-4.488
at-RA Distance from Heme (16-OH)	3.49 Å	2.77 Å
at-RA Docking Score (18-OH)	-9.552	-4.435
at-RA Distance from Heme (18-OH)	5.10 Å	3.10 Å
Tazarotenic Acid Docking Score	-11.016	-9.172
Tazarotenic Acid Distance from Heme	4.21 Å (to sulfur)	4.11 Å (to sulfur)
Tazarotenic Acid Sulfoxide Docking Score	-11.912	-9.843
Tazarotenic Acid Sulfoxide Distance from Heme	4.38 (to sulfur)	3.58 Å (to sulfur)

amino acid residues potentially capable of stabilizing the carboxylate moiety of *at*-RA in the active site of CYP26A1 (Arg64, Arg86 and Arg90) and CYP26B1 (W65, Arg76, Tyr372 and Arg373). Parameters detailing the structural evaluation of the template and the model are shown in Table 9-1 with the corresponding Ramachandran plots shown in Supplemental Figure 9-2. The active site volumes of CYP26A1 and CYP26B1 were estimated to be 918 Å^3 and 977 Å^3, respectively.

To further assess the validity of the homology models, *at*-RA was docked into the active site of the CYP26A1 and CYP26B1 homology models. In both models, the β-ionone ring of *at*-RA was oriented towards the heme iron, with the models confirming that the hydrogen atoms at

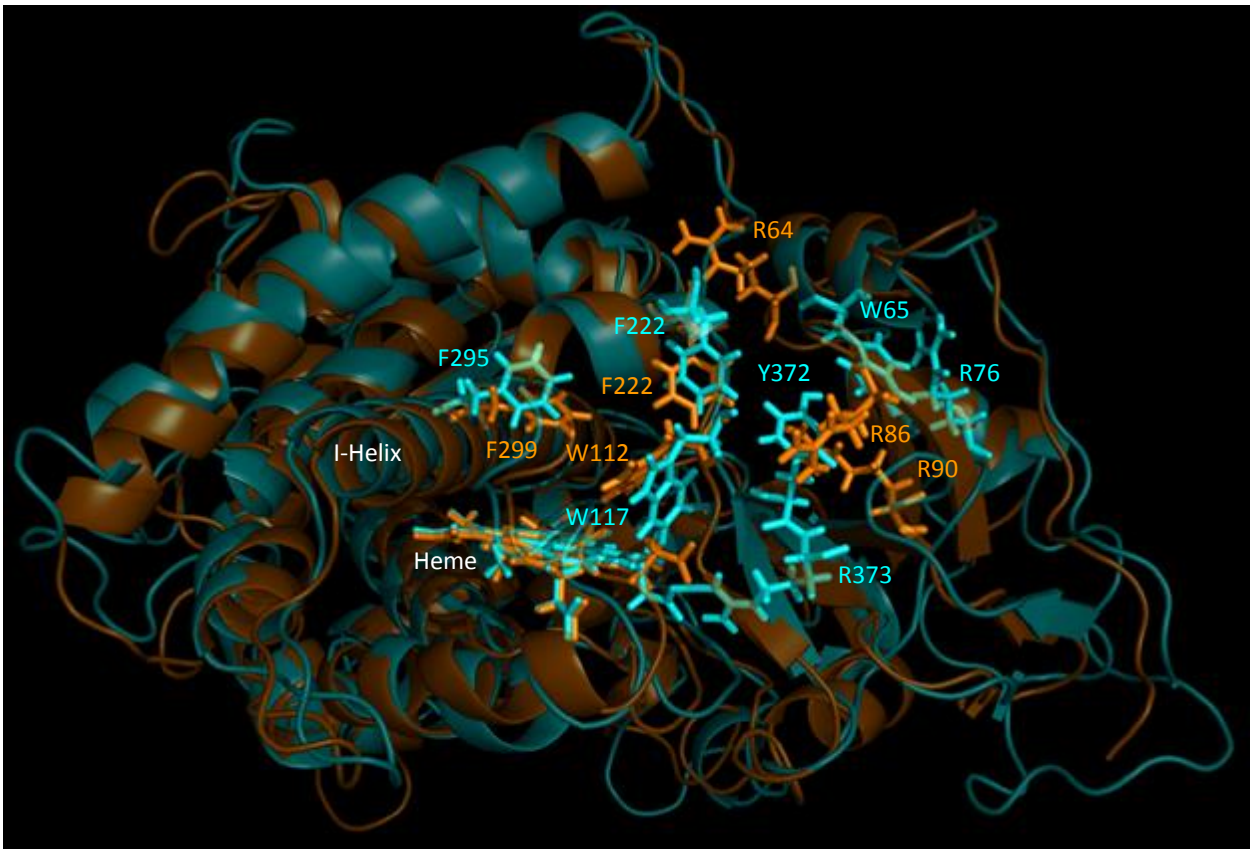

Figure 9-3. Structural alignment of CYP26A1 (orange) and CYP26B1 (cyan) homology models.

Sequence alignment of the two homology models indicated a structural identity of 44.26% and an RMSD value of 1.651. Structural similarity was observed for the portion of the active site of each enzyme that may contribute to hydrophobic binding interactions with a given ligand (Trp112, Phe222 and Phe299 for CYP26A1; Trp117, Phe222 and Phe295 for CYP26B1). The active site volumes of CYP26A1 and CYP26B1 were estimated to be 918 $Å^3$ and 977 $Å^3$, respectively.

the 4-, 16- or 18-position of the β-ionone ring of *at*-RA were positioned toward the heme iron. Similar to previously published homology model results, a single docking orientation of *at*-RA in the active site of CYP26A1 was able to account for oxidation at the 4-, 16- and 18- positions (Shimshoni et al., 2012). Further, only the hydrogen atom which when abstracted would lead to formation of the 4-(*S*)-hydroxyretinoic acid metabolite was directed toward the heme iron at a distance of 3.85 Å, with the hydrogen atoms at the 16- and 18- positions approximately 3.49 Å and 5.10 Å away from the heme iron, respectively (Figure 9-4A and Figure 9-5). In this

orientation, the corresponding hydrogen to form 4-(*R*)-hydroxyretinoic acid was directed away from the heme iron in a metabolically unfavorable position at a distance of 5.59 Å. The CYP26A1 homology model was unable to resolve an orientation of *at*-RA in the active site conducive with abstraction of the hydrogen in the 4-(*R*)-position. Conversely, docking orientations where either hydrogen atom on the carbon atom at the 4-position of the β-ionone ring was oriented toward the heme iron were identified using the CYP26B1 homology model (Figure 9-4B), suggesting that formation of 4-hydroxyretinoic acid by CYP26B1 would not be stereoselective. For formation of 4-(*R*)-hydroxyretinoic acid (Figures 9-4B (orange structure) and Figure 9-5), the hydrogen atom was located approximately 4.06 Å from the heme iron. When docked in such a way that the resulting product would be 4-(*S*)-hydroxyretinoic acid (Figures 9-4B (cyan structure) and Figure 9-5), the hydrogen atom to be abstracted was positioned approximately 2.99 Å from the heme iron. Docking of *at*-RA in the CYP26B1 homology model such that 16-hydroxyretinoic acid (Figures 9-4C and Figure 9-5) or 18-hydroxyretinoic acid (Figures 9-4D and Figure 9-5) would be the expected products positioned the sites of metabolism approximately 2.77 Å and 3.10 Å from the heme iron, respectively. The CYP26B1 docking score for the *at-RA* orientation leading to formation of 4-(*S*)-hydroxyretinoic acid was slightly more favorable than that leading to formation of 4-(*R*)-hydroxyretinoic acid and was similar to the docking scores observed when the 16- or 18-position was oriented toward the heme iron (Table 9-1). Arg90 (CYP26A1) and Ser369 or Arg373 (CYP26B1) were located within 3 Å of the carboxylic acid moiety of *at*-RA. Amino acid residues depicted in Figure 9-4 and Figure 9-5 are located within 3 Å of the docked *at*-RA ligand.

In order to select a non-endogenous retinoid-like molecule to include in the homology model analysis, a panel of retinoic acid receptor agonists was screened for inhibitory potency against CYP26A1 and CYP26B1. IC_{50} values ranged from 3.7 – 18 μM for CYP26A1 and from 0.13 – 31 μM for CYP26B1 (Table 9-2). Tazarotenic acid was the second most potent inhibitor

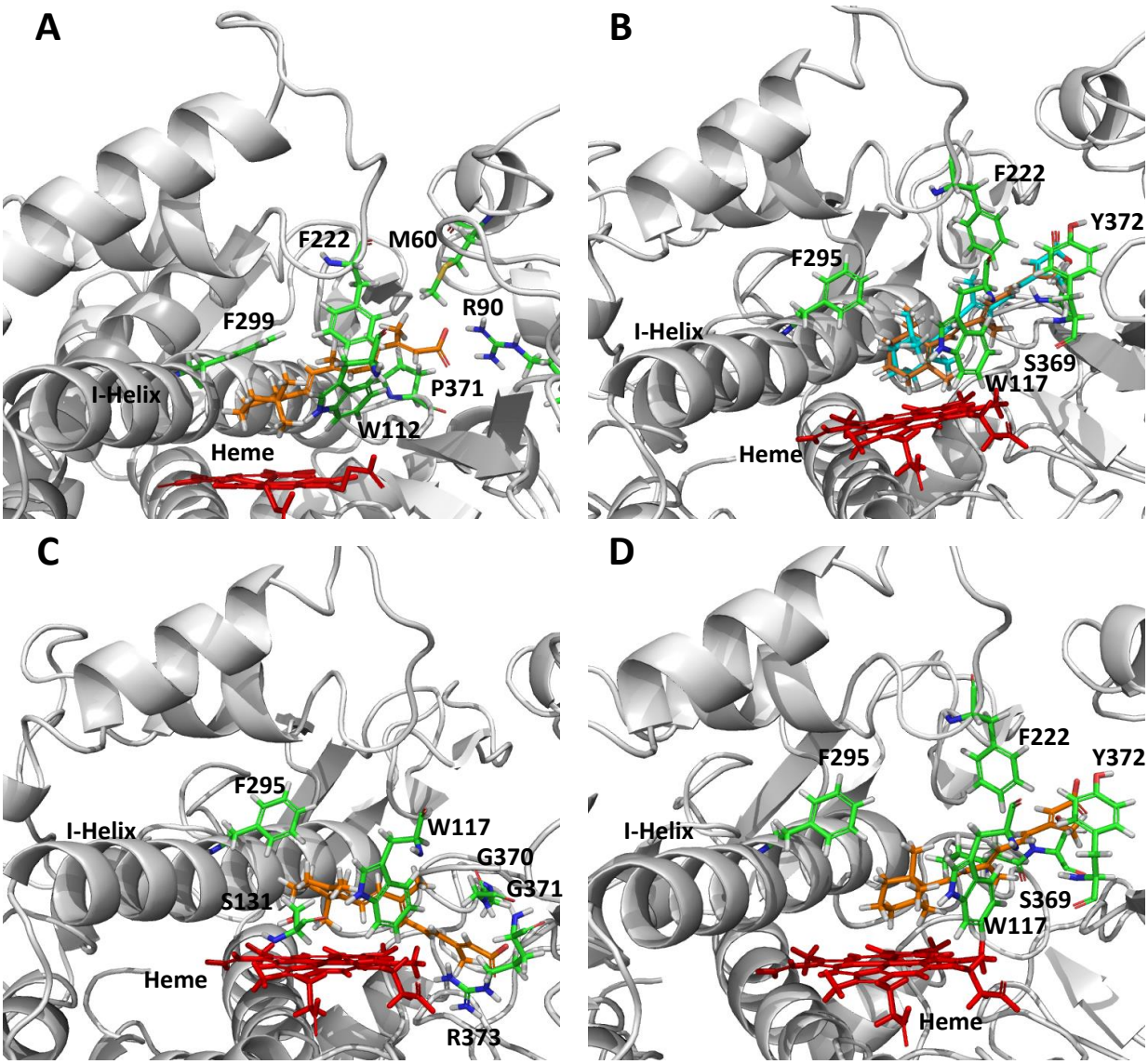

Figure 9-4. CYP26A1 (A) and CYP26B1 (B – D) homology models with *at*-RA docked in the active site.

A single docking orientation of *at*-RA in the CYP26A1 homology model accounted for 4-, 16- and 18-hydroxylation of *at*-RA and suggested that abstraction of the hydrogen atom leading to formation of 4-(*S*)-hydroxy-*at*-RA was the preferred binding orientation for CYP26A1, supporting the reported stereoselective metabolism of *at*-RA by CYP26A1 (A). Alternatively, docking of *at*-RA in the active site of CYP26B1 suggested that orientation of either hydrogen atom at the pro-chiral 4-position of the beta-ionone ring towards the heme iron was equally favorable, in agreement with the observed formation of both 4-(*R*)-hydroxy- (orange structure) and 4-(*S*)-hydroxy-*at*-RA (cyan structure) by CYP26B1 (B). The CYP26B1 model was also capable of docking *at*-RA such that the 16-hydroxy- or 18-hydroxyretinoic acid metabolites would be the predicted metabolite products (C and D).

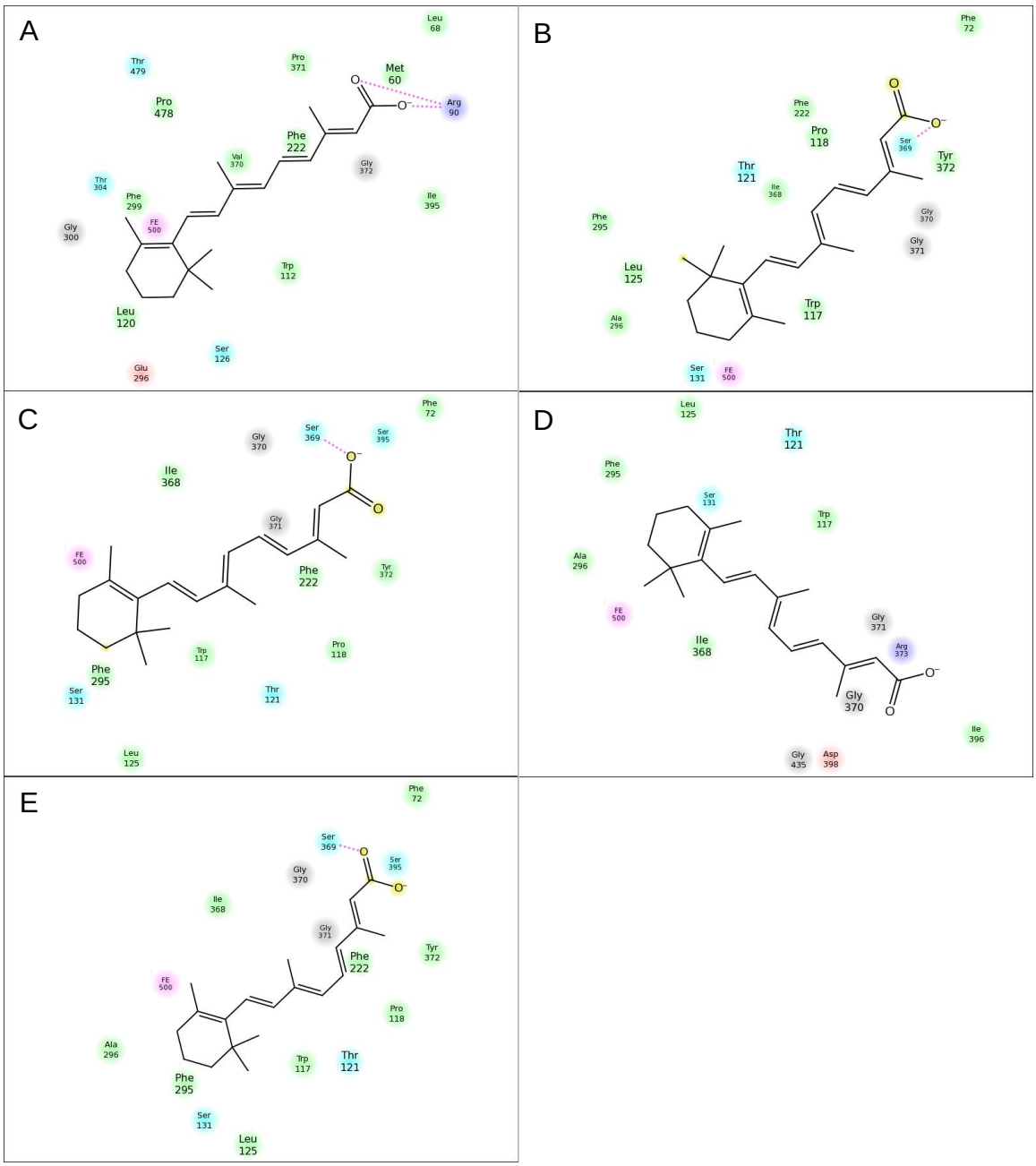

Figure 9-5. Ligand interaction diagram for *at*-RA docked in the active site of CYP26A1 and CYP26B1.

Analysis of the active site ligand interactions for *at*-RA docked in the active site of CYP26A1 (A) and CYP26B1 (4-(*R*)-OH, B; 4-(*S*)-OH, C; 16-OH, D; 18-OH, E) shows the hydrophobic (green), hydrophilic (blue), electrostatic (red/purple) and metal (pink) interactions located within 3.0 Å of *at*-RA. Hydrogen bonding interactions are depicted by dashed lines.

from the panel against CYP26A1, the most potent inhibitor against CYP26B1 and the only inhibitor to exhibit low to sub-micromolar inhibition potency in both assays. As such, it was selected for further evaluation in the CYP26A1 and CYP26B1 homology models.

Table 9-2. CYP26A1 and CYP26B1 IC_{50} values for retinoic acid receptor agonists and their derivatives (95% confidence interval is shown in parentheses).

RAR Agonist	CYP26A1 IC_{50} (μM)	CYP26B1 IC_{50} (μM)
AM80	12 (8.1 – 18)	6.6 (2.3 – 19)
AM580	5.6 (3.0 – 10)	2.2 (1.4 – 3.2)
BMS753	18 (4.4 – 76)	28 (21 – 37)
BMS961	14 (9.6 – 20)	31 (15 – 63)
Tazarotenic Acid	6.1 (3.2 – 12)	0.13 (0.09 – 0.19)
TTNPB	3.7 (1.4 – 9.8)	3.4 (2.2 – 5.2)

A single binding orientation was observed for tazarotenic acid in the CYP26A1 homology model with the heme iron located approximately 4.21 Å from the sulfur atom of the benzothiopyranyl ring and 5.15 Å from the adjacent aromatic hydrogen (Figure 9-6A). Key amino acids involved in ligand binding with CYP26A1 included Met60, Arg90, Trp112, Leu120, Phe222, Phe299, Thr304, Val370, Pro371, Gly372, Thr476, Pro478, and Thr479 (Figure 9-7). A hydrogen bonding interaction was predicted between the carboxylic acid moiety of tazarotenic

acid and Arg90. The observed docking pose would predict either sulfoxidation or hydroxylation to occur on the benzothiopyranyl ring of tazarotenic acid. Similar active site interactions were predicted when tazarotenic acid sulfoxide was docked in the active site of CYP26A1, with the sulfur atom and adjacent aromatic hydrogen atom 4.38 Å and 3.16 Å away from the heme iron, respectively (Figure 9-6B). Hydrogen bonding was predicted to occur between the carboxylate group of tazarotenic acid sulfoxide and Arg90 and between the pyridinyl nitrogen and Gly372 (Figure 9-7). Docking of tazarotenic acid in the active site of CYP26B1 resulted in a pose similar to that identified for 16-hydroxylation of *at*-RA, with hydrogen bonding interactions between the substrate and Arg373 and Ile396 stabilizing the carboxylic acid moiety of tazarotenic acid. In this orientation, the sulfur and adjacent aromatic hydrogen atom were located approximately 4.11 Å and 4.07 Å from the heme iron, respectively (Figures 9-6C and Figure 9-7). Tazarotenic acid sulfoxide bound in a similar manner in the active site of CYP6B1, with the sulfur and adjacent aromatic hydrogen atom located approximately 3.58 Å and 3.53 Å from the heme iron (Figure 9-6D). Hydrogen bonds were predicted between the carboxylate of tazarotenic acid sulfoxide and Arg373 and Ile396, as well as between the pyridinyl nitrogen of tazarotenic acid sulfoxide and Asp398 (Figure 9-7). Similar to the docking poses obtained with CYP26A1, results from the CYP26B1 homology model would predict metabolism to occur on the benzothiopyranyl moiety of tazarotenic acid or tazarotenic acid sulfoxide, with the sulfur atom generally in closest proximity to the heme iron.

9.3.2. Metabolic Profile.

The oxidative metabolites of tazarotenic acid whose formation are catalyzed by CYP26A1 and CYP26B1 were characterized using recombinant enzymes. Metabolism of tazarotenic acid by CYP26A1 and CYP26B1 resulted in the formation of tazarotenic acid sulfoxide, tazarotenic acid sulfone and a hydroxylated metabolite of tazarotenic acid (Figure 9-8). Comparison of the

electrospray ionization fragmentation patterns of the tazarotenic acid and tazarotenic acid sulfoxide synthetic standards with the hydroxylated metabolite of tazarotenic acid suggested that the location of the hydroxyl moiety was an aromatic hydroxylation on the benzothiopyranyl ring system (Figures 9-9 and 9-10). Formation of all tazarotenic acid metabolites was NADPH dependent. In order to assess the sequential metabolism of tazarotenic acid by CYP26A1 and CYP26B1, incubations were conducted using tazarotenic acid sulfoxide as the starting material. Both CYP26A1 and CYP26B1 catalyzed the metabolism of tazarotenic acid sulfoxide to tazarotenic acid sulfone (Figure 9-8). A proposed metabolic scheme is shown in Figure 9-11.

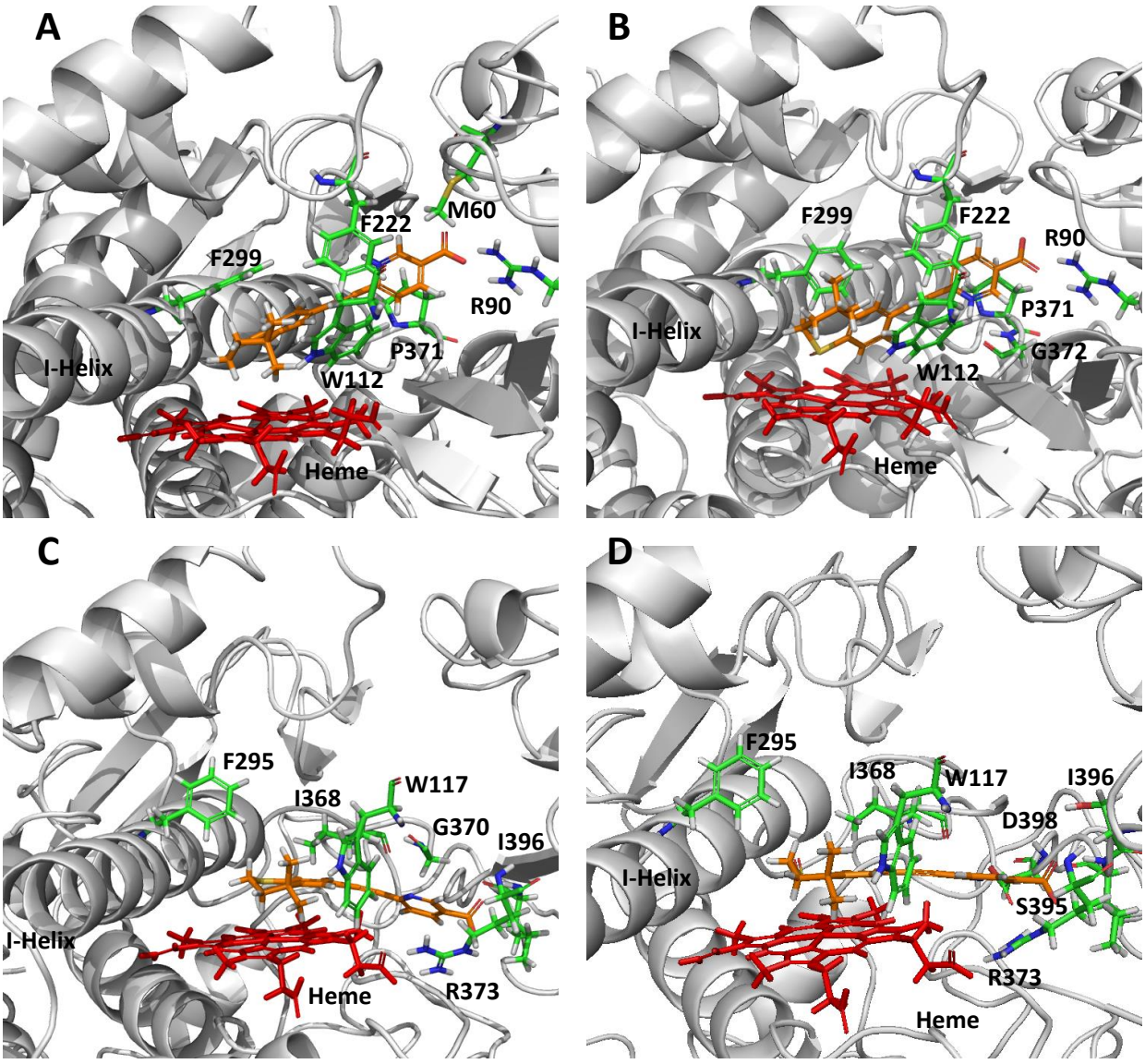

Figure 9-6. CYP26A1 and CYP26B1 homology models with tazarotenic acid docked in the active site.

Docking of tazarotenic acid in the active sites of CYP26A1 (A) and CYP26B1 (C) suggested metabolism at or near the sulfur atom of the benzothiopyranyl ring system was the preferred site of metabolism. Similar binding orientations were observed for tazarotenic acid sulfoxide in the active sites of CYP26A1 (B) or CYP26B1 (D).

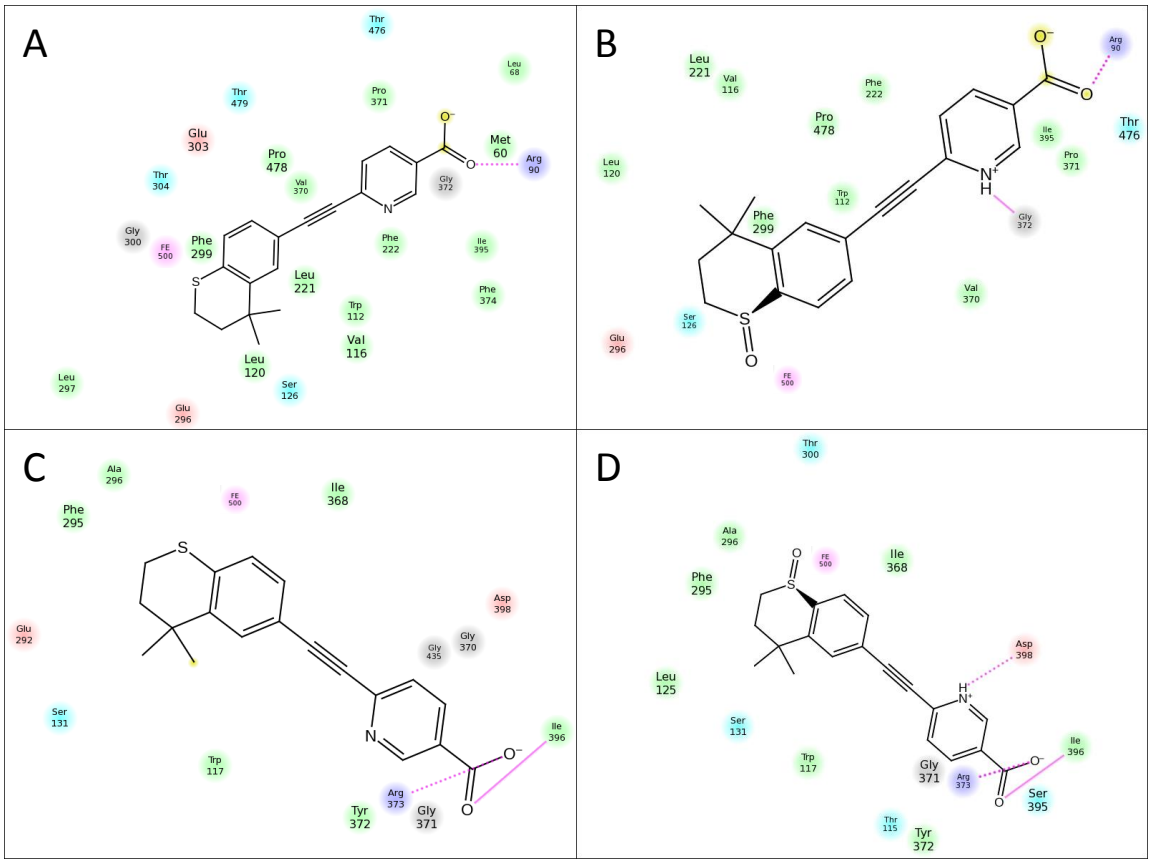

Figure 9-7. Ligand interaction diagram for tazarotenic acid or tazarotenic acid sulfoxide docked in the active site of CYP26A1 and CYP26B1.

Analysis of the active site ligand interactions for tazarotenic acid docked in the active site of CYP26A1 (A) and CYP26B1 (C) shows the hydrophobic (green), hydrophilic (blue), electrostatic (red/purple) and metal (pink) interactions located within 3.0 Å of tazarotenic acid. Ligand interactions for tazarotenic acid sulfoxide in the active site of CYP26A1 (B) and CYP26B1 (D) are also shown. Hydrogen bonding is depicted by dashed or solid lines.

9.3.3. In Vitro Enzyme Kinetics.

The enzyme kinetic parameters describing the formation of tazarotenic acid sulfoxide and hydroxytazarotenic acid were determined for CYP26A1 and CYP26B1. Enzyme kinetic parameters were determined using Michaelis-Menten kinetics and are reported in Table 9-3 and shown in Figure 9-12. In general, incubations with CYP26B1 resulted in slightly higher K_m and k_{cat} values as compared to incubations conducted with CYP26A1. Intrinsic clearance values (calculated as V_{max} / K_m) were slightly higher for CYP26A1 as compared to CYP26B1 owing

primarily to the difference in K_m values between the two enzymes. Both enzymes appeared to favor formation of the hydroxylated metabolite of tazarotenic acid. Formation of tazarotenic acid sulfone from tazarotenic acid sulfoxide was linear through a substrate concentration of 50 µM and as such no kinetic parameters were determined for this metabolic pathway.

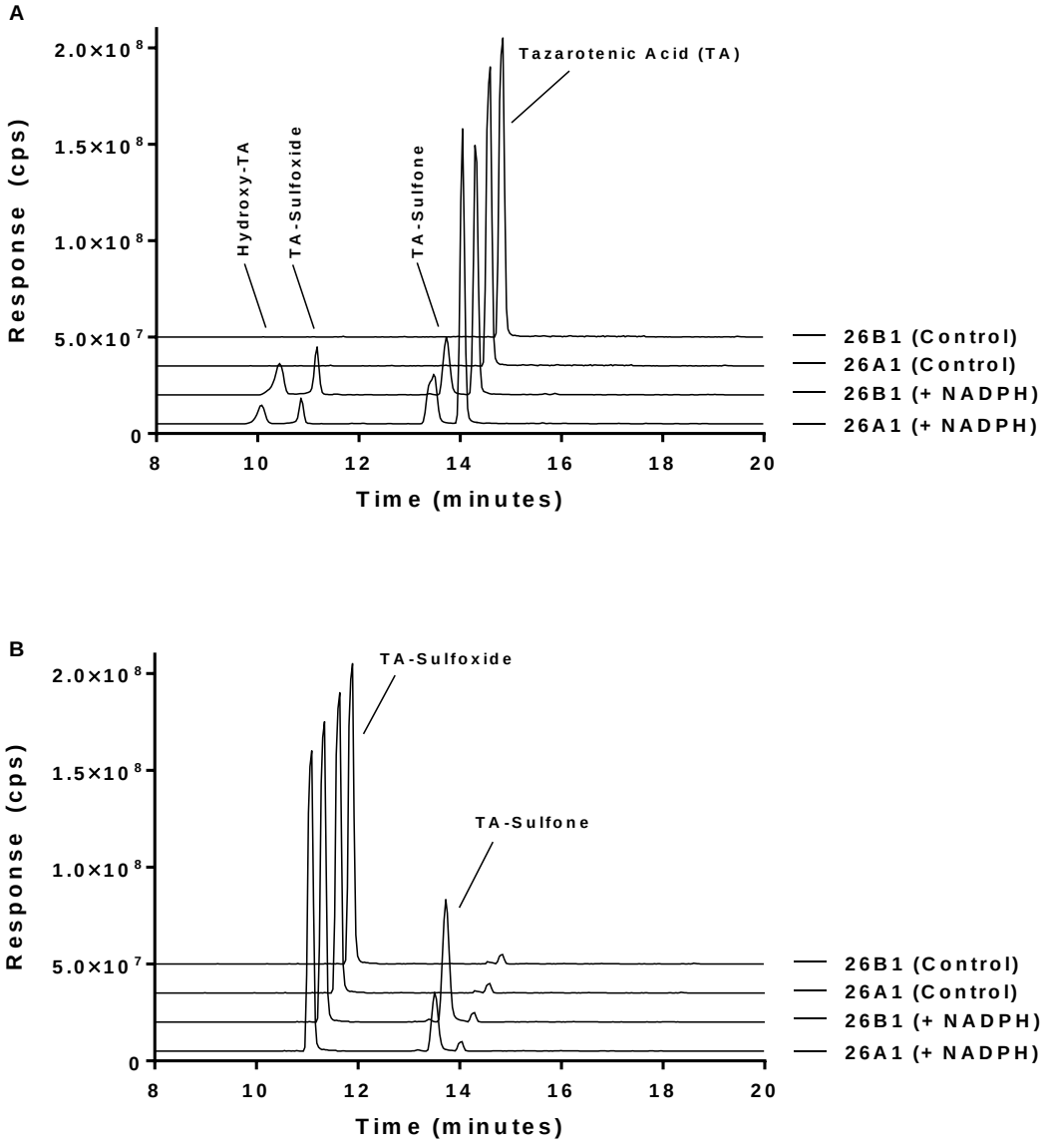

Figure 9-8. Extracted ion chromatograms for the metabolic profile of tazarotenic acid (A) and tazarotenic acid sulfoxide (B) by CYP26A1 and CYP26B1.

Data sets are offset for clarity and control traces represent incubations conducted in the absence of NADPH.

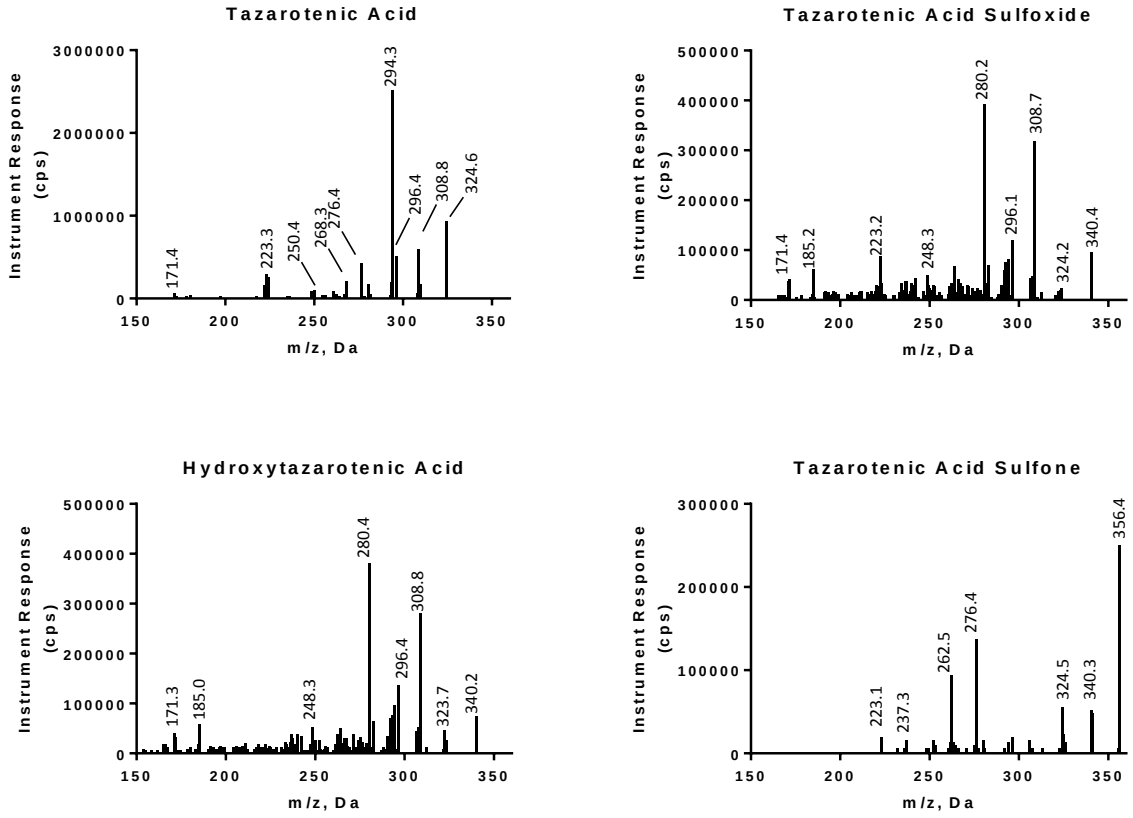

Figure 9-9. MRM spectra for tazarotenic acid and metabolites.

MS-MS Spectrum For Tazarotenic Acid (m/z 324.2), Tazarotenic Acid Sulfoxide (m/z 340.3), Hydroxy-Tazarotenic Acid (m/z 340.3) and Tazarotenic Acid Sulfone (m/z 356.3)

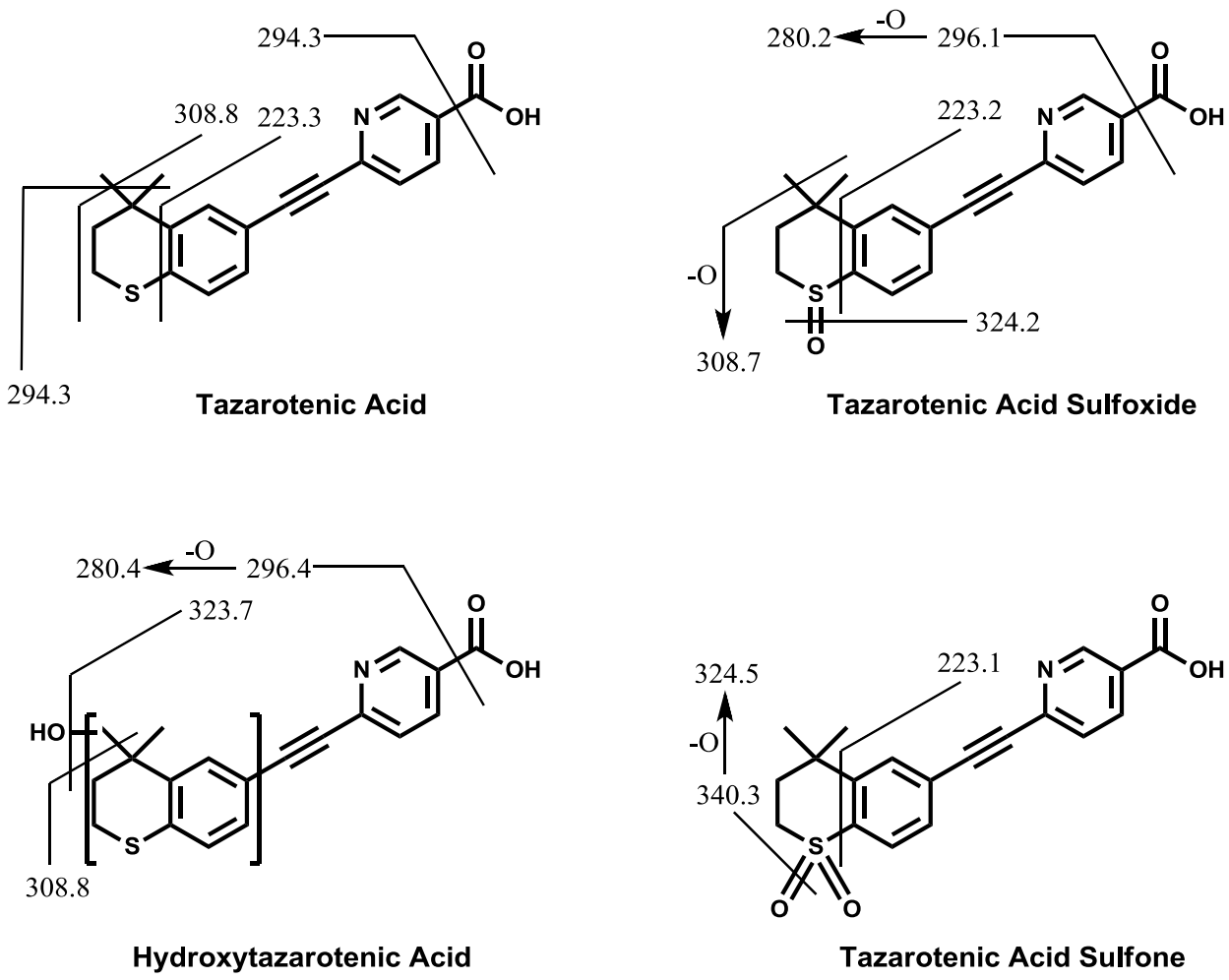

Figure 9-10. MS/MS fragmentation pattern for tazarotenic acid and metabolites.

Corresponding Fragmentation Pattern For Tazarotenic Acid (m/z 324.2), Tazarotenic Acid Sulfoxide (m/z 340.3), Hydroxytazarotenic Acid (m/z 340.3) and Tazarotenic Acid Sulfone (m/z 356.3)

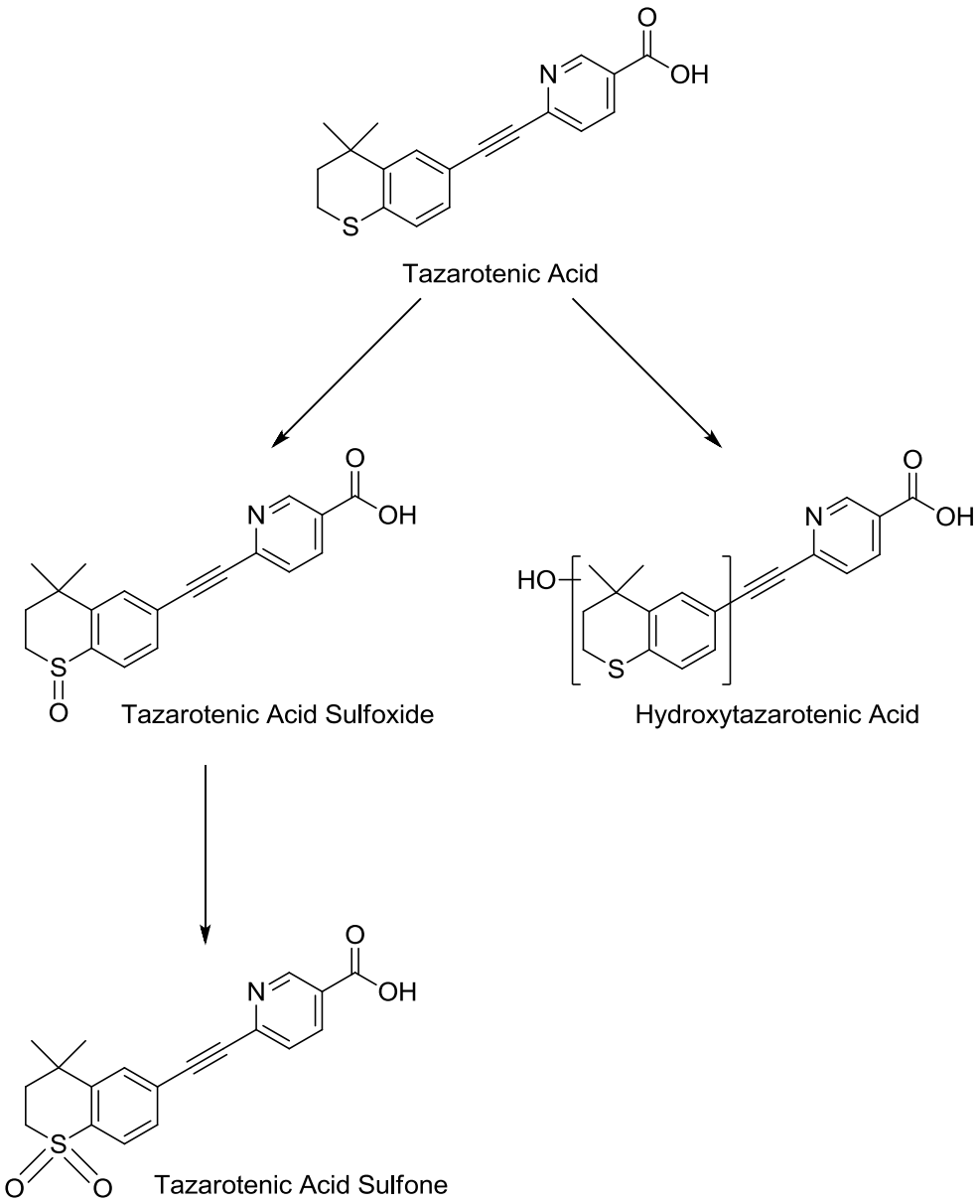

Figure 9-11. Proposed metabolic scheme of tazarotenic acid by CYP26A1 and CYP26B1.

CYP26A1 or CYP26B1 contributes to each of the metabolic steps identified in the metabolism of tazarotenic acid.

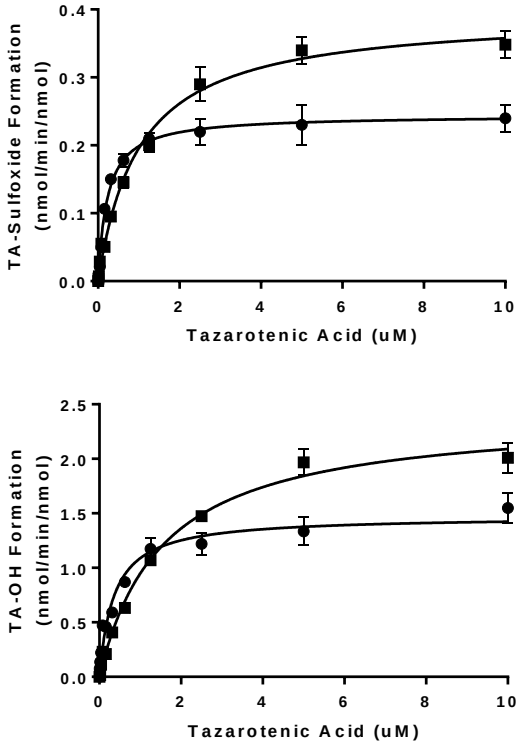

Figure 9-12. Enzyme kinetic plots for the formation of tazarotenic acid sulfoxide and hydroxytazarotenic acid by CYP26A1 (circles) and CYP26B1 (squares).

Formation was characterized by Michaelis-Menten kinetics with CYP26B1 having k_{cat} values that were approximately 1.3 – 1.6-fold higher than those observed for CYP26A1.

Table 9-3. Enzyme kinetic parameters for NADPH-dependent metabolism of tazarotenic acid to tazarotenic acid sulfoxide and hydroxytazarotenic acid (95% confidence interval is shown in parentheses).

	CYP26A1		CYP26B1		
Metabolite	K_m **(µM)**	Cl_{int} **(mL/min/nmol)**	K_m **(µM)**	Cl_{int} **(mL/min/nmol)**	$\frac{k_{cat,B1}}{k_{cat,A1}}$
TA-Sulfoxide	0.24 (0.18 – 0.27)	1.03 (0.87 – 1.18)	1.01 (0.85 – 1.18)	0.38 (0.34 – 0.44)	1.60 (1.52 – 1.68)
Hydroxy-TA*	0.39 (0.31 – 0.42)	4.01 (3.52 – 4.48)	0.56 (0.42 – 0.63)	3.67 (3.22 – 4.14)	1.32 (1.27 – 1.37)

* Metabolite Standard not available; Concentrations based on tazarotenic acid sulfoxide standard curve

9.3.4. Tazarotenic Acid Phenotyping.

Previous reports evaluating the enzymes responsible for tazarotenic acid metabolism in vitro have implicated CYP2C8, FMO1 and FMO3 in the formation of tazarotenic acid sulfoxide (Attar et al., 2003). Using an expanded drug metabolizing enzyme panel and clinically relevant concentrations of tazarotenic acid, additional enzymes were identified that may contribute to the metabolism of tazarotenic acid. The highest rates of tazarotenic acid sulfoxide formation were observed for CYP26A1 and CYP26B1, followed by CYP2C8 and CYP3A7 (Figure 9-13A). Formation of the sulfoxide metabolite was also observed in incubations with CYP2C9, CYP2J2, CYP3A4, CYP3A5 and aldehyde oxidase. Minor contributions were noted for CYP1A2 and CYP2B6. No metabolite formation was observed in incubations with FMO1, FMO3 or FMO5. The hydroxylated metabolite of tazarotenic acid was formed primarily by CYP26A1 and CYP26B1, with additional contributions from CYP2C8, CYP3A5 and CYP3A7 (Figure 9-13B). Similar to the formation of tazarotenic acid sulfoxide, trace amounts of the hydroxylated metabolite were also observed in incubations with the majority of the enzymes evaluated in the panel.

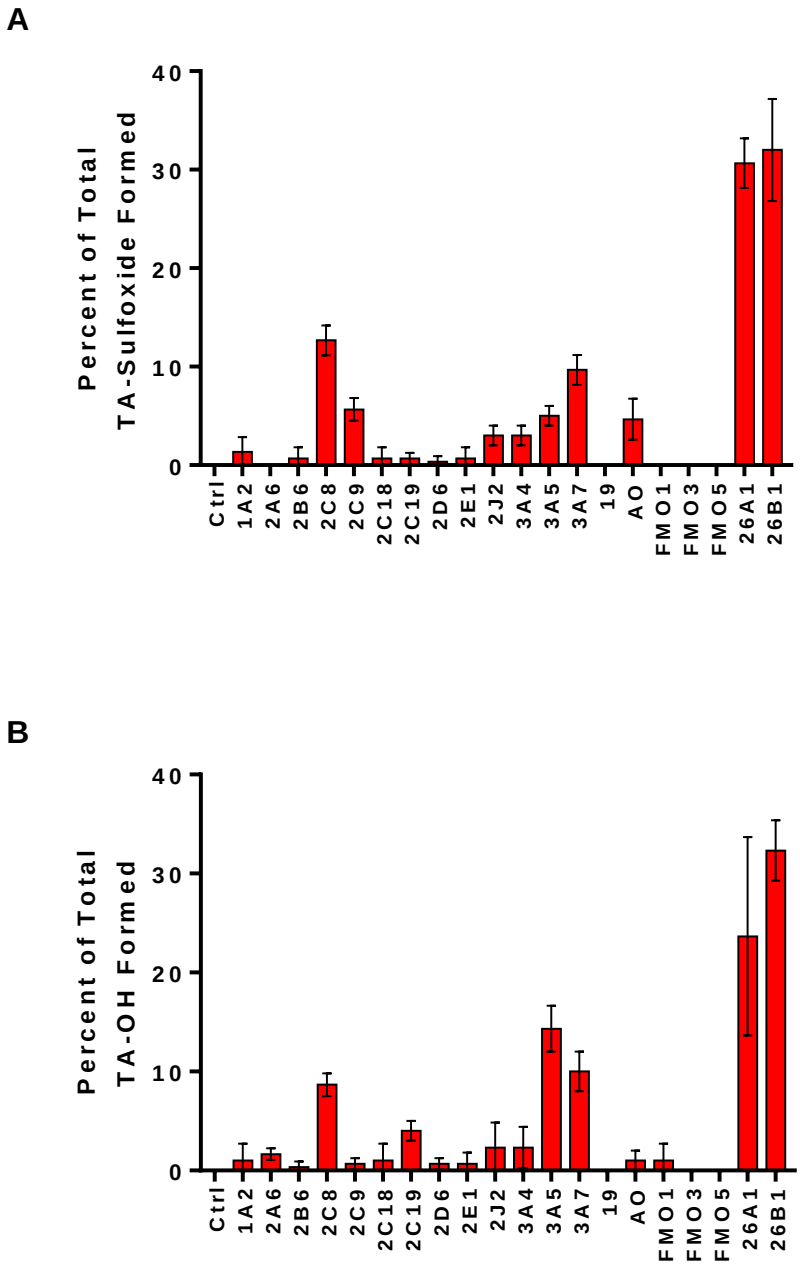

Figure 9-13. Formation of tazarotenic acid sulfoxide and hydroxytazarotenic acid in a panel of recombinant enzymes.

Formation of both enzymes was predominantly catalyzed by CYP26A1 and CYP26B1 with additional contributions from CYP3A and CYP2C isozymes.

9.4. Discussion

The CYP26 family of cytochrome P450s (CYP26A1, CYP26B1 and CYP26C1) has been identified as being responsible for the metabolism of *at*-RA and its metabolites (Ray et al., 1997; Taimi et al., 2004; Guengerich, 2006; Lee et al., 2007; Lutz et al., 2009; Thatcher and Isoherranen, 2009; Helvig et al., 2011; Ross and Zolfaghari, 2011; Nelson et al., 2013a). To date, however, no known xenobiotic compounds have been identified as substrates of CYP26A1 or CYP26B1, the two most characterized CYP26 isoforms. As both enzymes are expressed in human skin and many retinoid-based treatments are administered topically, the potential exists for these CYP26s to contribute to the metabolism and elimination of these compounds (Heise et al., 2006; Osanai and Lee, 2011; Topletz et al., 2012). Furthermore, a major focal point in the development of synthetic retinoids is to overcome the pharmacokinetic shortcomings of *at*-RA, such as the observed autoinduction of its clearance pathways. Tazarotene is an acetylenic retinoid which is readily converted via hydrolysis to tazarotenic acid upon topical administration (Duvic, 1997; Madhu et al., 1997; Tang-Liu et al., 1999; Menter, 2000; Yu et al., 2003; Attar et al., 2005; Talpur et al., 2009). It is prescribed for the treatment of abnormal keratinocyte proliferation, as is observed in patients with stable plaque psoriasis, mild to moderate acne and basal cell carcinoma (Tang-Liu et al., 1999; Talpur et al., 2009). The pharmacological mechanism of action described for tazarotene involves metabolism to tazarotenic acid which subsequently binds to retinoic acid receptors, primarily RAR-β and RAR-γ (Chandraratna, 1996). As an inhibitor of CYP26A1 and CYP26B1, tazarotenic acid may also serve to locally increase concentrations of retinoic acid in the skin, a mechanism that may hold potential in treating dermatological disorders. As such, a greater understanding of the structural characteristics of CYP26A1 and CYP26B1 which lend themselves to the catalytic and inhibitory properties of tazarotenic acid by these enzymes may have significant clinical relevance in terms of developing the next generation of topical pharmaceutics.

Homology models were designed in order to characterize the active site and substrate binding characteristics of CYP26A1 and CYP26B1. Prior to designing the homology models, the wild type gene sequence of CYP26B1 was verified from a panel of human livers as the initial clone differed in two amino acid residues from the currently available sequence of the enzyme (NCBI Reference Sequence: NP_063938.1; UniProtKB Q9NR63), which had been isolated from human retinal cDNA(White et al., 2000). Consistent with the commercially available clone, the amino acid sequence analysis showed that the amino acids residues at position 64 and 260 in the CYP26B1 sequence are an arginine and a serine residue, respectively, as opposed to the histidine and glycine originally reported from the retinal cDNA of a single human donor (Figure 9-1). However, as neither of these residues appears to be involved in substrate binding, it is unlikely that they influenced the results of previously published CYP26B1 homology models (Karlsson et al., 2008; Saenz-Mendez et al., 2012). Estimates of the active site volume for CYP26A1 (918 $Å^3$) and CYP26B1 (977 $Å^3$), suggest that each enzyme can bind ligands such as *at*-RA and tazarotenic acid with molecular volumes of approximately 300 $Å^3$ as well as much larger ligands, similar to the ligand binding profiles of other cytochrome P450 enzymes. Structural comparison of the two homology models suggests that selectivity between CYP26A1 and CYP26B1 may be dependent upon interactions with acidic binding residues as the active site amino acids involved in enzyme-ligand hydrophobic interactions appear to be fairly well conserved between the two enzymes (Figure 9-3).

The importance of being able to corroborate homology model data with supporting “site-of-metabolism” data cannot be understated. While successfully predicting the ability of an enzyme to bind an inhibitor suggests that the general active site characteristics of the homology model are representative of the actual enzyme, being able to predict the correct orientation of the ligand within the active site of the enzyme imparts an additional level of rigor to the homology model. As an initial attempt to validate the homology models, *at*-RA was docked into the active sites of CYP26A1 and CYP26B1. The mechanism for the formation of 4-

hydroxyretinoic acid by CYP26A1 and CYP26B1 involves hydrogen atom abstraction at a pro-chiral center, resulting in formation of either 4-(*S*)- or 4-(*R*)-*at*-RA. Previous in vitro data suggests that CYP26A1 preferentially catalyzes the stereoselective metabolism of *at*-RA to 4-(*S*)-hydroxy-*at*-RA while CYP26B1 catalyzes the formation of both 4-hydroxy-*at*-RA enantiomers, results which have also been rationalized through homology modeling of CYP26A1(Shimshoni et al., 2012; Topletz, 2013). In the case of the CYP26A1 homology model presented in this manuscript, all docking attempts resulted in the hydrogen atom leading to formation of 4-(*S*)-hydroxy-*at*-RA being oriented toward the heme, with the model unable to orient *at*-RA in the active site of CYP26A1 in a manner conducive with formation of 4-(*R*)-hydroxy-*at*-RA. Conversely, when *at*-RA was docked into the active site of CYP26B1 docking poses with either hydrogen atom at the 4-position toward the heme iron were observed. Taken together, this validation of the stereoselective metabolism of *at*-RA by the homology models suggests that the critical structural differences between the two enzymes which impart the stereoselective properties of *at*-RA metabolism by CYP26A1 and CYP26B1 are sufficiently captured by the models.

To apply the model to a xenobiotic ligand, the sites of metabolism of tazarotenic acid, an inhibitor of CYP26, were predicted. When tazarotenic acid was docked in the active sites of CYP26A1 or CYP26B1, a single orientation was observed with the benzothiopyranyl moiety directed toward the heme (Figure 9-6A and 9-6C). A number of the residues that appear to be important in orienting tazarotenic acid in the active sites of CYP26A1 and CYP26B1 have also been reported to be involved in the binding of *at*-RA in the active sites of these enzymes. For example, Trp112, Phe222, Phe299, Thr304, Pro369 and Val370 have been proposed to be involved in CYP26A1 binding of both *at*-RA as well as retinoic acid metabolism blocking agents (RAMBAs) that are able to inhibit the activity of CYP26A1 (Gomaa et al., 2008; Karlsson et al., 2008; Gomaa et al., 2011a; Gomaa et al., 2011b). Similarly, Trp65, Trp117, Thr121, Phe222, Phe295, Ser369, Val370 and Pro371 have been suggested to be key residues in binding *at*-RA

and other ligands of CYP26B1 (Karlsson et al., 2008; Saenz-Mendez et al., 2012). Results from metabolite identification studies confirmed the ability of CYP26A1 and CYP26B1 to contribute to the metabolism of tazarotenic acid and tazarotenic acid sulfoxide only at the benzothiopyranyl end of the molecule, and a proposed metabolic scheme is shown in Figure 9-11. Enzyme kinetic experiments suggest that the metabolism of tazarotenic acid by CYP26A1 and CYP26B1 represents a rare example of a substrate having higher k_{cat} values for CYP26B1 as compared to CYP26A1.

Finally, previously reported efforts to identify the enzymes responsible for the metabolism of tazarotenic acid have implicated CYP2C8, FMO1 and FMO3 in the metabolism of tazarotenic acid to a sulfoxide metabolite (Attar et al., 2003). As recent literature reports have highlighted the importance of conducting reaction phenotyping experiments at clinically relevant concentrations (Filppula et al., 2011; VandenBrink et al., 2011; Karonen et al., 2012), we have re-evaluated the enzymatic pathways responsible for the metabolism of tazarotenic acid. When reaction phenotyping experiments were conducted at the clinically relevant concentration of 100 nM, CYP26A1 and CYP26B1 were identified as the major cytochrome P450 isoforms involved in the formation of tazarotenic acid sulfoxide and hydroxytazarotenic acid in vitro (Figure 9-13). Other enzymes that contributed to the formation of the sulfoxide metabolite included CYP2C8, CYP2C9, CYP2J2, CYP3A4, CYP3A5 and CYP3A7 and aldehyde oxidase, though metabolite formation rates by the CYP26 isoforms were at least 2.5-fold higher than those observed for any other cytochrome P450 enzymes. No formation of the sulfoxide by FMO1, FMO3 or FMO5 was observed, suggesting that these enzymes do not play a role in the formation of the metabolite at sub-micromolar concentrations of tazarotenic acid.

To our knowledge, this manuscript describes the first known homology models of CYP26A1 and CYP26B1 that incorporate metabolic data from both endogenous and xenobiotic substrates. It also details the first known contributions of the CYP26 family of cytochrome P450 enzymes to the metabolism of a xenobiotic compound and provides additional computational

analyses of the active sites characteristics of each enzyme. Analysis of the active site features of the CYP26A1 and CYP26B1 homology models suggests that the greatest site of structural divergence is in the carboxylate-binding region of the active site and that the enzymes may be capable of binding much larger ligands as well, similar to other drug metabolizing cytochrome P450 enzymes. Further understanding of the active site characteristics of CYP26A1 and CYP26B1 which play a role in their substrate binding properties should serve to increase the likelihood of identifying CYP26-selective inhibitors that may ultimately prove useful in the treatment of various disease states.

10. Chapter III: Comparison of the Ligand Binding Site of CYP2C8 with CYP26A1 and CYP26B1: A Structural Basis for the Identification of New Inhibitors of the Retinoic Acid Hydroxylases

Accepted for Publication: Journal of Enzyme Inhibition and Medicinal Chemistry, 2016.

10.1. Introduction

Endogenous retinoic acid concentrations are highly regulated owing to their importance in cellular development with altered concentrations of retinoic acid known to have pharmacological and toxicological implications (Lotan, 1980; Sporn and Roberts, 1984; McCaffery and Drager, 2000; Ross et al., 2000; Clagett-Dame and DeLuca, 2002; Maden, 2002). In humans, retinoic acid binds to the retinoic acid and retinoid X receptors and plays a key role in the regulation of genes that affect the extent of cellular proliferation and differentiation as well as apoptosis (Levin et al., 1992; Mangelsdorf et al., 1992; Mark et al., 2006; Altucci et al., 2007; di Masi et al., 2015). The regulation of circulating retinoic acid concentrations can occur through modulation of its synthesis, which involves multiple enzymatic steps in the conversion of retinol to all-trans-retinoic acid (*at*-RA) or through its clearance, which is primarily mediated by cytochrome P450-catalyzed oxidation to 4-hydroxy-*at*-retinoic acid (Duester, 2008; Niederreither and Dolle, 2008). Within the cytochrome P450 superfamily of xenobiotic metabolizing enzymes, the CYP26 subfamily (CYP26A1, CYP26B1 and CYP26C1) are the primary enzymes involved in retinoic acid metabolism (Ray et al., 1997; Lutz et al., 2009; Thatcher and Isoherranen, 2009; Thatcher et al., 2010; Ross and Zolfaghari, 2011). While hepatic CYP26 content is primarily a function of CYP26A1 expression, CYP26A1 and CYP26B1 mRNA are ubiquitously expressed, with sites of expression including the skin, lungs, testes and brain (Ray et al., 1997; White et al., 2000; Wang et al., 2002; Xi and Yang, 2008; Tay et al., 2010; Thatcher et al., 2010; Topletz et al., 2012; Nelson et al., 2013a). Less information is available about the expression patterns and functional relevance of CYP26C1.

A significant amount of catalytic overlap is observed for CYP26A1 and CYP26B1 in regard to their metabolism of *at*-RA, though the sequence homology between the two isozymes is only 42% (Taimi et al., 2004; Topletz et al., 2012; Nelson et al., 2013a). Perhaps owing to their homeostatic role in the regulation of retinoic acid concentrations and the subsequent pharmacological or toxicological outcomes, the pursuit of selective chemical inhibitors of

CYP26A1 or CYP26B1 has received interest in both the inflammation and oncology therapeutic areas (Miller, 1998; Kuenzli and Saurat, 2001; Njar, 2002; Ahmad and Mukhtar, 2004; Njar et al., 2006; Verfaille et al., 2008). Many of the compounds designed to inhibit CYP26 activity, also known as retinoic acid metabolism blocking agents (RAMBAs), share a similar pharmacophore, with an extended hydrophobic region that bridges a hydrophobic or aromatic ring system on one end of the molecule to a hydrogen bond accepting group on the opposite end (Purushottamachar et al., 2012; Sun et al., 2015). In many cases, the aromatic group described above is an azole-containing ring system, designed to coordinate to the porphyrin iron of CYP26A1 or CYP26B1 and thus inhibit the enzyme (Njar, 2002; Njar et al., 2006; Gomaa et al., 2008; Gomaa et al., 2011a; Thatcher et al., 2011; Nelson et al., 2013a). Liarazole currently represents the most studied example of a RAMBA in clinical use (De Coster et al., 1992; Njar et al., 2006).

Approximately 5% to 8% of xenobiotic metabolism has been attributed to CYP2C8, with highly characterized substrates including amodiaquine, repaglinide, rosiglitazone, cerivastatin, paclitaxel and montelukast (Totah and Rettie, 2005; Lai et al., 2009; VandenBrink et al., 2011; Karonen et al., 2012). CYP2C8 has also been shown to metabolize *at*-RA, 9-cis-retinoic acid and 13-cis-retinoic acid (Nadin and Murray, 1999; McSorley and Daly, 2000; Marill et al., 2002; Marill et al., 2003; Rowbotham et al., 2010). Potent in vitro inhibitors of CYP2C8-catalyzed metabolism include montelukast (both substrate and inhibitor), candesartan cilexetil, zafirlukast, clotrimazole and fluconazole (Walsky et al., 2005; Nath et al., 2010; VandenBrink et al., 2011). Clinically relevant drug interactions attributed to CYP2C8 inhibition have been noted for rosiglitazone, repaglinide and cerivastatin when co-administered with the CYP2C8 inhibitor gemfibrozil (Backman et al., 2002; Niemi et al., 2003; Tornio et al., 2008; Honkalammi et al., 2011). The active site properties of CYP2C8 which contribute to its substrate and inhibitor profiles are fairly well understood, with the crystal structure of CYP2C8 having been solved with various ligands bound in the active site, including 9-cis-retinoic acid (Schoch et al., 2004). The

active site volume of CYP2C8 is relatively large (1438 $Å^3$) and it has been described as having a bifurcated Y-shaped geometry (Schoch et al., 2004; Schoch et al., 2008). Similar to the ligand profile of CYP26s, early pharmacophore models of CYP2C8 ligands suggested the need for a hydrophobic or aromatic group proximal to the site of oxidation, an extended hydrophobic chain distal to the site of oxidation and multiple hydrogen binding sites, properties which are often displayed by various retinoid or retinoid-like compounds (Kerdpin et al., 2004; Melet et al., 2004; Schoch et al., 2008; Lai et al., 2009).

Owing to the similar pharmacophore features described for CYP2C8 and CYP26 and as CYP2C8 has also been shown to catalyze the formation of 4-hydroxyretinoic acid from *at*-RA, the potential exists for the inhibitor binding profile of CYP26A1 and CYP26B1 to overlap with that of CYP2C8. As such, the primary aim of this work was to evaluate the potential for known inhibitors of CYP2C8 to inhibit CYP26A1 or CYP26B1 activity. In vitro inhibition assays were used to determine IC_{50} values for a set of known CYP2C8 inhibitors against CYP26A1 and CYP26B1. In the process, the use of tazarotenic acid, which has recently been shown to be metabolized by CYP26A1 and CYP26B1, as a probe substrate for CYP26 inhibition assays was evaluated. The mechanism of active site binding and inhibition of CYP26A1 and CYP26B1 was then characterized for compounds with azole moieties as well as those hypothesized to not inhibit the enzymes through type II binding interactions. Finally, in vitro inhibition parameters were compared to reported skin or plasma concentrations following clinically relevant doses of CYP2C8 inhibitors in an attempt to estimate the magnitude of the potential clinical interaction of known CYP2C8 inhibitors on CYP26 activity in vivo.

10.2. Materials and Methods.

10.2.1. Materials.

CYP26A1 and CYP26B1 were generous gifts from Dr. Nina Isoherranen (University of Washington). Recombinant CYP2C8 Supersomes® and purified human cytochrome P450 reductase were obtained from Corning Life Sciences (Tewksbury, MA). Tazarotenic acid, MM11253, liarazole, EC23, AM80 and candesartan were purchased from Tocris Chemicals (Bristol, United Kingdom). Montelukast, pioglitazone, rosiglitazone and zafirlukast were from Cayman Chemical (Ann Arbor, MI). Talarazole was purchased from MedChem Express (Monmouth Junction, NJ). Rapid equilibrium dialysis (RED) device kits were obtained from ThermoFisher Scientific (Waltham, MA). All other chemicals were from Sigma-Aldrich (St. Louis, MO) and were of the highest grade available.

10.2.2. Homology Modeling and Computational Docking Simulations.

CYP26A1 and CYP26B1 homology models based on the crystal structure of CYP120 (pdb 2VE3) were designed using Prime modeling software (Schrodinger LLC, New York) as previously described (Foti et al., 2016). The crystal structure of CYP2C8 was obtained from the RCSB Protein Data Bank (pdb 1PQ2). The CYP26A1 or CYP26B1 homology models were superimposed on the CYP2C8 crystal structure using the Super script within Pymol (Schrodinger LLC, New York; http://www.pymolwiki.org/index.php/Super). Structural similarity was determined by calculating the root mean square deviation (RMSD) between the protein structures. Amino acid residues 494 – 512 from the CYP26B1 homology model were not included in the RMSD calculation. Computational docking of clotrimazole (CYP26A1 and CYP26B1), zafirlukast (CYP26A1) or candesartan cilexetil (CYP26B1) was accomplished using an induced fit docking algorithm which incorporated decreased van der Waals radii, spatial repositioning of non-rigid protein side chains and additional energy minimization functions post-ligand docking (Sherman et al., 2006a; Sherman et al., 2006b). Compounds for docking

simulations were chosen based on inhibition potency as well as their potential (or lack thereof) for type II azole-heme interactions. Docking parameters required the center of mass of the inhibitors to be positioned within a 1728 $Å^3$ grid which was designed to be approximately 3 Å above the protoporphyrin ring system using Glide (Schrodinger LLC, New York). The OPLS_2005 force field constraints used by LigPrep (Schrodinger LLC, New York) were used to prepare the energy minimized structures of clotrimazole (hypothesized to bind through type II ligand interactions) and candesartan cilexetil and zafirlukast (two compounds not hypothesized to interaction through type II binding) prior to docking. Binding orientations obtained from the computational docking experiments were evaluated and scored using GlideScore and eModel, which incorporates aspects of the GlideScore, ligand score and grid score into the final assessment of the plausibility of the docking results.

10.2.3. In Vitro Inhibition Assays.

CYP2C8 in vitro IC_{50} values were obtained from previously reported literature sources and are noted in Table 10-1 (Walsky et al., 2005; Nath et al., 2010; VandenBrink et al., 2011). An initial single point inhibition screen (n = 3) was then used to estimate the inhibition potency of the set of known CYP2C8 inhibitors against CYP26A1 or CYP26B1. Talarazole and AM80 were included in the screening set as positive controls for CYP26 inhibition. In vitro screening conditions consisted of 10 µM inhibitor, 5 nM CYP26A1 or CYP26B1, 25 nM purified human cytochrome P450 reductase, and 200 nM tazarotenic acid, a compound which has recently been shown to be a substrate of CYP26 (Foti et al., 2016). The final volume of the incubation was 50 µL. Screening incubations were performed in triplicate and were pre-warmed at 37ºC for 3 minutes prior to addition of 1 mM NADPH (final concentration). Incubations were terminated after 10 minutes with three volumes (v/v) of 100 nM tolbutamide in acetonitrile and centrifuged for 20 minutes at 1240 x g. A portion of the resulting supernatant was transferred for liquid chromatography-tandem mass spectrometry (LC-MS/MS) analysis.

Table 10-1. Previously published CYP2C8 IC_{50} values ± standard error. All IC_{50} values were determined using recombinant CYP2C8 enzymes except where noted. (N.R. = Not Reported).

Inhibitor	CYP2C8 IC_{50} (μM)	Probe Substrate	Reference
Benzbromarone	0.38 (N.R.)	Montelukast (HLM)	VandenBrink et al., 2011
Candesartan	36.2 ± 1.7	Amodiaquine	Walsky et al., 2005
Candesartan Cilexetil	0.496 ± 0.190	Amodiaquine	Walsky et al., 2005
Clotrimazole	0.725 ± 0.116	Amodiaquine	Walsky et al., 2005
17α-Ethynylestradiol	6.54 ± 1.22	Amodiaquine	Walsky et al., 2005
Fluconazole	48.9 (N.R.)	Amodiaquine	Nath et al., 2010
Itraconazole	2.16 ± 0.41	Paclitaxel	Unpublished Data
Mometasone	0.813 ± 0.112	Amodiaquine	Walsky et al., 2005
Montelukast	0.00922 ± 0.00088	Amodiaquine	Walsky et al., 2005
Pioglitazone	11.7 ± 4.0	Amodiaquine	Walsky et al., 2005
Quercetin	3.94 ± 0.64	Amodiaquine	Walsky et al., 2005
Raloxifene	2.15 ± 0.90	Amodiaquine	Walsky et al., 2005
Repaglinide	11.1 (N.R.)	Montelukast (HLM)	VandenBrink et al., 2011
Ritonavir	3.03 ± 1.14	Amodiaquine	Walsky et al., 2005
Rosiglitazone	10.8 ± 3.1	Amodiaquine	Walsky et al., 2005
Tamoxifen	3.34 ± 1.55	Amodiaquine	Walsky et al., 2005
Zafirlukast	0.644 ± 0.273	Amodiaquine	Walsky et al., 2005

IC_{50} values were then determined for compounds exhibiting greater than 50% inhibition in the screening assay for at least one of the CYP26 isoforms. Incubations conditions (n = 3) were similar to those used in the screening assay except for the inhibition concentrations, which ranged from 0 – 100 μM. CYP26A1 and CYP26B1 IC_{50} values were estimated using a three parameter inhibition model as shown in Equation 1, where $Activity_{max}$ represents the observed probe substrate activity with no inhibitor, $Activity_{min}$ is the probe substrate activity at the maximum inhibitor concentration and [*I*] is the concentration of inhibitor in the incubation. IC_{50}

incubations were performed in triplicate. The organic content of each incubation was kept to less than 1% of the total volume and product formation under the conditions described above had previously been determined to be linear with respect to incubation time and protein content.

Equation 1 $$\%\ Remaining\ Activity = Activity_{min} + \frac{Activity_{max} - Activity_{min}}{1+10^{(log[I] - logIC50)}}$$

10.2.4. Spectral Binding Determination.

Spectral binding characterizations (n = 3) were carried out to determine the binding orientation of the most potent azole-containing compound (clotrimazole) for CYP26A1 and CYP26B1, as well as zafirlukast (CYP26A1) and candesartan cilexetil (CYP26B1). The binding of clotrimazole to CYP2C8 was also explored. Ligand concentrations ranged from 0 – 20 µM. A protein concentration of 500 nM was used in spectral binding assays. Following each addition of ligand, cuvettes (1 cm path length) were inverted multiple times and allowed to settle for 1 minute prior to measuring the difference spectra from 350 – 550 nm using a Cary 4000 UV-Vis spectrophotometer (Agilent Technologies, Santa Clara, CA). Spectral binding constants (K_s) were estimated using nonlinear regression of the absorbance difference (ΔAbs) for each enzyme (CYP26A1, $\lambda_{430nm} - \lambda_{413nm}$; CYP26B1, $\lambda_{430nm} - \lambda_{400nm}$; CYP2C8, $\lambda_{430nm} - \lambda_{390nm}$) as shown in Equation 2.

Equation 2 $$\Delta Abs = \frac{[S] * \Delta Abs_{max}}{[S] + K_s}$$

10.2.5. Assessment of In Vitro Free Fraction.

In order to determine the unbound fraction of clotrimazole in the IC_{50} and spectral binding assays, equilibrium dialysis was conducted under relevant conditions. Experiments were performed in triplicate using the Rapid Equilibrium Dialysis Device (Thermo Fisher Scientific, Waltham, MA) which was prepared according to the manufacturer's recommendations. In brief, 1 µM of clotrimazole was added to 5 nM or 500 nM CYP26A1 or CYP26B1 in potassium phosphate buffer (100 µL, pH 7.4) and was dialyzed for 12 hours at 37 ºC against 300 µL of control potassium phosphate buffer. The plate was agitated using an orbital shaker set to 200 rpm. Upon completion of the incubation period, a 50 µL aliquot was removed from each side of the equilibrium dialysis membrane and added to 50 µL of control enzyme or buffer to normalize for potential matrix effects. Protein precipitation was achieved by adding three volumes of 100 nM tolbutamide in ice cold acetonitrile and centrifuging the samples for 20 minutes at 1240 x g. A portion of the resulting supernatant was transferred for liquid chromatography-tandem mass spectrometry (LC-MS/MS) analysis. The unbound fraction was determined as shown in Equation 3.

Equation 3 $$f_u = \frac{Concentration\ in\ Buffer\ Chamber}{Concentration\ in\ Sample\ Chamber}$$

10.2.6. In Vitro Stability of Candesartan Cilexetil.

Candesartan is the pharmacologically active form of the prodrug candesartan celexetil, which is hydrolyzed by intestinal esterases following oral administration (Gleiter and Morike, 2002). In order to determine whether the observed inhibition potency of candesartan cilexetil was due to the prodrug or to the hydrolysis product, the in vitro stability of candesartan cilexetil was determined using CYP26A1, CYP26B1 and CYP2C8. Briefly, 1 µM candesartan cilexetil was added to incubations containing 5 nM CYP26A1, CYP26B1 or CYP2C8 and 25 nM purified

human cytochrome P450 reductase in 100 mM potassium phosphate buffer (pH 7.4; n = 3). Incubations were performed at 37 ºC and initiated through addition of 1 mM NADPH (final concentration) in order to mirror the conditions of the IC_{50} assay. Aliquots were removed at 0, 1, 5 and 10 minutes and immediately placed into ice cold acetonitrile containing 100 nM tolbutamide as an internal standard. Samples were vortex-mixed and centrifuged for 20 minutes at 1240 x g. A portion of the supernatant was transferred for LC-MS/MS analysis of candesartan cilexetil degradation and candesartan formation in the incubations.

10.2.7. Calculation of Cmax,u / IC_{50}.

Previously reported C_{max} and unbound fraction values in plasma were obtained for 17 known inhibitors of CYP2C8 (benzbromarone, candesartan, candesartan cilexetil, clotrimazole, 17α-ethynylestradiol, fluconazole, itraconazole, mometasone furoate, montelukast, pioglitazone, quercetin, raloxifene, repaglinide, ritonavir, rosiglitazone, tamoxifen and zafirlukast) at clinically relevant doses (http://www.drugbank.ca/; Walter-Sack et al., 1988; Saperstein et al., 1989; Boulton et al., 1998; Daley-Yates et al., 2004; Goodman and Gilman, 2006; Moon et al., 2008; Uchida et al., 2010; Karonen et al., 2011; Deshpande, 2013). As no reported plasma concentrations of clotrimazole after oral administration were available, skin concentrations following a topical administration were used. The ratio of the unbound C_{max} values to the in vitro IC_{50} values was calculated using Equation 4.

Equation 4 $$\frac{C_{max,unbound}}{IC_{50}} = \frac{C_{max} * f_{u,plasma}}{IC_{50}}$$

10.2.8. Liquid Chromatography – Mass Spectrometry Analysis.

Tazarotenic acid sulfoxide, clotrimazole, candesartan and candesartan cilexetil was monitored using LC-MS/MS. The mass spectrometer incorporated electrospray ionization coupled to an Applied Biosystems 4000 QTrap (Applied Biosystems, Foster City, CA). Samples were injected (10 µL) using a LEAP CTC HTS PAL autosampler (CTC Analytics, Carrboro, NC) and introduced to the mass spectrometer using two LC-20AD binary pumps with an in-line DGU-20A5 solvent degasser (Shimadzu, Columbia, MD). A rapid gradient using 0.1% formic acid (v/v) in water (A) and 0.1% formic acid in methanol:acetonitrile (1:1; B) with a Synergi 2.5 µm Hydro RP 100 Å (50 x 2.0 mm) column (Phenomenex, Torrance, CA) was utilized. Gradient conditions were as follows: 2.0% B (0 – 0.2 minutes), 2.0% B – 95% B (from 0.2 – 1.0 minutes), 95% B (from 1.0 – 1.5 minutes) and re-equilibration at 2.0% B for 0.3 minutes. Tazarotenic acid sulfoxide (positive ion, 340.3 / 280.3) clotrimazole (positive ion, 345.4 / 277.0), candesartan (positive ion, 441.0 / 263.1), candesartan cilexetil (positive ion, 611.1 / 567.2) and the internal standard tolbutamide (positive ion, 271.2 / 91.1; negative ion, 268.9 / 169.7) were detected under MRM (multiple reaction monitoring) conditions. Additional parameters that were used in the tazarotenic acid analytical method included the source temperature (500 °C), curtain gas (12 arbitrary units), ion spray voltage (5000 V), CAD gas (medium), and ion source gas 1 and gas 2 (30 arbitrary units, each).

10.3. Results

10.3.1. Evaluation of tazarotenic acid sulfoxide formation as a probe substrate of CYP26.

Tazarotenic acid (Figure 10-1) has recently been identified as a xenobiotic substrate of CYP26A1 and CYP26B1 (Foti et al., 2016). Prior to utilizing the tazarotenic acid assay to screen new compounds for inhibition of CYP26A1 and CYP26B1, IC_{50} values were generated for a test set of known CYP26 inhibitors using tazarotenic acid as the probe substrate and compared to previously published results obtained when 9-cis-retinoic acid was the probe substrate (Table 10-2). Inhibitor potency rankings were generally the same and a statistically significant correlation was observed between the IC_{50} values obtained using the two assays. Correlation coefficients (r^2) for the IC_{50} values obtained using tazarotenic acid assay and the 9-cis-retinoic acid assay were 0.78 and 0.62 for CYP26A1 and CYP26B1, respectively, suggesting that formation of tazarotenic acid sulfoxide is an appropriate probe reaction for determining inhibition of CYP26 activity (Figure 10-2).

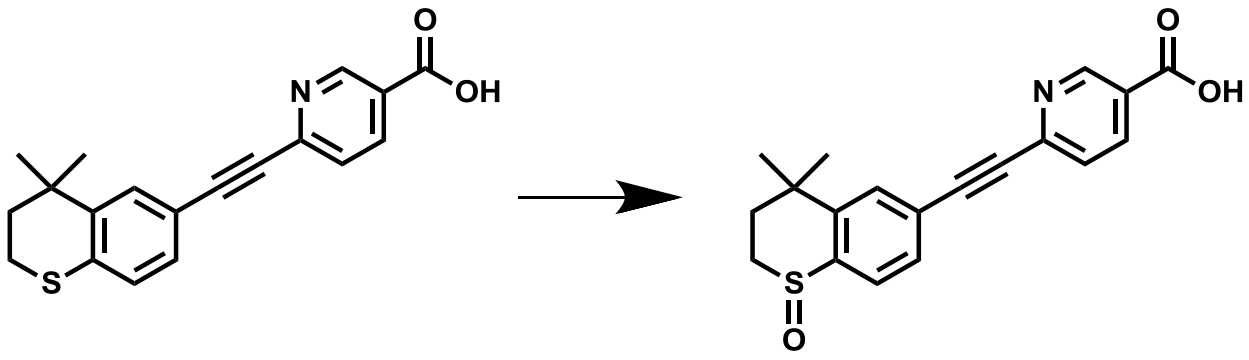

Tazarotenic Acid **Tazarotenic Acid Sulfoxide**

Figure 10-1. CYP26-catalyzed metabolism of tazarotenic acid to tazarotenic acid sulfoxide.

Table 10-2. Inhibition of tazarotenic acid sulfoxide formation in recombinant CYP26 enzymes by known inhibitors of retinoic acid hydroxylation.

Values in parenthesis represent the 95% confidence intervals for the nonlinear regression calculations, except for ketoconazole and liarazole with 9-cis-retionic acid, where standard error values were reported (Thatcher et al., 2011; Buttrick, 2012). (N.R. = Not Reported).

	IC_{50} (µM)			
	CYP26A1		CYP26B1	
Inhibitor	Tazarotenic Acid	9-cis-Retinoic Acid	Tazarotenic Acid	9-cis-Retinoic Acid
CD437	0.01 (0.01-0.03)	0.04 (N.R.)	0.14 (0.09-0.22)	0.03 (N.R.)
MM11253	0.02 (0.01-0.03)	0.06 (N.R.)	1.25 (0.81-1.91)	1.03 (N.R.)
Talarazole	0.02 (0.01-0.04)	0.005 (0.003-0.007)	0.001 (0.001-0.002)	0.0005 (0.00007-0.0009)
Ketoconazole	0.13 (0.05-0.31)	0.55 (1.3)*	0.19 (0.06-0.42)	0.14 (0.03-0.56)
SR11237	0.81 (0.34-1.91)	3.3 (N.R.)	6.86 (3.12-14.2)	14.2 (N.R.)
Liarazole	0.84 (0.31-2.48)	2.1 (1.1)*	0.01 (0.01-0.03)	0.02 (0.013-0.027)
Bexarotene	1.31 (0.54-4.22)	12.3 (N.R.)	1.60 (0.42-6.07)	4.0 (N.R.)
EC23	1.60 (0.61-4.94)	8.3 (4.0-17)	3.45 (1.47-8.44)	0.94 (0.44-2.0)
AM80	2.89 (1.52-7.43)	12 (8.1-18)	9.21 (3.69-24.2)	6.6 (2.3-19)

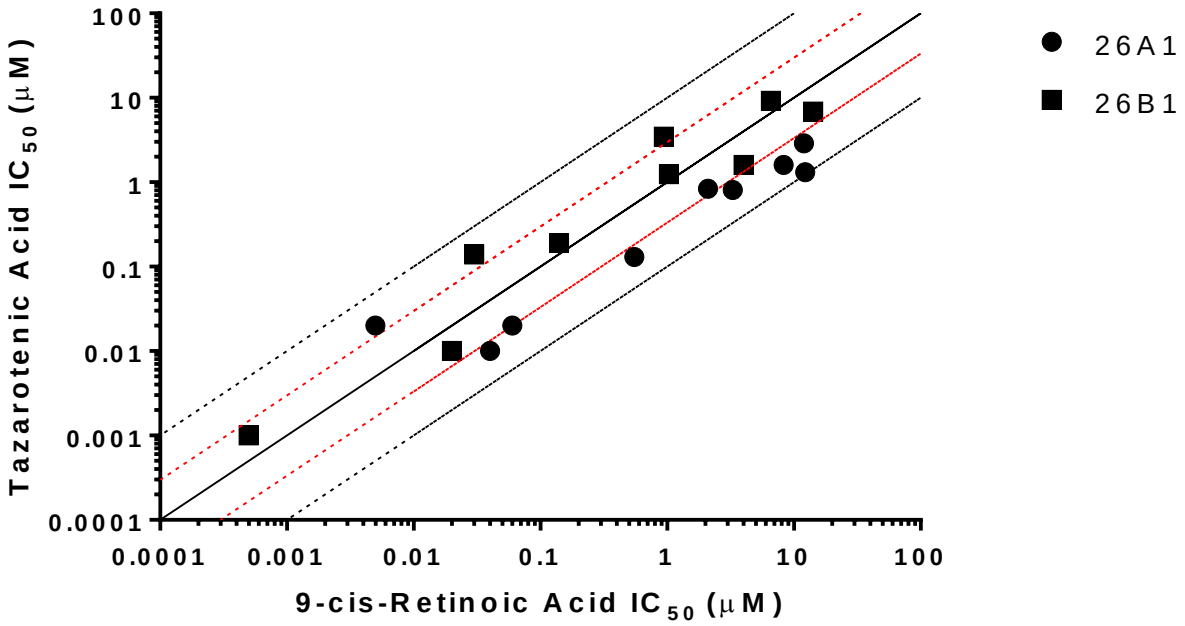

Figure 10-2. Correlation between tazarotenic acid and 9-cis-retinoic acid derived IC50s.

Correlation between previously reported CYP26 IC_{50} values using 9-cis-retinoic acid as a probe substrate and IC_{50} values generated using tazarotenic acid as a probe substrate for for CYP26A1 (r^2 = 0.78) or CYP26B1 (r^2 = 0.62) in vitro activity in recombinant CYP enzymes. Lines represent unity (solid black), 3-fold difference (dotted red) and 10-fold difference (dotted black).

10.3.2. In Vitro Inhibition Screening and IC_{50} Determination.

An initial set of 29 known CYP2C8 inhibitors was screened for inhibition of CYP26A1- or CYP26B1-catalyzed tazarotenic acid sulfoxide formation using a single inhibitor concentration (10 µM). Inhibition values ranged from no inhibition to greater than 90% inhibition (Figure 10-3). IC_{50} values were determined for 17 compounds which exhibited greater than 50% inhibition in the single concentration inhibition screen for either CYP26A1 or CYP26B1. Clotrimazole was the most potent inhibitor of CYP26 activity with IC_{50} values of 20 nM and 50 nM for CYP26A1 and CYP26B1, respectively (Table 10-3; Figure 10-4). The most potent inhibitors hypothesized to not inhibit through type II azole-heme interactions were zafirlukast for CYP26A1 (IC_{50} = 60

nM) and candesartan cilexetil for CYP26B1 (IC_{50} = 270 nM) (Figure 10-4). To determine whether the observed inhibition by candesartan cilexetil was due to the prodrug or degradation to candesartan, the stability of the prodrug in the three in vitro enzyme systems was assessed. Minimal degradation of candesartan cilexetil was observed in incubations with CYP26A1, CYP26B1 or CYP2C8 with only CYP2C8 showing any appreciable formation of the ester-hydrolyzed product (Figure 10-5). While all of the inhibitors tested exhibited some degree of inhibition of both CYP26A1 and CYP26B1, benzbromarone (12.0-fold), fluconazole (28.3-fold), quercetin (39.9-fold) and zafirlukast (11.8-fold) were all identified as relatively selective inhibitors for CYP26A1 while repaglinide (12.6-fold) showed selectivity towards inhibition of CYP26B1. IC_{50} values obtained with the set of 17 compounds for CYP26A1 and CYP26B1 were then compared to previously reported CYP2C8 IC_{50} values (Table 10-1). A positive and statistically significant correlation was observed for CYP26A1 and CYP2C8 IC_{50} values (r^2 = 0.849; Figure 10-6A). Only a weak correlation (r^2 = 0.258) was observed between the IC_{50} values obtained for CYP26B1 and CYP2C8 (Figure 10-6B).

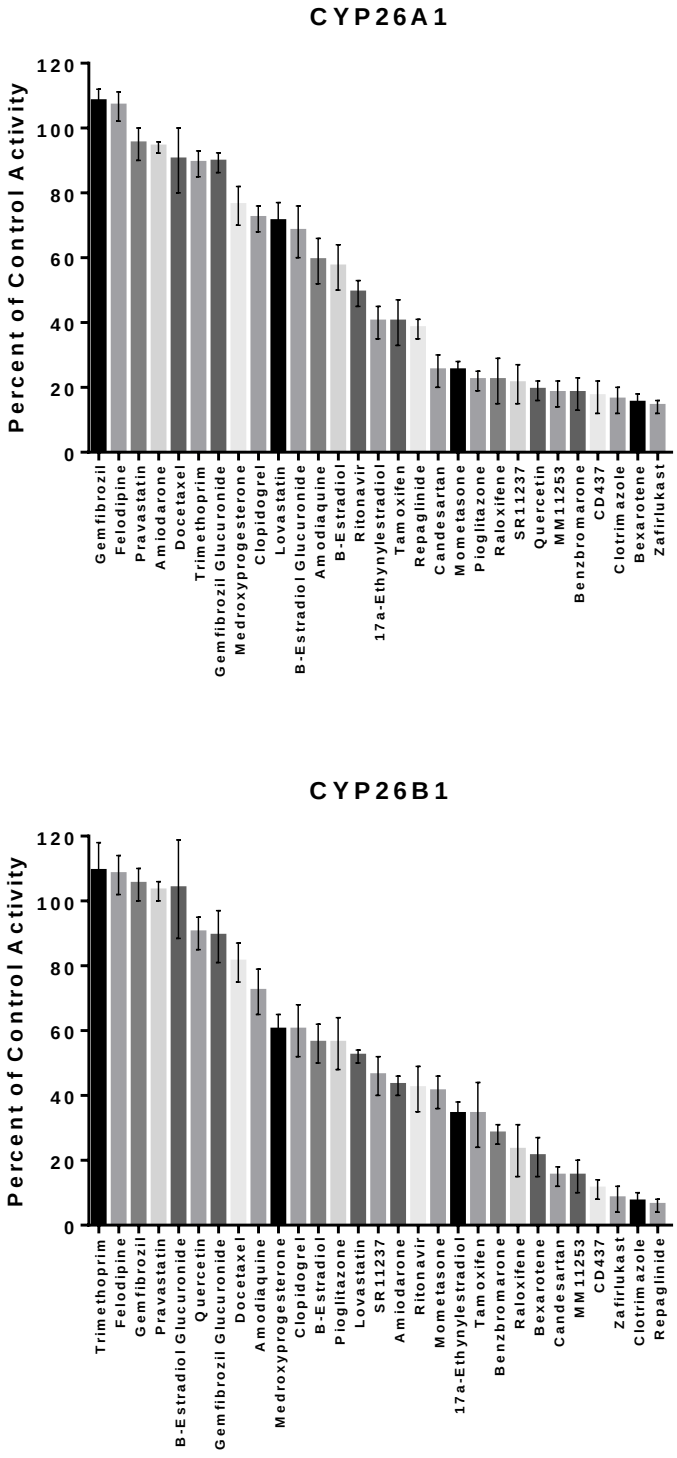

Figure 10-3. Single concentration (10 μM) inhibition screen using tazarotenic acid as a probe substrate of CYP26 activity.

Table 10-3. IC_{50} values for tazarotenic acid sulfoxide formation in recombinant CYP26 enzyme preparations by inhibitors of CYP2C8. Values in parenthesis represent the 95% confidence intervals for the nonlinear regression analysis.

	IC_{50} (μM)		
Inhibitor	**CYP26A1**	**CYP26B1**	**26B1 IC_{50} / 26A1 IC_{50}**
Benzbromarone	0.63 (0.56-0.71)	7.57 (3.62-15.9)	12
Candesartan	25.6 (8.21-72.3)	58.3 (24.2-473)	2.3
Candesartan Cilexetil	0.41 (0.17-0.96)	0.27 (0.20-0.36)	0.7
Clotrimazole	0.02 (0.01-0.03)	0.05 (0.04-0.07)	2.5
17α-Ethynylestradiol	2.24 (0.79-6.33)	6.73 (3.52-12.9)	3.0
Fluconazole	0.70 (0.53-1.0)	19.8 (8.61-26.5)	28
Itraconazole	0.55 (0.44-0.68)	0.16 (0.13-0.20)	0.3
Mometasone	0.90 (0.32-2.54)	6.81 (1.64-28.2)	7.6
Montelukast	0.12 (0.09-0.14)	0.61 (0.49-0.73)	5.1
Pioglitazone	0.93 (0.62-1.26)	8.48 (2.25-31.9)	9.1
Quercetin	1.92 (1.49-2.46)	76.2 (9.26-628)	40
Raloxifene	1.78 (1.06-2.97)	3.28 (2.15-5.01)	1.8
Repaglinide	7.73 (5.14-11.6)	0.61 (0.36-1.01)	0.1
Ritonavir	3.84 (1.69-8.70)	2.56 (0.93-7.09)	0.7
Rosiglitazone	11.9 (4.77-30.1)	8.47 (3.57-20.1)	0.7
Tamoxifen	21.4 (7.85-58.3)	14.0 (5.84-33.4)	0.7
Zafirlukast	0.06 (0.04-0.08)	0.71 (0.48-1.05)	12

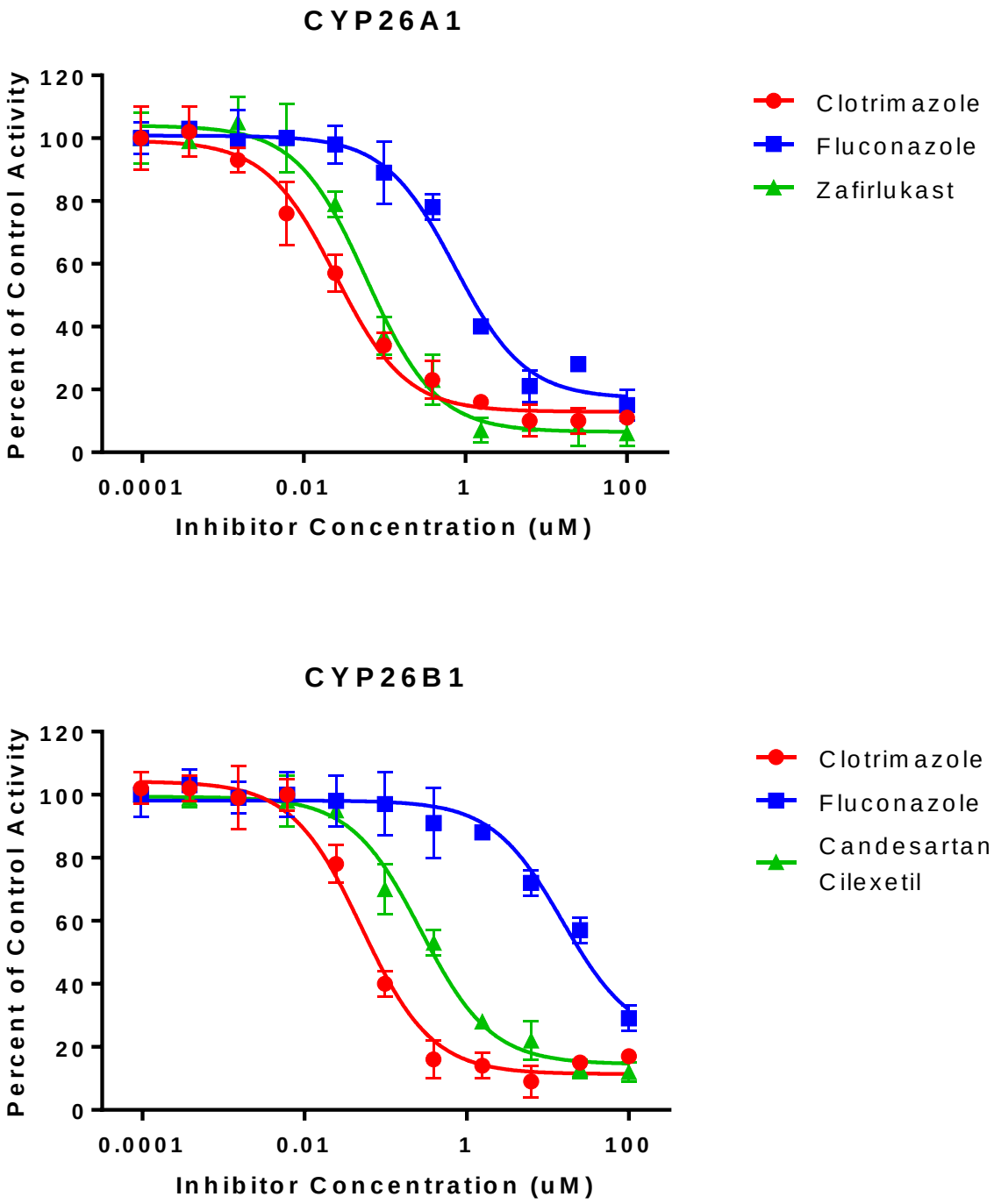

Figure 10-4. In vitro IC_{50} curves for select CYP26A1 or CYP26B1 inhibitors using tazarotenic acid as a probe substrate.

Data points represent the average of incubations conducted in triplicate and IC_{50} values were calculated using a three-parameter inhibition model with the Hill slope fixed to 1.

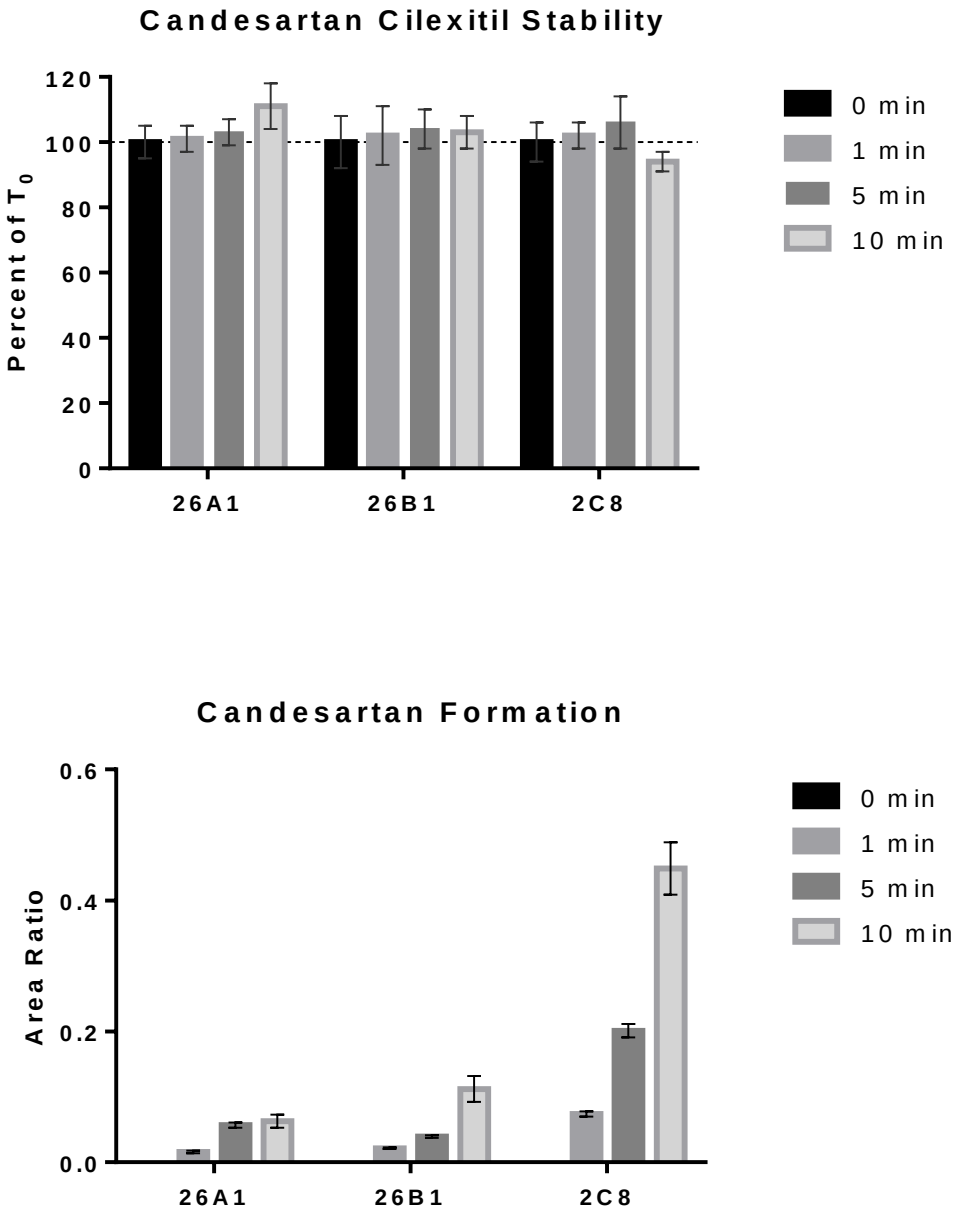

Figure 10-5. Stability of candesartan cilexetil in recombinant CYP26A1, CYP26B1 and CYP2C8 enzymes.

No degradation of candesartan cilexetil was observed under conditions similar to those used in the IC_{50} assays with only CYP2C8 showing any appreciable formation of candesartan.

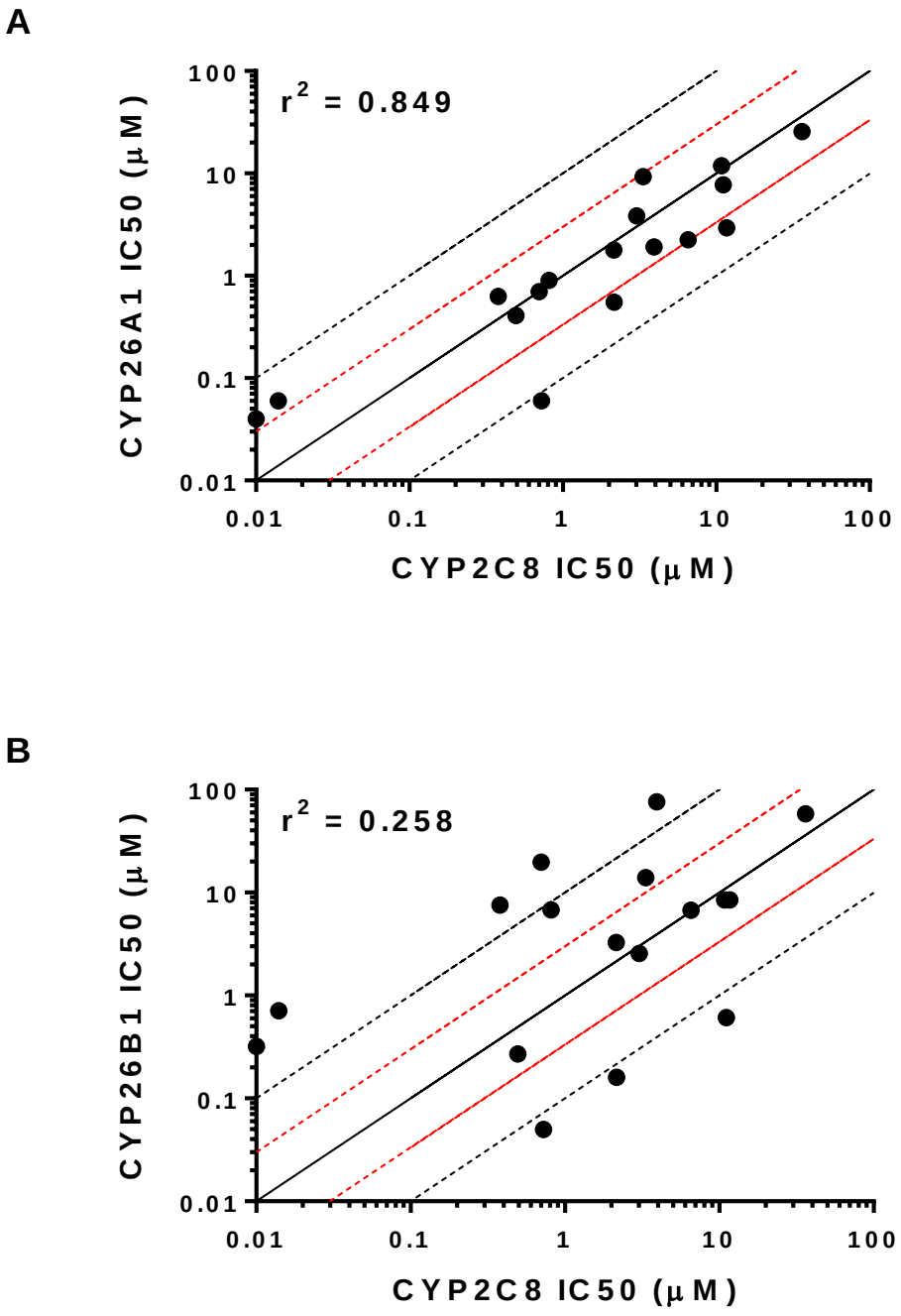

Figure 10-6. Correlation Between IC_{50} Values for CYP2C8 and CYP26A1 or CYP26B1.

Correlation between previously reported CYP2C8 IC_{50} values and CYP26A1 (r^2 = 0.849) or CYP26B1 (r^2 = 0.258) IC_{50} values generated using tazarotenic acid as a probe substrate. Lines represent unity (solid black), 3-fold difference (dotted red) and 10-fold difference (dotted black).

10.3.3. Computational Docking Simulations.

Previous reports have implicated CYP2C8 in the metabolism of *at*-RA, the primary substrate of CYP26A1 and CYP26B1 (Nadin and Murray, 1999; Marill et al., 2000; McSorley and Daly, 2000). In order to compare the structural similarities between the active sites of CYP2C8 and either CYP26A1 or CYP26B1, homology models of the CYP26 isozymes were superimposed on the crystal structure of CYP2C8 (pdb 1PQ2). Comparison of the CYP26A1 homology model to CYP2C8 resulted in an RMSD value of 3.013 between the two protein structures. The RMSD value for the CYP26B1 protein structure and CYP2C8 was 4.624. Visual examination of the active sites of the three cytochrome P450 isozymes revealed carboxylic acid binding residues located in comparable regions of the active site of CYP2C8 (Gly98, Asn99, Ser100), CYP26A1 (Arg 86, Arg90) and CYP26B1 (Tyr372, Arg373) that have been suggested to interact with the carboxylic acid moiety of 9-cis-retinoic acid, *at*-RA, or tazarotenic acid (Gomaa et al., 2006; Karlsson et al., 2008; Schoch et al., 2008; Foti et al., 2016).

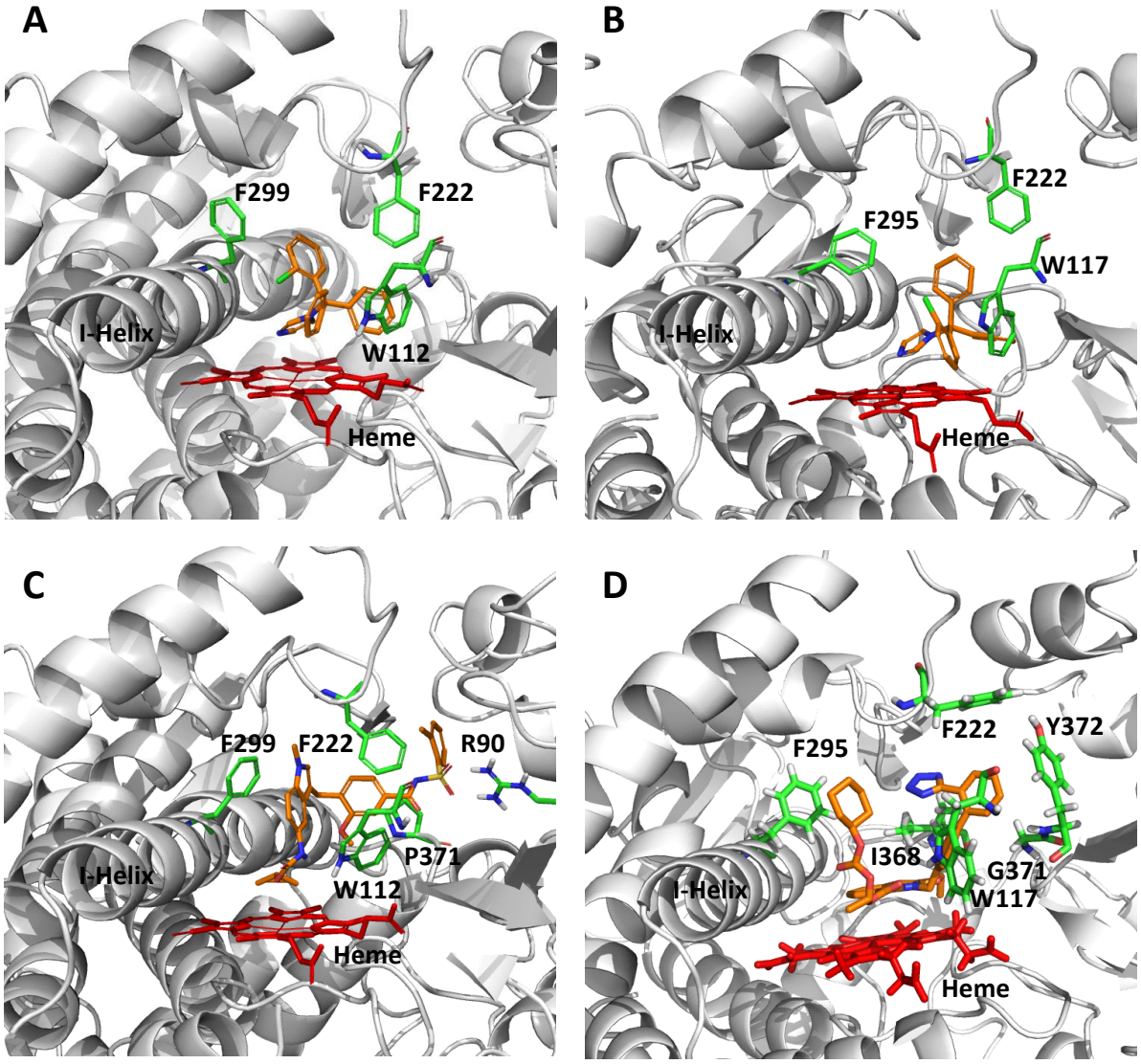

Figure 10-7. Computational Docking of Clotrimazole, Zafirlukast and Candesartan Cilexitil into CYP26 Homology Models.

Computational docking of clotrimazole (A, CYP26A1; B, CYP26B1), zafirlukast (C, CYP26A1) and candesartan cilexetil (D, CYP26B1) into the active sites of CYP26. The docking orientation of clotrimazole in the active sites of CYP26A1 and CYP26B1 suggests the potential for the imidazole moiety to inhibit the enzyme through type II binding interactions. Active site residues involved in the binding of zafirlukast in the active site of CYP26A1 (R90, W112, F222, and F299) and candesartan cilexetil in the active site of CYP26B1 (W117, F295, F299 and Y372) are similar to the active site residues known to be involved in retinoic acid binding for each isoform.

In order to rationalize the ligand binding of the known CYP2C8 inhibitors in the active sites of either CYP26A1 or CYP26B1, a number of computational docking experiments were performed. Docking simulations were carried out for the most potent azole-containing compound (clotrimazole for both CYP26A1 and CYP26B1) as well as zafirlukast for CYP26A1 and candesartan cilexetil for CYP26B1, two compounds hypothesized to not inhibit the enzymes through azole-heme interactions. As shown in Figures 10-7a and 10-7b, docking clotrimazole in the active sites of the CYP26A1 and CYP26B1 homology model predicted the sp^2 nitrogen of the imidazole ring to be oriented toward the iron of the heme prosthetic group at a distance of 3.104 Å for CYP26A1 and 2.655 Å for CYP26B1. Docking scores were similar for both CYP26A1 (-8.602) and CYP26B1 (-7.148). When zafirlukast was docked in the active site of CYP26A1 (docking score = -11.688), the cyclopentyl moiety was predicted to be oriented towards the heme iron at an approximate distance of 3.316 Å (Figure 10-7c). Key active site interactions included π-stacking between the methylindole ring and F222 and F299, as well as between the tolyl ring and P371. Hydrogen bonding was predicted to occur between the sulfonyl oxygens of zafirlukast and R90. For CYP26B1 and candesartan cilexetil, a favorable docking score of -11.200 was achieved with the benzene ring of the benzimidazole moiety located approximately 3.424 Å from the heme iron (Figure 10-7d). The amino acid residues predicted to be involved in orienting candesartan cilexetil in the active site of CYP26B1 included Y372 (π-stacking interaction with the phenyl ring adjacent to the tetrazole moiety) as well as W117, I368 and G371.

10.3.4. Spectral Binding Studies.

To further evaluate the results of the computational docking simulations with clotrimazole, zafirlukast and candesartan cilexetil, spectral binding studies were performed. Clotrimazole exhibited type II binding characteristics when incubated with CYP26A1, CYP26B1 and CYP2C8

as indicated by the observed maxima and minima of the UV-difference spectra (Figure 10-8). Spectral binding constants (K_s) were determined by nonlinear regression and were 533 nM, 4945 nM and 1574 nM for CYP26A1, CYP26B1 and CYP2C8, respectively (Table 10-4). No binding spectra could be obtained for zafirlukast or candesartan cilexetil in any of the systems tested (data not shown).

As the clotrimazole spectral binding constants for CYP26A1 and CYP26B1 were approximately 21.6-fold and 98.9-fold higher than their respective IC_{50} values, the protein binding of clotrimazole under the relevant in vitro conditions was explored. Under the conditions used in the in vitro CYP26A1, CYP26B1 and CYP2C8 IC_{50} assays, clotrimazole had f_u values of 0.661, 0.430 and 0.155, respectively. In the spectral binding assay, clotrimazole f_u values were 0.025, 0.005 and 0.048 for CYP26A1, CYP26B1 and CYP2C8, respectively. When corrected for protein binding, the $IC_{50,u}$ and $K_{s,u}$ values for clotrimazole were within two-fold of each other for each isozyme, suggesting that coordination of the imidazole nitrogen of clotrimazole to the heme iron is the most likely mechanism of clotrimazole inhibition for these three enzymes.

Table 10-4. Spectral binding properties for clotrimazole in recombinant CYP26A1, CYP26B1 and CYP2C8. Values in parenthesis represent the 95% confidence intervals for the nonlinear regression analysis. Standard error values are reported for fu and Ks data.

	CYP26A1	**CYP26B1**	**CYP2C8**
IC_{50} (nM)	24.7 (16.7-36.6)	50.1 (33.5-76.4)	725 (422-1120)
f_u (*IC_{50} assay*)	0.661 ± 0.042	0.430 ± 0.031	0.155 ± 0.024
$IC_{50,unb}$ (nM)	**16.3**	**21.5**	**112**
K_s (nM)	533 ± 71.8	4954 ± 640	1574 ± 569
f_u (*spectral binding assay*)	0.025 ± 0.001	0.005 ± 0.0006	0.048 ± 0.002
$K_{s,unb}$ (nM)	**13.3**	**24.7**	**75.5**
Binding Mechanism	Type II	Type II	Type II

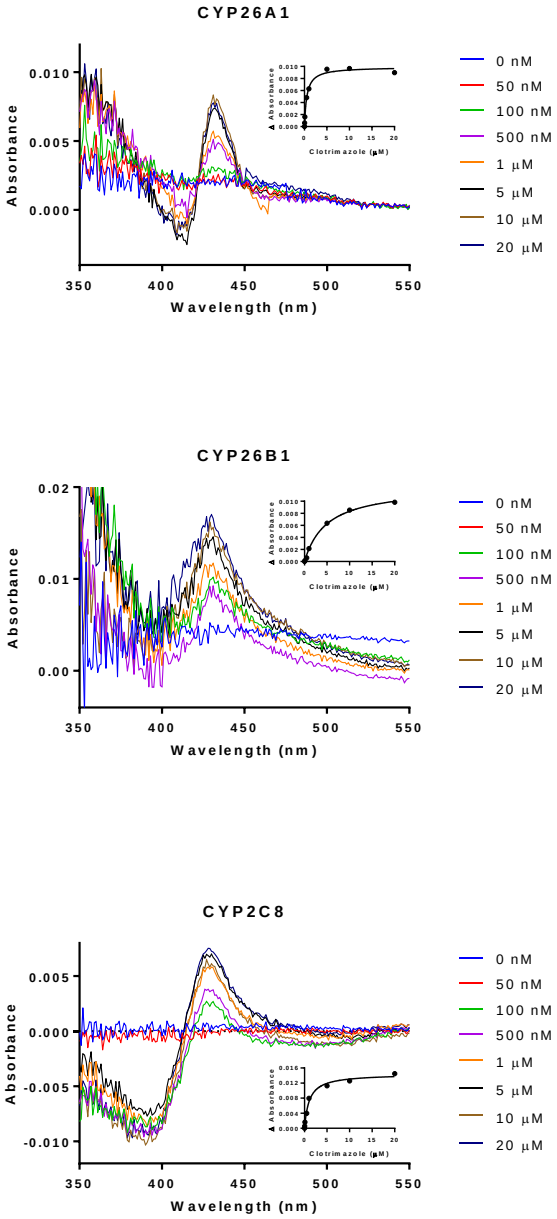

Figure 10-8. Spectral binding results for clotrimazole with recombinantly expressed CYP26A1, CYP26B1 or CYP2C8.

Data suggests enzyme inhibition occurs through type II binding interactions with the heme. $K_{s,unb}$ affinity constants for CYP26A1 (13.3 nM), CYP26B1 (24.7 nM) and CYP2C8 (75.5 nM) were determined through nonlinear regression analysis (inset Figures) and corrected for nonspecific binding in the in vitro assays.

10.3.5. Calculation of $C_{max,u}$ / IC_{50}.

To characterize the potential clinical ramifications of the observed in vitro inhibition of CYP26A1 and CYP26B1 by known inhibitors of CYP2C8, reported clinical plasma C_{max} values following typical oral or topical doses were obtained from the literature. C_{max} values were corrected for plasma protein binding and compared to the in vitro IC_{50} values to obtain a $C_{max,u}$ / IC_{50} ratio for CYP26A1 and CYP26B1 (Table 10-5). While total plasma concentrations following oral or topical administration for a number of the inhibitors exceeded their in vitro IC_{50} values, only clotrimazole and fluconazole exhibited maximum unbound concentrations which would suggest the potential for a meaningful interaction in vivo. Following topical administration, total skin concentrations of clotrimazole were reported to be 67.3 µM. Using plasma protein binding as a surrogate for the unbound fraction in the skin, $C_{max,u}$ / IC_{50} values for clotrimazole were 337 for CYP26A1 and 135 for CYP26B1. The predicted $C_{max,u}$ / IC_{50} values following 200 mg BID oral administration of fluconazole were 44.0 and 1.56 for CYP26A1 and CYP26B1, respectively.

10.4. Discussion.

Retinoic acid is a highly regulated signaling molecule that is involved in a host of dermatological, immunological and neurological functions through binding to the retinoic acid receptors and retinoid X receptors (Asselineau et al., 1989; Duester, 2008; Niederreither and Dolle, 2008; Raverdeau et al., 2012; Ransom et al., 2014; Raverdeau and Mills, 2014; Cunningham and Duester, 2015). As such, the metabolic pathways that are involved in the regulation of retinoic acid represent potential targets that can be exploited to alter concentrations of retinoic acid in vivo. Synthesis of retinoic acid begins with conversion of vitamin A (retinol) to retinal by alcohol dehydrogenases and short-chain dehydrogenases followed by the conversion of retinal to retinoic acid by retinaldehyde dehydrogenases (Roos et al., 1998; Chen et al., 2000b; Zhang et al., 2000; Marill et al., 2002). Degradation of retinoic

Table 10-5. $C_{max,u}$ / IC_{50} values for inhibitors of tazarotenic acid sulfoxidation.

C_{max} and f_u data compiled from literature references as noted in the Materials and Methods.

					$C_{max,u}/IC_{50}$	
Inhibitor	**Oral Dose**	**C_{max} (nM)**	**$f_{u,plasma}$**	**$C_{max,u}$ (nM)**	**CYP 26A1**	**CYP 26B1**
Benzbromarone	100 mg	9236	0.010	92.4	0.147	0.012
Candesartan	16 mg QD	270	0.002	0.38	< 0.001	< 0.001
Clotrimazole	1% Topical	67300*	0.100	6730	337	135
17α-Ethynylestradiol	30 µg	0.5	0.002	0.00085	< 0.001	< 0.001
Fluconazole	200 mg BID	34606	0.890	30794	44.0	1.56
Itraconazole	200 mg QD	919	0.002	1.80	0.003	0.011
Mometasone	50 µg Inhaled	0.05	0.010	0.0005	< 0.001	< 0.001
Montelukast	10 mg	925	0.010	8.90	0.077	0.015
Pioglitazone	45 mg	4489	0.010	38.0	0.048	0.005
Quercetin	500 mg TID	50.9	0.009	0.45	< 0.001	< 0.001
Raloxifene	1 mg/kg	1.05	0.050	0.50	< 0.001	< 0.001
Repaglinide	4 mg	104	0.026	2.60	< 0.001	0.004
Ritonavir	600 mg BID	15258	0.010	150	0.040	0.060
Rosiglitazone	8 mg	1673	0.002	3.40	< 0.001	< 0.001
Tamoxifen	10 mg BID	323	0.020	6.40	< 0.001	< 0.001
Zafirlukast	20 mg BID	1125	0.010	3.00	0.188	0.016

***** Represents reported clotrimizole concentration in skin (stratum corneum) following topical administration of a 1% clotrimazole cream formulation.

acid occurs through oxidation to 4-hydroxy-, 16-hydroxy-, and 18-hydroxyretinoic acid, which is catalyzed primarily by the CYP26-family (CYP26A1, CYP26B1 and CYP26C1) as well as by CYP2C8, CYP2C9 and CYP3A (Leo et al., 1989; Sonneveld et al., 1998; Nadin and Murray, 1999; Chen et al., 2000a; Marill et al., 2000; McSorley and Daly, 2000; Marill et al., 2002; Taimi et al., 2004; Lutz et al., 2009; Thatcher and Isoherranen, 2009; Thatcher et al., 2010; Helvig et al., 2011; Topletz et al., 2012). As such, the ability to modulate these pathways may prove to have a significant therapeutic benefit.

CYP2C8 was one of the first enzymes identified in the formation of 4-hydroxyretinoic acid and is the only drug metabolizing enzyme for which a crystal structure with a retinoic acid isomer bound in the active site exists (Leo et al., 1989; Nadin and Murray, 1999; Schoch et al., 2008). The enzyme is the major hepatic isoform involved in 13-cis-retinoic acid metabolism and can be inhibited by retinol and retinoic acid (Yamazaki and Shimada, 1999; McSorley and Daly, 2000; Marill et al., 2002). Given the propensity for CYP26A1, CYP26B1 and CYP2C8 to both metabolize and to be inhibited by the same retinoids, the potential exists for the inhibitory pharmacophores of CYP2C8 and CYP26 to overlap. Indeed, when homology models of CYP26A1 and CYP26B1 built using CYP120 (pdb 2VE3) as a template were superimposed on the CYP2C8 crystal structure (pdb 1PQ2), RMSD values of 3.013 and 4.624 were calculated, respectively. Furthermore, closer inspection of the active sites of CYP26A1, CYP26B1 and CYP2C8 suggest the presence of carboxylic acid binding residues in similar spatial proximity to the heme prosthetic group. Previous work to solve the crystal structure of CYP2C8 with 9-cis-retinoic acid bound in the active site suggests Gly98, Asn99 and Ser100 are important residues in anchoring the carboxylate moiety of the retinoic acid molecule which undergoes catalysis (CYP2C8 simultaneously binds two molecules of 9-cis retinoic acid) while CYP26A1 or CYP26B1 homology models built off of various templates have indicated that the carboxylate of retinoic acid forms hydrogen bonds with Arg64 (Shimshoni et al., 2012), Arg86 (Gomaa et al.,

2006) or Arg90 (Karlsson et al., 2008; Foti et al., 2016) for CYP26A1 and Arg95 and Ser369 (Karlsson et al., 2008; Saenz-Mendez et al., 2012) or Tyr372 and Arg373 (Foti et al., 2016) for CYP26B1. The estimated active site volumes of CYP26A1 (918 $Å^3$) and CYP26B1 (977 $Å^3$) based on homology modeling are somewhat smaller than the volume of the active site measured from the crystal structure of CYP2C8 (1438 $Å^3$), though it would appear they are large enough to accommodate larger xenobiotic compounds, similar to other CYP isoforms (Schoch et al., 2004; Foti et al., 2016).

In order to test the hypothesis of whether CYP26A1 and CYP26B1 were capable of binding xenobiotics with a similar pharmacophore profile as CYP2C8, a set of known CYP2C8 inhibitors was screened for inhibition activity against CYP26A1 and CYP26B1. Recently, tazarotenic acid has been identified as a substrate of CYP26A1 and CYP26B1 (Foti et al., 2016). To verify the use of tazarotenic acid sulfoxide formation as a probe for CYP26 activity, inhibition data was generated for known CYP26 inhibitors and compared to IC_{50} values previously obtained using 9-cis-retinoic acid. The observed r^2 values suggest that tazarotenic acid is an appropriate probe substrate to assess the inhibition of CYP26A1 and CYP26B1 in vitro (Figure 10-2), though the possibility of substrate-dependent inhibition profiles cannot be ruled out. While the compounds rank-ordered in a similar fashion between the two assays, some notable differences were observed. Calculated IC_{50} values for CYP26A1 using tazarotenic acid as a probe substrate were lower than those using 9-cis-retinoic acid. Interestingly, the reverse was generally true for CYP26B1, with 9-cis-retionic acid IC_{50} values being lower than those generated using tazarotenic acid.

The inhibition profile of CYP2C8 has received a great deal of attention owing to its role in clinically relevant drug interactions. Inhibition of CYP2C8 is thought to be partially responsible for the observed drug interactions between fluvoxamine and rosiglitazone as well as between gemfibrozil and montelukast, rosiglitazone, pioglitazone, repaglidide, cerivastatin and

loperamide (Backman et al., 2002; Niemi et al., 2003; Deng et al., 2005; Jaakkola et al., 2005; Niemi et al., 2006; Tornio et al., 2008; Karonen et al., 2010; Honkalammi et al., 2011). To further characterize the drug interaction profile of CYP2C8, a significant amount of in vitro efforts have been reported, with compounds such as montelukast, candesartan cilexetil, zafirlukast and clotrimazole having sub-micromolar IC_{50}s (Walsky et al., 2005; VandenBrink et al., 2011). In the current study, multiple CYP2C8 inhibitors were identified as potent inhibitors of both CYP26 isoforms. Selective inhibitors of CYP26A1 (versus CYP26B1) included quercetin, fluconazole, benzbromarone, and zafirlukast while repaglinide was the only compound with a 10-fold or greater selectivity for CYP26B1 inhibition. The difference in inhibition profiles between the two enzymes suggests differences in the active site characteristics which lead to inhibitor binding as well as to the potential to identify novel chemical scaffolds with which to achieve selective inhibition of CYP26A1 or CYP26B1. When the IC_{50} values were compared to previously reported CYP2C8 IC_{50} values, a statistically significant correlation was observed for CYP26A1 (r^2 = 0.849), suggesting that compounds which are inhibitors of CYP2C8 may also be inhibitors of CYP26A1. Perhaps further supporting the possibility for substrate-dependent inhibition profiles for CYP26 are the IC_{50} values observed for clotrimazole, fluconazole, quercetin and tamoxifen, four compounds previously reported to not be inhibitors of CYP26A1-catalyzed 4-hydroxyretinoic acid formation from 9-cis-retinoic acid in vitro (Foti et al., 2011).

To further characterize the active site binding interactions that lead to inhibition of CYP26A1 and CYP26B1, the spectral binding characteristics of the most potent azole-containing compound for each enzyme, clotrimazole, were evaluated. In addition, the binding of the most potent inhibitor of CYP26A1 (zafirlukast) and CYP26B1 (candesartan cilexetil) which was hypothesized to not inhibit each enzyme through heme-azole interactions was characterized. Computational simulations with homology models of CYP26A1 or CYP26B1 predicted that clotrimazole would bind in the active site of each enzyme with the sp^2 nitrogen of

the imidazole ring oriented toward the heme (Figure 10-7a and 10-7b). Zafirlukast, which does not contain any structural moieties amenable to heme coordination, docked with its cyclopentyl moiety oriented towards the heme (Figure 10-7c). Interestingly, CYP26B1 docking of candesartan cilexetil, which contains a tetrazole moiety theoretically capable of coordinating to the heme iron, suggested that interactions with active site residues, rather than heme-azole coordination, were responsible for orienting candesartan cilexetil in the active site of CYP26B1 with the tetrazole moiety oriented in a distal fashion from the heme (Figure 10-7d). Indeed, when spectral studies were conducted, only clotrimazole exhibited a type II binding spectra for both CYP26A1 and CYP26B1, indicating that the imidazole nitrogen of clotrimazole was coordinated to the heme. Other known type II inhibitors of CYP26 activity in vitro include ketoconazole, R115866 and R116010 (Thatcher et al., 2011).

The comparison of unbound inhibitor concentrations in vivo, [I], to in vitro IC_{50} or K_i values is a commonly used method to predict clinically relevant drug interactions. For reversible inhibitors, $[I]/K_i$ values of between 0.1 and 1 suggest the possibility of a clinically relevant drug interaction while an $[I]/K_i$ greater than 1 implies the interaction is likely (Bjornsson et al., 2003a; Bjornsson et al., 2003b; Kosugi et al., 2012). Using IC_{50} values as a surrogate for K_i, the ratio of unbound C_{max} values for clotrimazole and fluconazole to their respective inhibition potencies suggest the potential for these two compounds to inhibit CYP26 activity either locally (clotrimazole) or systemically (fluconazole). The low bioavailability of clotrimazole implies that even with high skin concentrations of the drug, systemic effects are unlikely (Sawyer et al., 1975). The effect of antifungal drugs such as clotrimazole and fluconazole on retinoic acid concentrations has been previously reported, though the overall role of CYP26 in these interactions remains to be determined. For example, the C_{max} and AUC of orally administered retinoic acid were shown to increase 6-fold and 4-fold, respectively, in a patient with acute promyelocytic leukemia upon co-administration of oral fluconazole (Schwartz et al., 1995). A

second case study on a patient with the same form of leukemia receiving oral retinoic acid described the onset of pseudotumor cerebri, a CNS toxicity, upon administration of oral fluconazole, a condition which resolved after discontinuation of the fluconazole treatment (Vanier et al., 2003). While inhibition of CYP2C8, CYP2C9 and CYP3A4 by fluconazole may also be involved in the reported drug interactions, the contribution of CYP26A1 or CYP26B1 cannot be ruled out, and may provide an plausible mechanism for the teratogenicity often associated with fluconazole in humans and animal models (Tiboni, 1993; Menegola et al., 2001; Lopez-Rangel and Van Allen, 2005; Tiboni and Giampietro, 2005). In addition to clinical drug interactions, additional evidence exists in vitro and in pre-clinical species in regard to the effects of antifungal drugs on retinoic acid metabolism. For example, the combination of clotrimazole and *at*-RA has been shown to initiate cellular differentiation in retinoic acid-resistant cell lines and to inhibit retinoic acid metabolism in embryonic carcinoma cells, while a modest induction of murine CYP26 embryonic mRNA expression is observed after administration of teratogenic doses of fluconazole, perhaps in response to an increase in *at*-RA concentration (Williams and Napoli, 1987; Kizaki et al., 1996; Tiboni et al., 2009). Similar to the clinical drug interactions observed between retinoic acid and fluconazole, while not definitive, the role of CYP26 in these in vitro interactions warrants further consideration.

In conclusion, the results demonstrate that CYP26A1 and CYP26B1 are inhibited by many known inhibitors of CYP2C8. The overlap in inhibitory pharmacophores between CYP2C8 and CYP26A1 or CYP26B1 may be driven by similarities in the active site binding characteristics of each enzyme and may open the possibility to expand upon the known pharmacophores related to inhibition of retinoic acid metabolism. Further, the potential for inhibition of CYP26 to cause clinically relevant drug interactions suggests care should be taken when co-administering retinoic acid and potent inhibitors such as fluconazole or clotrimazole. Ultimately, the results expand upon the contributions of CYP26A1 and CYP26B1 to drug

metabolism and drug interactions and should serve to increase the understanding of the enzymes as both a drug target and in regard to patient safety.

11. Chapter IV: Contribution of CYP26 to the Metabolism and Clearance of Retinoic Acid Receptor Agonists and Antagonists

11.1. Introduction.

The cytochrome P450 family of drug metabolizing enzymes is responsible for the oxidative metabolism of many endogenous compounds and most xenobiotics (Nelson, 2006; Zanger and Schwab, 2013). Within the cytochrome P450 family, CYP26A1, CYP26B1 and CYP26C1 are involved to varying extents in the regulation of endogenous retinoic acid concentrations (Ray et al., 1997; Taimi et al., 2004; Guengerich, 2006; Lutz et al., 2009; Thatcher and Isoherranen, 2009; Ross and Zolfaghari, 2011). While CYP26A1 and CYP26B1 are expressed in multiple tissues throughout the adult human body, expression of CYP26C1 is believed to be relatively limited (Xi and Yang, 2008; Thatcher and Isoherranen, 2009; Thatcher et al., 2010; Topletz et al., 2012; Brown et al., 2014). On the basis of mRNA expression, primary sites of CYP26A1 expression include the testes, lung, kidney and skin, with CYP26B1 also being expressed in the testes, lung and skin, as well as the intestine, placenta and ovaries (Xi and Yang, 2008; Osanai and Lee, 2011; Topletz et al., 2012). The known catalytic activities of CYP26A1 and CYP26B1 highly overlap, with substrates including retinoic acid isomers, metabolites of retinoic acid and at least one known xenobiotic compound, tazarotenic acid (White et al., 1996; Sonneveld et al., 1998; White et al., 2000; Taimi et al., 2004; Lutz et al., 2009; Thatcher et al., 2010; Ross and Zolfaghari, 2011; Shimshoni et al., 2012; Topletz et al., 2012; Topletz et al., 2014; Foti et al., 2016).

In order to maintain cellular homeostasis, the regulation of endogenous retinoic acid concentrations is a highly ordered process with alterations often resulting in the onset of pharmacological and toxicological effects (Lotan, 1980; Sporn and Roberts, 1984; McCaffery and Drager, 2000; Ross et al., 2000; Clagett-Dame and DeLuca, 2002; Maden, 2002). The mechanism of action for the observed effects in humans involves the binding of retinoic acid to retinoic acid receptors (α, β and γ) as well as retinoid X receptors (α, β and γ) with the subsequent downstream effects including changes in gene expression which ultimately can impact cellular proliferation and differentiation (Levin et al., 1992; Mangelsdorf et al., 1992; Mark

et al., 2006; Altucci et al., 2007; di Masi et al., 2015). As such, the development of retinoic acid receptor agonists and antagonists represents an area of scientific interest throughout a number of therapeutic areas and disease states (Pawson et al., 1982).

Multiple of retinoic acid receptor agonists and antagonists, often structurally related to retinoic acid, are either in use clinically or in development for various indications, including dermatological disorders and multiple forms of cancer (Charpentier et al., 1995; di Masi et al., 2015). While it is quite common to assess the selectivity of such compound across the panel of retinoic acid- or retinoid X receptors, often much less is known about the adsorption, distribution, metabolism and excretion (ADME) properties of these compounds, and in particular, very little information currently exists with regard to the drug metabolizing enzymes responsible for their biotransformation. Recently, tazarotenic acid, the active metabolite of tazarotene (a retinoic acid receptor β/γ agonist), was shown to be a substrate for CYP26A1 and CYP26B1 in vitro (Foti et al., 2016). As such, the possibility exists for other RAR agonists and antagonists to be substrates for the CYP26 family of drug metabolizing enzymes.

The primary aim of this work was to characterize the ability of the CYP26s (CYP26A1, CYP26B1 and CYP26C1) to metabolize various retinoic acid receptor agonists and antagonists in vitro. In vitro clearance assays were used as an initial screen to determine the clearance parameters for thirteen compounds. Based on the rates of metabolite formation by all three CYP26 isozymes, adapalene was selected for further evaluation, including a full phenotyping assessment as well as more in-depth metabolite identification studies. Finally, computational docking experiments were used to rationalize the ligand interactions leading to the observed metabolic profile of adapalene and des-adamantyl adapalene for each of the CYP26 isozymes. The results presented herein further support the role of the CYP26 family of drug metabolizing enzymes in the metabolism of xenobiotic compounds, especially those structurally related to retinoic acid.

11.2. Materials and Methods.

11.2.1. Materials.

Retinoic acid receptor agonists, antagonists and metabolites were obtained from Tocris Chemicals (Bristol, United Kingdom). Des-adamantyl adapalene was a generous gift from Dr. Philippe Diaz (University of Montana). Recombinant CYP26A1, CYP26B1 and CYP26C1 were generous gifts from Dr. Nina Isoherranen (University of Washington). All other in vitro enzymes were purchased from Corning (Tewksbury, MA). The remainder of the reagents and solvents were purchased from Sigma-Aldrich (St. Louis, MO) and were of the highest grade available.

11.2.2. In Vitro Clearance of Retinoic Acid Receptor Agonists and Antagonists by Recombinant CYP26s, CYP2C8 and CYP3A4.

Incubations to determine the intrinsic clearance of a set of RAR ligands (Figure 11-1) in recombinant CYP2C8, CYP3A4, CYP26A1 and CYP26B1 consisted of 5 nM of the relevant cytochrome P450 enzyme, 25 nM purified human reductase, 200 nM substrate and 1 mM NADPH in 100 mM potassium phosphate buffer (pH 7.4; final volume = 750 µL). An initial screen using a single end point (20 minutes) was initially conducted to assess turnover in each in vitro system. For compounds exhibiting more than 20% turnover by any single enzyme, in vitro clearance experiments were repeated with aliquots being removed at 0, 1, 2.5, 5, 15, 30, 45 and 60 minutes and immediately quenched with 3 volumes of ice-cold acetonitrile containing tolbutamide as an internal standard and centrifuged as noted above prior to analysis by LC-MS/MS. Control incubations were carried out in the absence of NADPH.

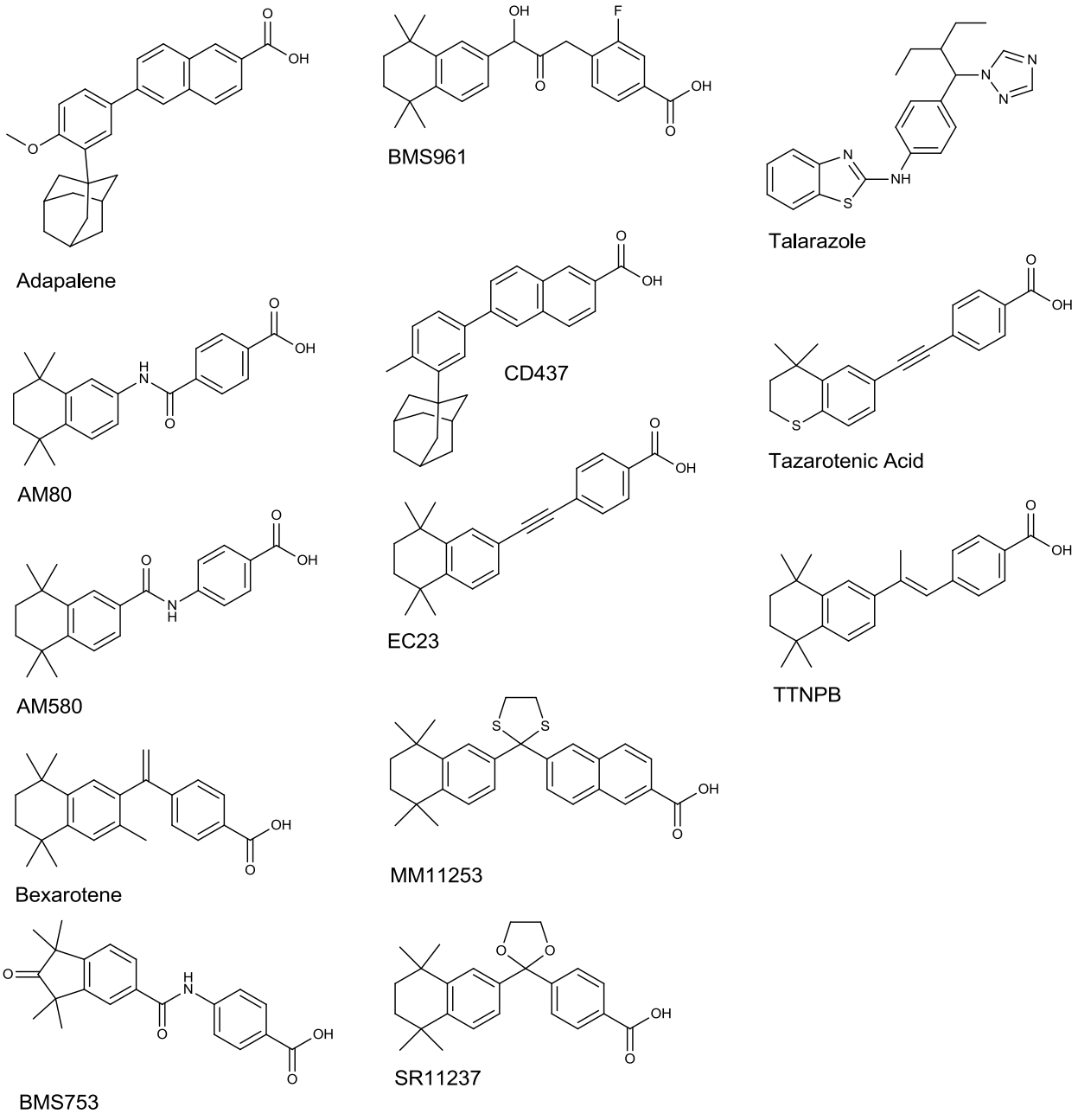

Figure 11-1. Retinoic acid receptor agonists and antagonists included in intrinsic clearance experiments in recombinant CYP26A1, CYP26B1, CYP26C1, CYP2C8 and CYP3A4.

11.2.3. Adapalene Phenotyping.

Incubations performed to determine the enzymes responsible for the metabolism of adapalene contained recombinant enzyme (5 nM, final concentration), purified human reducatase (50 nM, final concentration) and adapalene (500 nM, final concentration) in potassium phosphate buffer (100 mM, pH 7.4). After a pre-incubation period of three minutes at 37 ºC, NADPH (1 mM, final concentration) was added to all incubations. Incubations which contained flavin-containing monooxygenase (FMO) enzymes were pre-incubated with enzyme and NAPDH and initiated by addition of adapalene because of the lack of stability of FMOs at 37 ºC (Foti and Fisher, 2004). All incubations (50 µL, final volume) were kept at 37 ºC for 20 minutes before being stopped through addition of 3 volumes (v/v) of ice-cold acetonitrile. Tolbutamide (500 nM, final concentraition) was utilized as the internal standard. Samples were mixed and subject to centrifugation (3000 RPM) for fifteen minutes before analysis by LC-MS/MS.

11.2.4. Metabolite Identification of Adapalene and Des-Adamantyl Adapalene in Recombinant CYP26s.

In vitro experiments to elucidate the metabolic pathways of adapalene in CYP26A1, CYP26B1 or CYP26C1 recombinant preparations were carried out using 50 nM recombinant enzyme, 200 nM purified human reducatase and adapalene (10 µM) in 100 mM potassium phosphate buffer (pH 7.4). Incubations were initiated with the addition of 1 mM NADPH (final concentration) and incubated at 37 ºC for 30 minutes. Control incubations were performed in the absence of NADPH. Upon completion, in vitro incubations were extracted into 4 volumes of ethyl acetate, dried under a gentle stream of N_2 at 40 ºC and reconstituted in 100 µl methanol prior to LC-MS/MS analysis and compared to commercially available synthetic standards of each metabolite.

11.2.5. Computational Docking of Adapalene and Des-Adamantyl Adapalene in CYP26A1, CYP26B1 and CYP26C1 homology models.

Three dimensional homology models of CYP26A1 and CYP26B1 were designed and validated as described in previous chapters. Subsequently, a three dimensional homology model of CYP26C1 was also designed using Prime (Schrodinger LLC, New York). The CYP26C1 amino acid sequence was obtained from the NCBI protein server (UniProtKB/Swiss-Prot Accession Number: Q6V0L0.2; Gene ID 340665). As with the CYP26A1 and CYP26B1 homology models, the crystal structure of CYP120 (pdb 2VE3) was also used as the template for the CYP26C1 homology model. Sequence similarity between CYP26C1 and CYP120 was indicated by a 35% sequence identity and 52% positive sequence coverage (Table 11-1). A heme prosthetic group was introduced into the homology model and covalently bound to Cys459 upon which an energy minimization step using OPLS_2005 force field constraints (contained within the MacroModel algorithm (Schrodinger LLC, New York)) was conducted. For docking of adapalene or des-adamantyl adapalene in the active site of the CYP26C1 homology model, the available docking space was defined by a 12 x 12 x 12 Å cube to constrain the center of mass of the ligands using Glide (Schrodinger LLC, New York). The structural plausibility of the CYP26C1 homology model was evaluated through Ramachandran plots, calculation of unacceptable bond lengths and angles and scoring of model flexibility using PSIPRED (University College London, UK) and SSPro (Schrodinger). Adapalene and des-adamantyl adapalene three dimensional structures were energy minimized using the OPLS_2005 force field constraints as defined within the LigPrep algorithms (Schrodinger LLC, New York). Multiple scoring algorithms were used to assess the docking poses of the ligands within the active site of each enzyme (Perola et al., 2004).

Table 11-1. Estimated parameters for the CYP26C1 homology model.

Parameter	CYP26C1 Model
Template	CYP120 (pdb 2VE3)
Template Sequence Identity	35%
Template Positive Sequence Coverage	52%
BLAST Query Coverage	89%
BLAST E-Value	3e-83
RMSD vs Template	0.789
Favorable Bond Angles	84.7%
Allowable and Favorable Bond Angles	94.9%
I-Helix Residues	M283 – L312
Active Site Volume (A^3)	1090.1

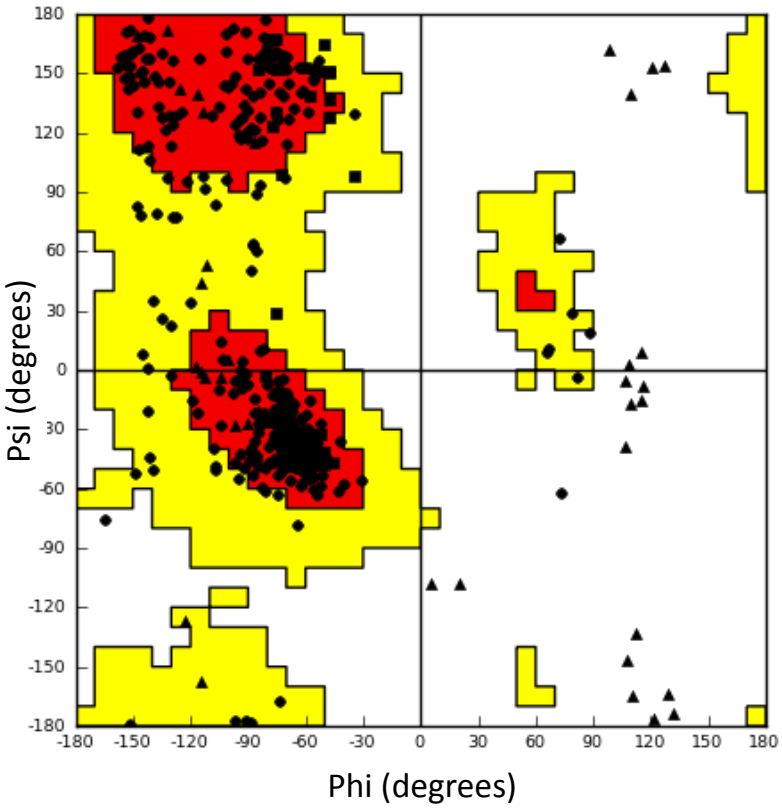

Figure 11-2. CYP26C1 Ramachandran Plot.

Analysis of the Phi-Psi angles in the CYP26C1 homology model demonstrated 94.9% of the angles were in the favorable or allowable regions.

11.2.6. LC-MS/MS Analysis.

Analysis of the retinoic acid receptors and their metabolites was conducted using LC-MS/MS methods. The analytical instrumentation was identical to that described in previous chapters. In brief, an Applied Biosystems API4000 utilizing an electrospray ionization source (Applied Biosystems, Foster City, CA) was coupled to a liquid chromatography / sample introduction system that was comprised of LC-20AD binary pumps and an in-line solvent degasser (Shimadzu, Columbia, MD). The injection volume used for all analytical samples was 10 µL. For intrinsic clearance experiments, peak separation was accomplished using 0.1% formic acid (v/v) in water (mobile phase A) or acetonitrile (mobile phase B) and a Synergi 2.5 µm Hydro RP 100 Å (50 x 2.0 mm) analytical column (Phenomenex, Torrance, CA). A rapid gradient similar to that described in previous chapters was used. For adapalene and des-adamantyl adapalene metabolite elucidation experiments, a Kinetex 2.6 µm C18 100 Å (100 x 2.1 mm) column (Phenomenex, Torrance, CA) was used to achieve peak separation. A longer gradient was used for metabolite elucidation samples, beginning with 2.5% B (0 – 3 minutes), increasing from 2.5% B to 95% B (from 3 – 14 minutes), holding at 95% B (from 14 – 17 minutes) and re-equilibrating at 2.5% B for 3 minutes prior to the injection of the next sample. LC-MS/MS analyses for intrinsic clearance experiments utilized multiple reaction monitoring (MRM). A rapid screen for the formation of oxidative metabolites (+16 amu) was performed by increasing the Q1 mass value by 16 amu and by both increasing the Q3 mass value by 16 amu as well as by holding it constant for each metabolite. Additional metabolite identification analyses for adapalene and des-adamantyl adapalene also utilized full Q1 scans (100 – 1000 amu). Generic parameters that were utilized for all analytes included the curtain gas (14 arbitrary units), CAD gas (medium), ion spray voltage (4500 V), source temperature (550 °C) and ion source gas 1 and gas 2 (35 arbitrary units, each).

11.2.7. Data Analysis.

Analysis of raw data was was performed through Analyst (version 1.5; Applied Biosystems, Foster City, CA). Concentrations of each analyte of interest were calculated by comparing the peak areas of an unknown sample to the peak area that was determined from standard curves with synthetic standards. Parameter fitting for intrinsic clearance was accomplished with WinNonlin (Phoenix64, Cetara, Princeton, NJ) as described below.

Intrinsic clearance values were calculated by first determining substrate depletion rates through the normalization of remaining analyte concentrations to a percent of initial concentration remaining (T_0). Linear regression was employed to calculated the slope (-k) of the ln(percent remaining) values as a function of time as previously described (Obach et al., 1997). An in vitro clearance value (mL/min/nmol cytochrome P450) was then determined by converting the resulting rate value (k) to an in vitro half-life ($T_{1/2}$ = 0.693 / k) as shown in Equation 1.

Equation 1

$$Cl_{InVitro,app} = \frac{0.693}{T_{1/2}} * \frac{Incubation\_Volume}{CYP\_Content}$$

11.3. Results

11.3.1. In Vitro Clearance of Retinoic Acid Receptor Agonists and Antagonists by Recombinant CYP26s, CYP2C8 and CYP3A4.

An initial metabolic stability screen was conducted in order to determine the percent remaining for each of the 13 retinoic acid receptor ligands after a 20 minute incubation in recombinant CYP26A1, CYP26B1, CYP26C1, CYP2C8 or CYP3A4 (Table 11-2). The retinoic acid receptor agonists with the highest degree of turnover were SR11237 (CYP26A1 and CYP3A4), tazarotenic acid (CYP26B1), and MM11253 (CYP26C1 and CYP2C8).

Table 11-2. Percent remaining of RAR ligands at 20 min in CYP 26A1, 26B1, 26C1, 2C8 and 3A4.

	Percent Parent Compound Remaining at 20 minutes				
Compound	**CYP26A1**	**CYP26B1**	**CYP26C1**	**CYP2C8**	**CYP3A4**
Adapalene	96	78	68	102	102
AM80	104	88	93	99	94
AM580	93	44	102	105	96
Bexarotene	98	74	103	4	18
BMS 753	82	106	104	107	83
BMS 961	104	102	16	38	76
CD437	108	95	97	2	106
EC23	71	98	103	107	68
MM11253	46	87	9	0	46
SR11237	35	72	81	3	7
Talarozole	98	86	88	96	68
Tazarotenic Acid	51	42	52	86	104
TTNPB	68	66	58	105	81

Intrinsic clearance values were determined for any retinoic acid receptor ligand which displayed greater than 20% depletion over the 20 minute incubation (Table 11-2). Both adapalene (CYP26B1 and CYP26C1) and tazarotenic acid (CYP26A1, CYP26B1 and CYP26C1) were shown to be primarily cleared by the CYP26s with only minimal involvement by either CYP2C8 or CYP3A4. The highest intrinsic clearance observed for any of the CYP26-catalyzed reactions was with CYP26A1 and SR11237, which had an intrinsic clearance of 3.76

± 0.28 mL/min/nmol P450 (Table 11-3, Figure 11-3). Conversely, the highest rates of metabolite formation were observed with AM580 (CYP26A1) and adapalene (CYP26B1 and CYP26C1) (Figure 11-4).

Table 11-3. Intrinsic clearance parameters for RAR ligands in recombinant CYP26A1, CYP26B1, CYP26C1, CYP2C8 and CYP3A4.

Compound	Enzyme	Clint (mL/min/nmol P450)
Adapalene	CYP26B1	0.24 ± 0.01
	CYP26C1	0.38 ± 0.03
AM580	CYP26B1	0.84 ± 0.02
Bexarotene	CYP26B1	0.30 ± 0.04
	CYP2C8	3.22 ± 0.12
	CYP3A4	1.71 ± 0.18
BMS961	CYP26C1	2.49 ± 0.21
	CYP2C8	0.96 ± 0.16
	CYP3A4	0.27 ± 0.08
CD437	CYP2C8	3.91 ± 0.31
EC23	CYP26A1	0.84 ± 0.05
	CYP3A4	1.26 ± 0.24
MM11253	CYP26A1	0.78 ± 0.16
	CYP26C1	2.41 ± 0.41
	CYP2C8	7.37 ± 0.69
	CYP3A4	1.21 ± 0.09
SR11237	CYP26A1	3.76 ± 0.28
	CYP26B1	0.33 ± 0.08
	CYP2C8	15.6 ± 2.61
	CYP3A4	2.66 ± 0.24
Talarazole	CYP3A4	0.39 ± 0.09
Tazarotenic Acid	CYP26A1	0.67 ± 0.07
	CYP26B1	1.08 ± 0.21
	CYP26C1	0.65 ± 0.11
TTNPB	CYP26A1	1.05 ± 0.05
	CYP26B1	0.42 ± 0.06
	CYP26C1	0.54 ± 0.12

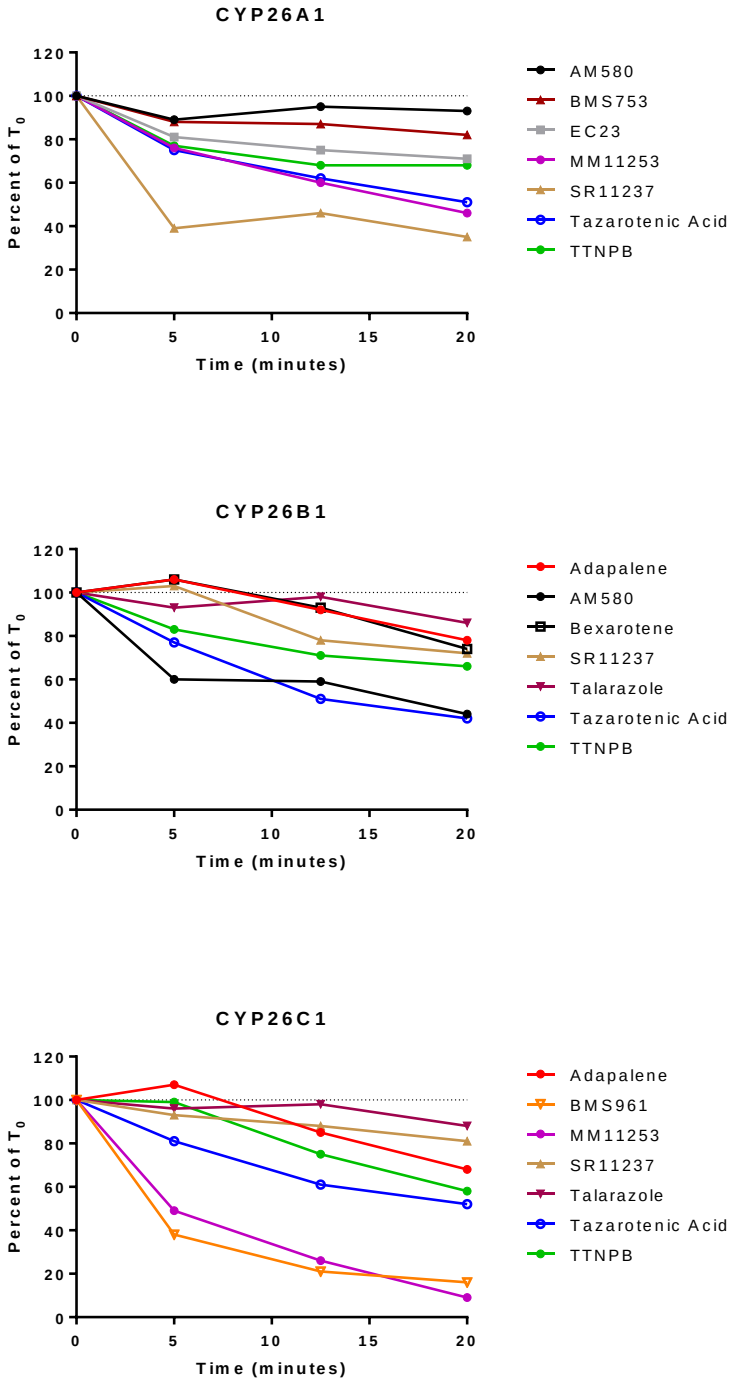

Figure 11-3. Depletion rates of retinoic acid receptor agonists and antagonists in recombinant CYP26A1, CYP26B1 and CYP26C1.

Substrates were incubated at 200 nM for 20 minutes at 37 °C. SR11237, tazarotenic acid and MM11253 exhibited the highest degrees of depletion by CYP26A1, CYP26B1 and CYP26C1, respectively.

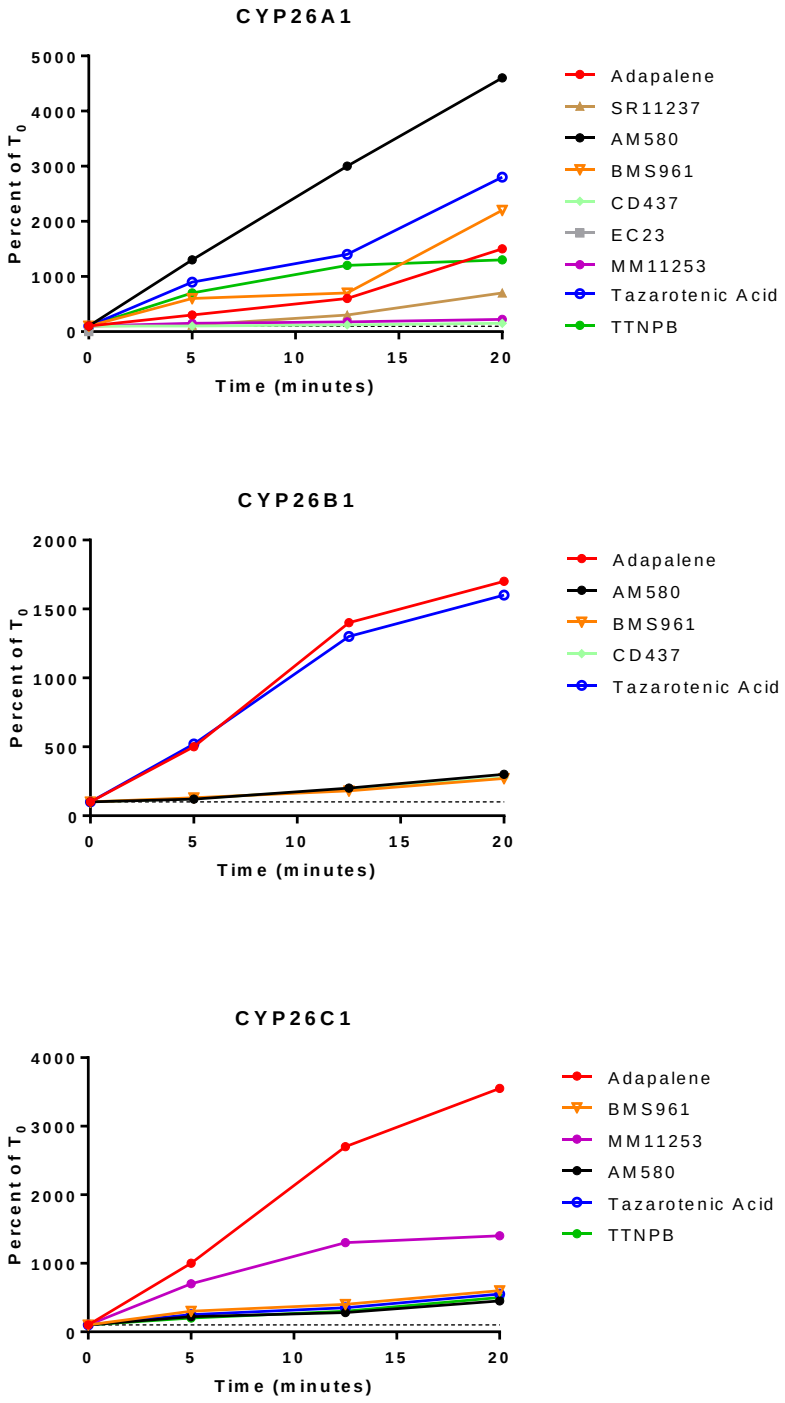

Figure 11-4. Metabolite formation rates of retinoic acid receptor agonists and antagonists 1n recombinant CYP26A1, CYP26B1 and CYP26C1.

Oxidative metabolism (+16 amu) was monitored over 20 minutes by LC-MS/MS. AM580 (CYP26A1) and adapalene (CYP26B1 and CYP26C1) exhibited the highest rates of metabolite formation over the 20 minute incubation period. Dashed lines represent 100% of T_0.

11.3.2. Metabolite Identification of Adapalene and Des-Adamantyl Adapalene in Recombinant CYP26s.

Experiments were conducted to deduce the major sites of metabolism for adapalene and des-adamantyl adapalene in recombinant CYP26 incubation. In incubations with adapalene and CYP26A1, CYP26B1 and CYP26C1, the only metabolite observed was hydroxylation of the adamantane ring (Figure 11-5). To assess the steric effects of the adamantyl moiety, a des-adamantyl analog of adapalene was also profiled. When des-adamantyl adapalene was used as the substrate with any of the CYP26 isozymes, the only metabolite observed was O-demethylation of the methoxyphenyl moiety (Figure 11-6). No additional sites of oxidative metabolism were observed for either adapalene or des-adamantyl adapalene.

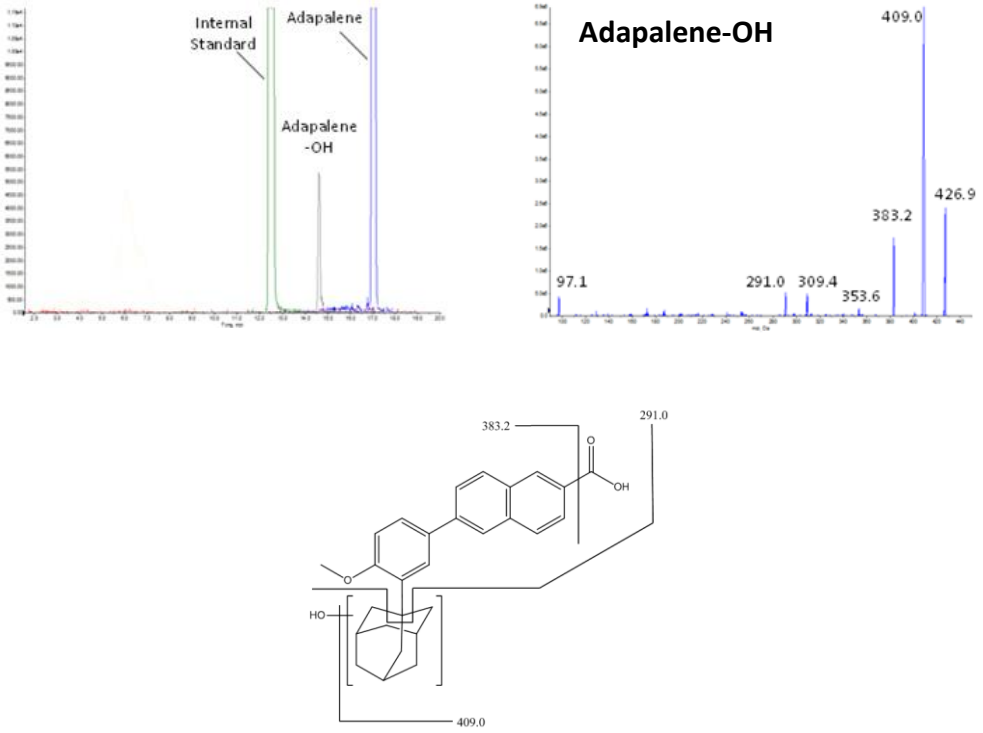

Figure 11-5. Metabolite elucidation of adapalene in recombinant CYP26C1.

Incubating adapalene with recombinant CYP26C1 produced a single hydroxylated metabolite. Analysis of mass spectrometry fragmentation patterns suggests the adamantyl moiety is the site of hydroxylation. Similar data was observed with recombinant CYP26A1 and CYP26B1 (data not shown).

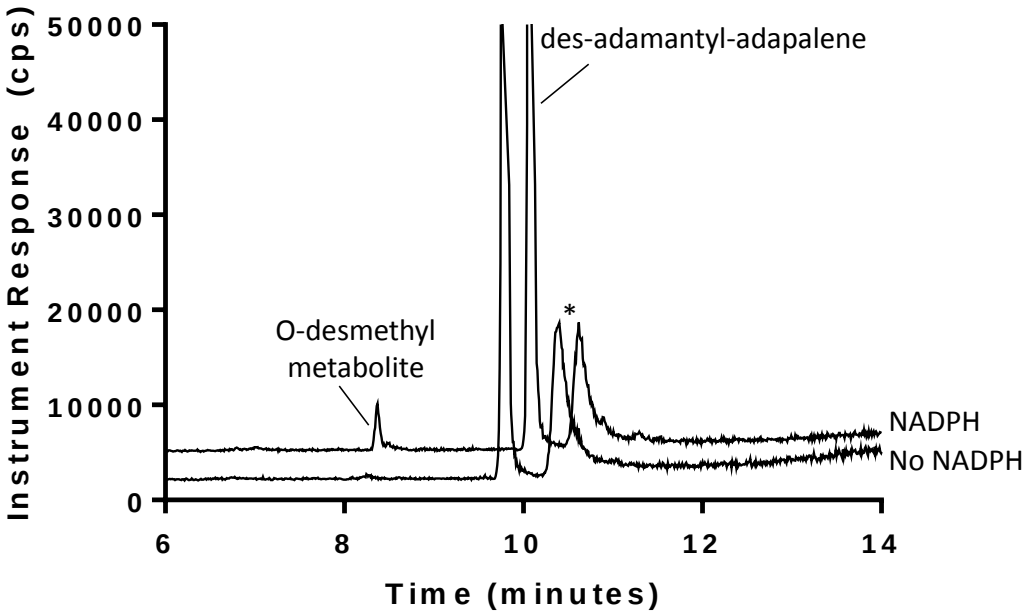

Figure 11-6. Assessment of des-adamantyl adapalene metabolite formation in recombinant CYP26C1.

Incubation of des-adamantyl adapalene with recombinant CYP26C1 produced a single metabolite at a molecular weight of 14 amu less that the parent molecule. Analysis of mass spectrometry fragmentation patterns suggests the metabolite is O-desmethyl-desadamantyl adapalene. Similar data was observed with recombinant CYP26A1 and CYP26B1 (data not shown).

11.3.3. Computational Docking of Adapalene and Des-Adamantyl Adapalene in CYP26A1, CYP26B1 and CYP26C1 homology models.

To characterize the ligand-protein interactions of adapalene that lead to its observed metabolic profile by CYP26A1, CYP26B1 and CYP26C1, the compound was computationally docked into homology models of each enzyme. The design and validation of the CYP26A1 and CYP26B1 homology models are as previously described. A BLAST search using the amino acid sequence of CYP26C1 (UniProtKB/Swiss-Prot Accession Number: Q6V0L0.2; Gene ID 340665) identified the crystal structure of CYP120 (pdb 2VE3) as being the closest match upon which to base the homology model, similar to what was observed for CYP26A1 and CYP26B1.

Comparison of the protein sequences for CYP26C1 and CYP120 revealed a sequence identity of 35%, a positive sequence coverage of 52% and a BLAST query coverage of 89%. An RMSD value of 0.789 was calculated by superimposing the CYP26C1 homology model on the crystal structure of CYP120. A number of similarities to the CYP26A1 and CYP26B1 active sites were observed, namely aromatic, hydrophobic interactions with Phe222, Phe295 and W117 as well as amino acid residues able to interact with a carboxylate moiety distal from the heme iron (Trp65, His73 and Tyr387). Additional amino acid residues involved in defining the active site of CYP26C1 included Glu292, Val383 and Ser384. The I-helix was defined by residues Met283 through Leu312. Homology model parameters are shown in Table 11-1 and the resulting Ramachandran plot in Figure 11-2. Estimation of the active site volume of CYP26C1 indicated a cavity of approximately 1090 $Å^3$ (Figure 11-7)

Prior to docking adapalene into the CYP26C1 homology model, the model was further evaluated by docking *at*-RA into the active site. As expected, *at*-RA was positioned with the β-ionone moiety proximal to the heme prosthetic group with the carboxylate of *at*-RA distal to the heme and predicted to have a hydrogen bonding interaction with Trp65 (Figure 11-8). Other amino acid residues located within 4 Å of the *at*-RA molecule included Trp117, Phe222, Phe295, Val383 and Ser384. In this orientation, the hydrogen atoms whose abstraction would facilitate formation of 16-hydroxy-*at*-RA were positioned approximately 3.37 Å from the heme iron. The model was unable to resolve binding orientation conducive to 4- or 18 hydroxylation of *at*-RA, though it should be noted that the metabolic profile of *at*-RA in vitro has yet to be fully characterized.

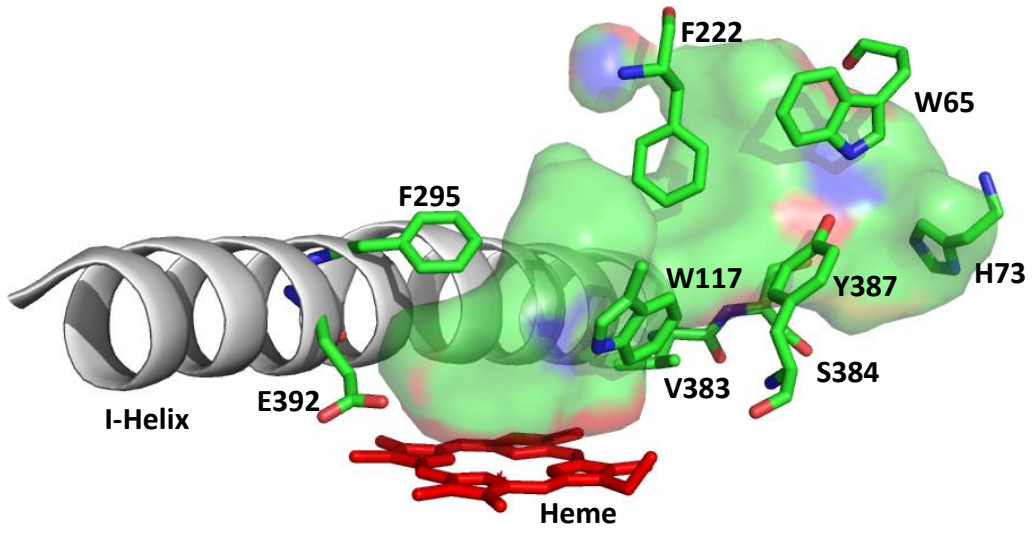

Figure 11-7. Characterization of the active site of the CYP26C1 homology model.

The ligand binding site of CYP26C1 was defined primarily by lipophilic aromatic amino acid residues (W117, F222 and F295) and by ionizable hydrogen bonding residues capable of interacting with the carboxylate moiety of retinoic acid (W65, H73 and Y387).

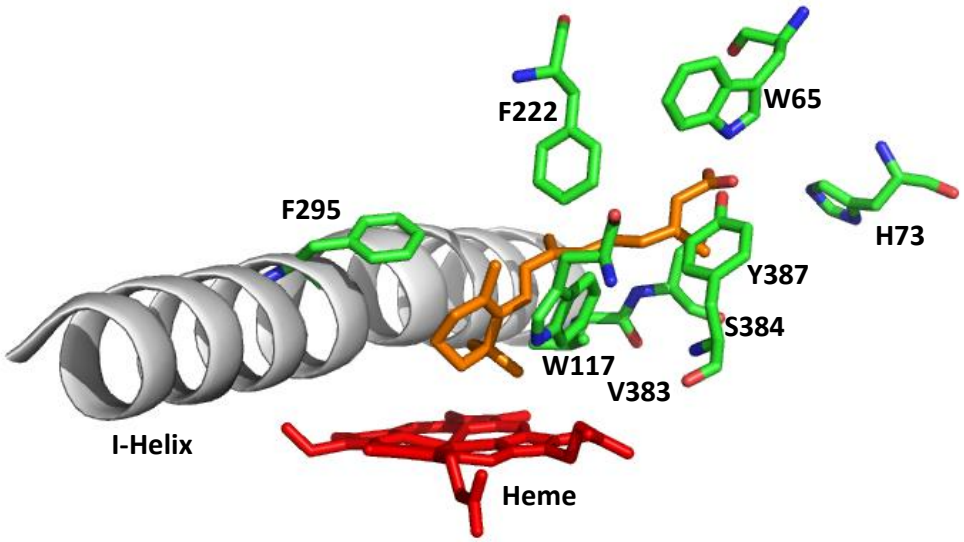

Figure 11-8. CYP26C1 homology model with *at*-RA docked in the active site.

Docking of *at*-RA in the active site of CYP26C1 suggested that 16-hydroxylation would be the preferred site of metabolism by CYP26C1. In this orientation, *at*-RA was located approximately 3.37 Å from the heme iron and within 4 Å of W117, F222, F295, V383 and S384. The Glide score for this docking simulation was –9.387.

In order to rationalize the observed metabolic profile of adapalene by CYP26 enzymes, the compound was docked into the homology models for all three CYP26 isozymes (Figure 11-9). In each case, the adamantyl ring was located in proximity to the heme iron, at a distance of approximately 2.864 Å, 2.833 Å and 2.873 Å from the heme of CYP26A1, CYP26B1 and CYP26C1, respectively. Arg90 (CYP26A1), Arg373 (CYP26B1) and Trp65 (CYP26C1) were predicted to stabilize this conformation through hydrogen bonding interactions with the carboxylate moiety of adapalene. No orientations supportive of O-demethylation of adapalene were observed. Conversely, when des-adamantyl adapalene was docked in the three homology models in an attempt to rationalize the observed switch in metabolic sites, the molecule was positioned with the methoxy group oriented towards the heme for all three enzymes at an approximate distance of 2.598 Å (CYP26A1), 4.226 Å (CYP26B1) and 2.579 Å (CYP26C1). As with adapalene, Arg90 (CYP26A1) and Arg373 (CYP26B1) were hypothesized to stabilize the binding of des-adamantyl adapalene in the respective active sites through hydrogen bonding interactions with its carboxylate moiety (Figure 11-9). In the CYP26C1 homology model, the carboxylate moiety of des-adamantyl adapalene was located within 3 Å of Ser384.

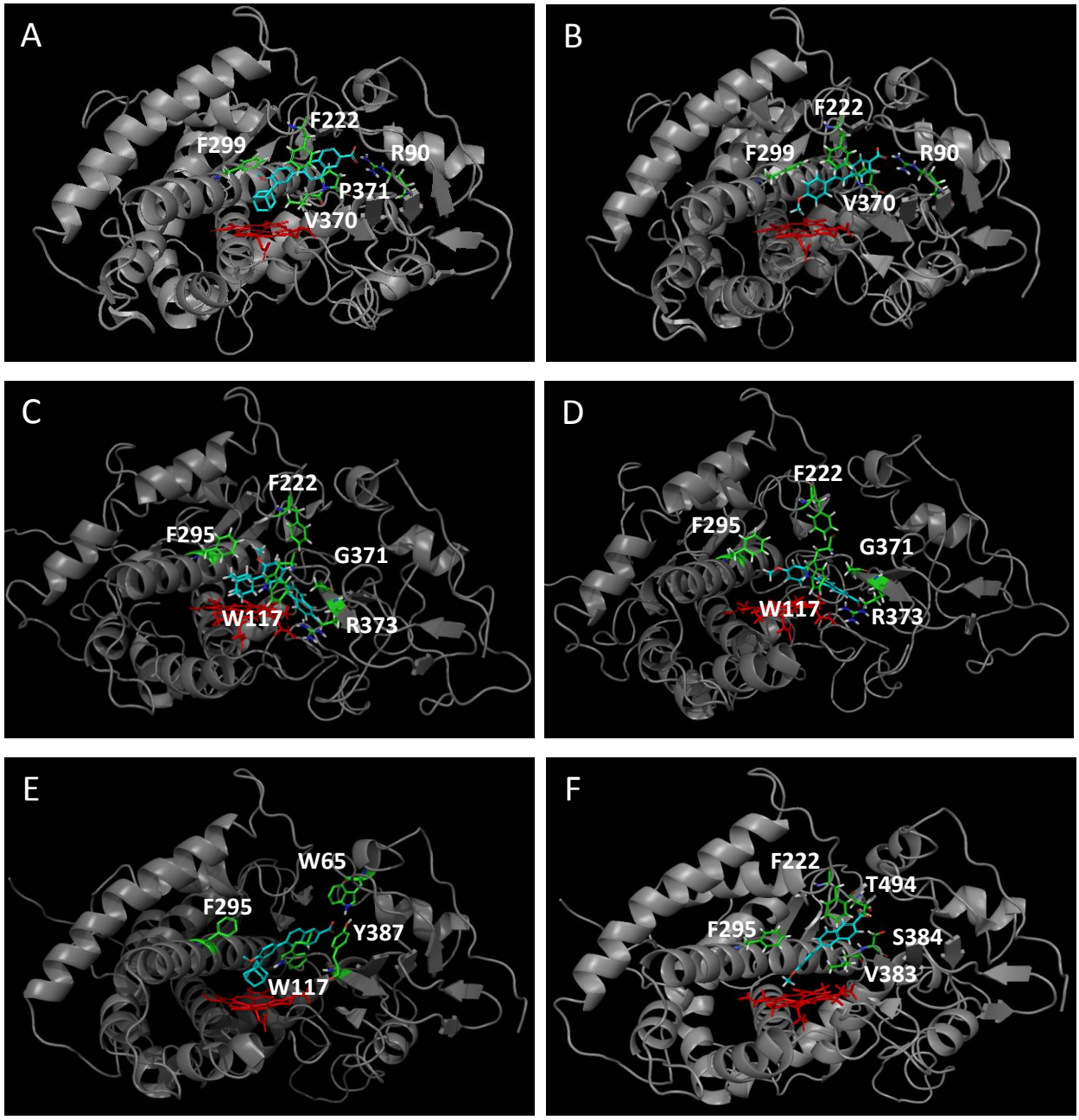

Figure 11-9. CYP26A1, CYP26B1 and CYP26C1 homology models with adapalene and des-adamantyl adapalene docked in the active site.

Docking of adapalene in the active sites of CYP26A1 (A), CYP26B1 (C) and CYP26C1 (E) suggested the preferred site of metabolism would be oxidation of the adamantyl moiety with no ability for the methoxy group to access the heme iron. Conversely, docking of des-adamantyl adapalene in the active site of CYP26A1 (B), CYP26B1 (D) or CYP26C1 (F) suggested O-demethylation as the primary route of metabolism.

11.3.4. Adapalene Phenotyping.

Adapalene was a chosen as a representative retinoic acid receptor agonist for further reaction phenotyping experiments because of its rates of metabolite formation in all of the recombinant CYP26 incubations. Using a full drug metabolizing enzyme panel, the enzymes responsible for the hydroxylation of adapalene were profiled. The highest rate of adapalene hydroxylation was observed with CYP26C1. Additional enzymes which contributed to the formation of the hydroxylated metabolite were CYP26B1, CYP3A5, CYP26A1 and CYP2C8 (Figure 11-10). Minor contributions were noted for CYP1A2, CYP3A4 and FMO5.

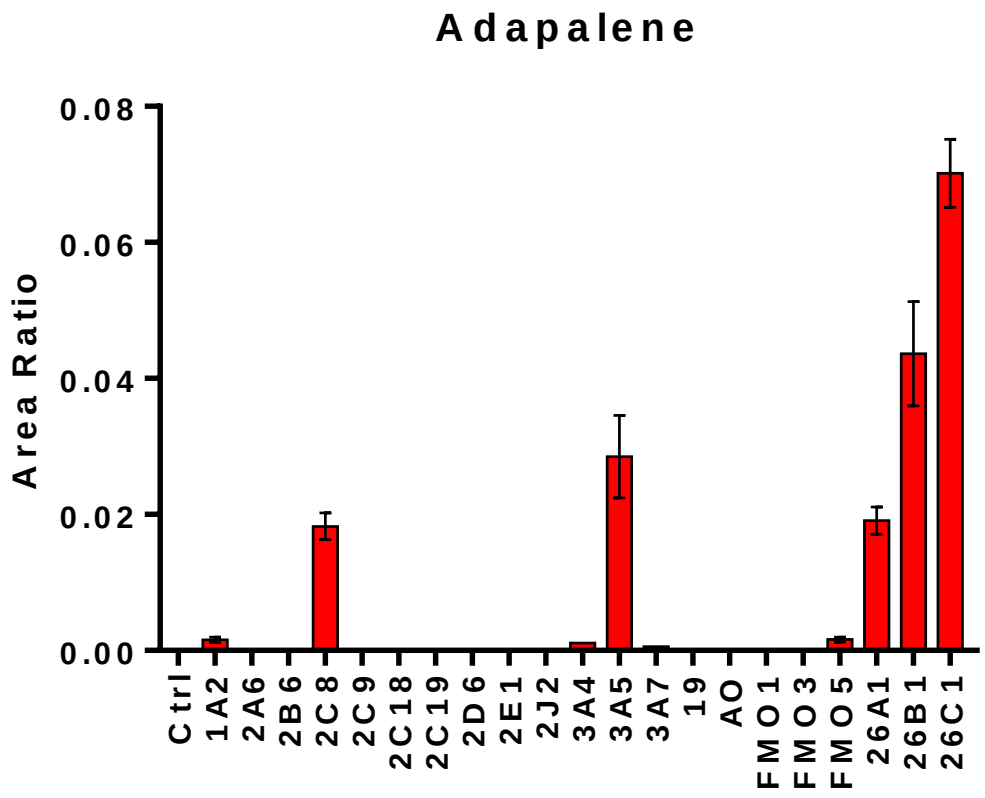

Figure 11-10. Formation of hydroxylated adapalene by recombinant drug metabolizing enzymes.

Reaction phenotyping experiments in recombinant enzymes identified the CYP26 enzymes, as well as CYP2C8 and CYP3A5, as major contributors to the hydroxylation of the adamantyl moiety of adapalene.

11.4. Discussion

Within the cytochrome P450 family of drug metabolizing enzymes, the CYP26 sub-family (CYP26A1, CYP26B1 and CYP261) plays a role in the homeostatic regulation of retinoic acid and has been shown to be capable of metabolizing the xenobiotic compound tazarotenic acid (Ray et al., 1997; Taimi et al., 2004; Guengerich, 2006; Lutz et al., 2009; Thatcher and Isoherranen, 2009; Ross and Zolfaghari, 2011; Foti et al., 2016). As mentioned previously, while both CYP26A1 and CYP26B1 share relatively broad expression patterns (less so for CYP26C1), relatively little information exists about the role the enzymes may play in the metabolism of xenobiotic compounds (Xi and Yang, 2008; Thatcher and Isoherranen, 2009; Thatcher et al., 2010; Topletz et al., 2012; Brown et al., 2014). To that end, the primary focus of the work presented in this manuscript was the further characterization of the in vitro metabolic capabilities of CYP26A1, CYP26B1 and CYP26C1.

While multiple homology models designed to assess the active site characteristics of CYP26A1 and CYP26B1 have been reported, much less is known about CYP26C1 (Gomaa et al., 2006; Karlsson et al., 2008; Gomaa et al., 2011a; Gomaa et al., 2011b; Saenz-Mendez et al., 2012; Foti et al., 2016). It has been previously determined that while CYP26C1 shares a 43% and 51% similarity in regard to the amino acid sequences of CYP26A1 and CYP26B1, respectively, its enzymatic profile differs somewhat from the other CYP26 isozymes (Taimi et al., 2004). Examination of the CYP26C1 homology model suggested that similar to CYP26A1 and CYP26B1, ligand interactions within the active site of CYP26C1 are primarily driven by lipophilic interactions coupled with amino acid residues capable of hydrogen bonding a carboxylate moiety as would be expected for an enzyme whose primary function is the metabolism of endogenous retinoids. The lipophilic triad of one tryptophan residue and two phenylalanine residues as key determinants of active site architecture appear to be conserved across the three CYP26 isozymes (CYP26A1: Trp112, Phe222, Phe299; CYP26B1 and CYP26C1: Trp117, Phe222 and Phe295). Similar to CYP26A1 (Arg90), a single binding

orientation within the active site of CYP26C1 appear to predominate, with the location of the carboxylate moiety being determined through interactions with Trp65, His73 and Tyr387 (Figure 11-7). Conversely, CYP26B1 appears to be capable of accommodating multiple binding orientations through carboxylate interactions with either Trp65 or Arg373 (Figure 9-3) (Foti et al., 2016). Interestingly, when *at*-RA was docked in the active site of CYP26C1, the preferred orientation suggested that formation of 16-hydroxy-*at*-RA would be the predominant metabolite, as opposed to what was observed with homology models of CYP26A1 and CYP26B1, where the models predicted formation of 4-hydroxy-*at*-RA to predominate. Though limited, in vitro data suggests that CYP26C1 is capable of catalyzing the metabolism of *at*-RA at multiple locations (Taimi et al., 2004).

Initial experiments aimed at determining the ability of the CYP26 enzymes to metabolize retinoic acid receptor agonists and antagonists indicated many of the compounds are metabolized by the CYP26s, many to an appreciable extent (Table 11-2). The compound with the greatest depletion over 20 minutes differed for each enzyme (CYP26A1, SR11237; CYP26B1, tazarotenic acid; CYP26C1, MM11253), suggesting differences in the catalytic profiles of each enzyme, and differences in the extent of metabolism between CYP26 and CYP2C8 or CYP3A4, two enzymes with overlapping substrate specificities with CYP26, were also observed. A screen for oxidative metabolites of the retinoic acid receptor agonists and antagonists identified a number of +16 amu metabolites which, as expected, were located on the end of the molecule most distal from the carboxylate moiety. Earlier in silico efforts also suggested the potential for adapalene and other retinoic acid-like compounds to be oxidized at multiple sites that were generally distal from the carboxylate moiety (Sloczynska et al., 2015). In a number of cases, however, discrepancies were observed when the rates of metabolite formation (Figure 11-4) were compared to the rates of compound depletion (Figure 11-3), as in the case of SR11373 and CYP26A1, where substrate depletion appears to be rapid but

metabolite formation is low compared to the other compounds. The finding suggests alternative routes of metabolism which were not adequately captured by the screen for +16 amu metabolites and warrants further investigation.

Adapalene was selected for further profiling based on its selectivity for the CYP26 isoforms over CYP2C8 or CYP3A4 as well as the observed rates of substrate depletion and metabolite formation (especially CYP26B1 and CYP26C1) as shown in Figures 11-3 and 11-4. The retinoic acid receptor agonist is a structurally-related naphthoic acid analog of retinoic acid that is primarily prescribed in the treatment of acne vulgaris (Brogden and Goa, 1997; Waugh et al., 2004; Alirezai et al., 2007; Irby et al., 2008). The introduction of the relatively large adamantyl moiety to the molecule presumably serves three purposes, namely mimicking the β-ionone ring of *at*-RA, limiting its percutaneous flux for toxicological purposes and providing steric hindrance around a metabolically favorable O-demethylation site (Pierard et al., 2009). Information around the routes of metabolism for adapalene is sparse, perhaps due to its limited absorption into circulation following topical administration (DIFFERIN_(Adapalene)_Prescribing_Information). When adapalene was incubated with recombinant CYP26A1, CYP26B1 or CYP26C1, a single hydroxylated metabolite was observed, with fragmentation patterns from mass spectral analyses suggesting hydroxylation on the adamantyl ring (Figure 11-5), with no evidence of adapalene O-demethylation observed. To test the hypothesis that lack of O-demethylation was due to steric hindrance from the adamantyl moiety, a des-adamantyl analog of adapalene was incubated in vitro with the three CYP26 isozymes. Upon incubation, a single O-demethylated metabolite was observed, with no additional metabolites being identified (Figure 11-6). Indeed, when adapalene was computationally docked into the active sites of CYP26A1, CYP26B1 and CYP26C1, a single binding orientation was observed, with the adamantyl ring system positioned within 3 Å of the heme prosthetic group (Figure 11-9). In this orientation, the methoxy group was unable to

obtain a metabolically favorable position in the active site, supporting the observed in vitro data and the role of the adamantyl ring in sterically hindering access of the methoxy hydrogens to the heme. Further, when the des-adamantyl analog was docked, the models predicted the methoxy group to be oriented towards the heme iron, suggesting O-demethylation to be the primary site of metabolism (Figure 11-9). The docking orientation of adapalene in the CYP26A1 and CYP26B1 models was similar to that previously reported for tazarotenic acid (Foti et al., 2016).

Given the observed catalysis of adapalene oxidation by CYP26A1, CYP26B1 and CYP26C1, experiments were undertaken to assess the relative contribution of the CYP26 enzymes versus other P450 isoforms to the overall metabolism of adapalene. Monitoring for the single hydroxylation product observed, CYP26C1, CYP26B1, CYP3A5, CYP2C8 and CYP26A1 were the major contributors to adapalene hydroxylation in vitro. Minor contributions were noted for CYP1A2, CYP3A4 and FMO5. The expression of CYP26A1, CYP26B1 and CYP26C1 mRNA in human skin cells has been reported, and as such, the potential exists for these enzymes to play a role in the metabolism of topically administered adapalene (Loudig et al., 2000; Abu-Abed et al., 2002; Taimi et al., 2004). However it is important to note that the relative protein expression levels of the CYP26 enzymes compared to the other cytochrome P450 enzymes is not yet understood and as such, additional efforts will be needed to conclusively determine the role of the CYP26s in the metabolism of adapalene and other retinoic acid receptor agonists and antagonists.

In conclusion, the results presented in this chapter further support the role of the CYP26 family of cytochrome P450 family of drug metabolizing enzymes in the metabolism of xenobiotic compounds. To our knowledge, it also describes the first homology model of CYP26C1 based on the crystal structure of CYP120. Comparison of the active site features of the CYP26C1 homology model to models of CYP26A1 and CYP26B1 suggest similar binding interactions that facilitate ligand recognition across the CYP26 isozymes. The data presented herein also

suggest that for topically administered compounds such as adapalene, enzymes such as CYP26A1, CYP26B1 or CYP26C1 may play a role in their metabolism. The increased understanding gained from characterizing the active sites of all three CYP26 enzymes and applying those learnings to identify their contributions to the metabolism of xenobiotics serves to significantly increase the awareness of the importance of CYP26A1, CYP26B1 and CYP26C1 in the field of drug metabolism.

12. Chapter V: General Conclusions

Retinoic acid is a homeostatically-controlled signaling molecule that regulates gene expression through interactions with the retinoic acid receptors, resulting in its key role in dermatological, immunological and neurological function (Asselineau et al., 1989; Duester, 2008; Niederreither and Dolle, 2008; Raverdeau et al., 2012; Ransom et al., 2014; Raverdeau and Mills, 2014; Cunningham and Duester, 2015). The initial steps in retinoic acid synthesis involve the formation of retinal from retinol (vitamin A), catalyzed by alcohol dehydrogenases and short-chain dehydrogenases, and the subsequent conversion of retinal to retinoic acid, catalyzed by retinaldehyde dehydrogenases (Roos et al., 1998; Chen et al., 2000b; Zhang et al., 2000; Marill et al., 2002). Retinoic acid is oxidatively metabolized to 4-hydroxy-, 16-hydroxy-, and 18-hydroxyretinoic acid, with CYP26A1, CYP26B1 and CYP26C1 having been characterized as the primary metabolic enzymes involved in the metabolism of *at*-RA and its metabolites with minor contributions from CYP2C8, CYP2C9 and CYP3A (Leo et al., 1989; Ray et al., 1997; Sonneveld et al., 1998; Nadin and Murray, 1999; Chen et al., 2000a; Marill et al., 2000; McSorley and Daly, 2000; Marill et al., 2002; Taimi et al., 2004; Guengerich, 2006; Lee et al., 2007; Lutz et al., 2009; Thatcher and Isoherranen, 2009; Thatcher et al., 2010; Helvig et al., 2011; Ross and Zolfaghari, 2011; Topletz et al., 2012; Nelson et al., 2013a).

While the understanding around the role of CYP26s in the metabolism of endogenous ligands has rapidly increased, knowledge of the role of these enzymes in the metabolism of xenobiotic compounds has been lacking. Combining the fact that CYP26A1 and CYP26B1 are expressed in human skin with the topical administration route of current retinoid-based interventions, there is clear possibility for the CYP26s to also contribute to the metabolism of synthetic retinoids (Heise et al., 2006; Osanai and Lee, 2011; Topletz et al., 2012). Though less is known about the expression and functional relevance of CYP26C1, the isoform shares a 43% and 51% sequence similarity in regard CYP26A1 and CYP26B1, respectively, and its catalytic preferences are thought to differ slightly from CYP26A1 and CYP26B1 (Taimi et al., 2004). Adding importance are the current efforts to design retinoids that do not have the

pharmacokinetic liabilities of *at*-RA, namely autoinduction of CYP26A1 and CYP26B1 (Muindi et al., 1992; Ray et al., 1997; Sonneveld et al., 1998; Tay et al., 2010). Further, while various efforts are underway to evaluate the inhibition of CYP26 in regard to pharmacological outcomes, less attention has been focused on the potential for clinically relevant drug interactions as a result of their inhibition. To that end, efforts to understand and characterize the structural aspects of CYP26A1, CYP26B1 and CYP26C1 which define the metabolic and inhibitory properties of the enzymes are highly warranted and may lend additional understanding around the development of new retinoid-like therapies.

A homology model approach based on the crystal structure of cyanobacterial CYP120 (pdb 2VE3) was chosen as the desired method to characterize the active sites and ligand binding properties of CYP26A1, CYP26B1 and CYP26C1. While CYP26A1 and CYP26C1 sequences were used directly from the currently available sequences (CYP26A1: GenBank ID: 2688846, UniProtKB O43174; CYP26C1: GenBank ID: 340665, UniProtKB Q6V0L0), previous work suggested potential discrepancies between the currently accepted gene sequence for CYP26B1 (NCBI Reference Sequence: NP_063938.1; UniProtKB Q9NR63, GenBank ID: 56603) and that of commercially available clones. It was determined that the amino acid residues at position 64 and 260 of the CYP26B1 protein sequence were an arginine (64) and serine (260), rather than a histidine and glycine as previously reported (White et al., 2000). From a functional aspect, however, neither residue appears to be directly involved in ligand binding.

A comprehensive analysis of three homology models suggests that all three CYP26 isoforms have relatively conserved hydrophobic regions within the active site and unique domains capable of stabilizing interactions with acidic groups such as the carboxylate moiety of *at*-RA. Three hydrophobic amino acids including a tryptophan residue and two phenylalanine residues appear to combine to delineate the active site boundaries of each enzyme and be involved in key hydrophobic bonding interactions: CYP26A1 – Trp112, Phe222, Phe299;

CYP26B1 and CYP26C1 – Trp117, Phe222 and Phe295. Spatially, CYP26A1 (Arg90) and CYP26C1 (Trp65, His73 and Tyr387) appear to promote a single binding orientation for molecules with a terminal acidic moiety while the active site of CYP26B1 appears to have two regions (Trp65/Tyr372 or Arg373) capable of interacting with acidic molecules (Foti et al., 2016). Earlier homology models of CYP26A1 or CYP26B1 have proposed Arg64 (Shimshoni et al., 2012), Arg86 (Gomaa et al., 2006) or Arg90 (Karlsson et al., 2008) for CYP26A1 and Arg95 and Ser369 for CYP26B1 (Karlsson et al., 2008; Saenz-Mendez et al., 2012). The models in this thesis, along with the CYP26A1 model in the paper by Shimshoni et al., are the only models currently supported by site of metabolism data for *at*-RA or other retinoids. Analysis of the active site volume of CYP26A1 (918 $Å^3$), CYP26B1 (977 $Å^3$) and CYP26C1 (1090 $Å^3$) identified similar binding capabilities for all the CYP26 isoforms and suggest the ability to bind not only endogenous retinoic acid but also larger xenobiotics, perhaps similar to what is observed for many of the other drug metabolizing cytochrome P450 enzymes.

While the homology models used in the current work were based on CYP120, previously published homology models of CYP26 have also evaluated CYP2C8 as a possible template, as it has been shown to be capable of binding retinoic acid and structurally related analogs and is currently the only metabolic enzyme which has been successfully crystallized while binding a retinoic acid isomer (Leo et al., 1989; Nadin and Murray, 1999; Yamazaki and Shimada, 1999; McSorley and Daly, 2000; Marill et al., 2002; Schoch et al., 2008; Saenz-Mendez et al., 2012). Given the functional similarities of CYP26A1, CYP26B1 and CYP2C8, the question of whether or not similarities exist among the active site characteristics of the three enzymes must be addressed. As inferred, superimposition of the crystal structure of CYP2C8 (pdb 1PQ2) with the CYP26 homology models indicated a high degree of similarity and identified amino acid residues capable of hydrogen bonding with carboxylic acid moieties in similar regions of their respective active sites. Similar to the CYP26 residues noted above, analysis of the crystal structure of CYP2C8 identified a key role for Gly98, Asn99 and Ser100 in orienting the

carboxylate of 9-cis-retinoic acid in the active site of CYP2C8 (Schoch et al., 2004; Schoch et al., 2008). The overall similarities provide a strong basis for the pharmacophores of CYP2C8 and CYP26A1 or CYP26B1 to exhibit significant similarities.

Though the ability to computationally dock a known enzyme inhibitor into a homology model of the enzymes implies that the structural characteristics of the model sufficiently capture the key attributes of the actual enzyme, the results give no indication as to whether or not the proposed binding orientation of the inhibitor is correct or not. Conversely, being able to correctly predict the orientation of a ligand in the active site of the enzyme that is consistent with known sites of metabolism of the ligand suggests the model is also capable of correctly orienting the ligand in the active site of the enzyme. As the reaction mechanism for the metabolism of *at*-RA to 4-hydroxyretinoic acid includes a hydrogen atom abstraction step at a pro-chiral center, the resulting orientations of *at*-RA in the active sites of the CYP26 models presented a key opportunity to test the robustness of each model. Further, previously published reports have shown that CYP26A1 stereoselecively catalyzes the formation of 4-(*S*)-hydroxy-*at*-RA while CYP26B1 is non-stereoselective in the metabolism of *at*-RA (Shimshoni et al., 2012; Topletz, 2013). Suggesting a high degree of structural integrity of the current models, when *at*-RA was computationally docked in the active site of the CYP26A1 model, only the hydrogen atom which when abstracted would lead to the formation of 4-(S)-hydroxy-*at*-RA was oriented towards the heme iron, with no resolved poses being able to support formation of 4-(R)-hydroxy-*at*-RA. Alternatively, the CYP26B1 homology model was able to resolve docking orientations which would lead to formation of either enantiomer of 4-hydroxy-*at*-RA, indicating that the key structural anomalies between the CYP26A1 and CYP26B1 which result in the stereoselective (or lack thereof) formation of 4-hydroxy-*at*-RA are adequately described by the models. Somewhat surprisingly, when *at*-RA was computationally docked in the CYP26C1 homology model, formation of 16-hydroxy-*at*-RA was suggested to the preferred metabolic transformation,

contrary to the results from the CYP26A1 and CYP26B1 homology models. This is perhaps supported by the limited in vitro data suggesting that the CYP26s metabolize *at*-RA at multiple locations (Taimi et al., 2004).

Though the ligand binding and resulting metabolism of *at*-RA by the CYP26s has been extensively characterized, there have not been any xenobiotic compounds identified as substrates for metabolism by the CYP26 family of enzymes. However, given the reported expression of CYP26A1 and CYP26B1 mRNA in human skin combined with the topical route of administration used for many retinoids and retinoic acid agonists and antagonists, we hypothesized that CYP26 may also play a role in the metabolism of these compounds (Heise et al., 2006; Osanai and Lee, 2011; Topletz et al., 2012). Utilizing in vitro metabolic stability assays, a number of retinoids were identified as substrates of CYP26, some to significant extents. Interestingly, the metabolic pattern was both substrate and enzyme dependent. For example, the retinoid with the highest rate of clearance over 20 minutes was different for each of the CYP26 isoforms, with SR11237, tazarotenic acid, and MM11253 being metabolized to the greatest extent by CYP26A1, CYP26B1 and CYP26C1, respectively. When quantitatively looking at the sites of metabolism of these compounds by CYP26, as expected, all of the compounds were oxidatively metabolized on the portion of the retinoid most opposite from the carboxylic acid functional group. This is in agreement with previously published computational studies suggesting that compounds such as adapalene generally tend to be oxidized at multiple sites by cytochrome P450 enzymes on the portion of the molecule most distal from the carboxylic acid (Sloczynska et al., 2015). Finally, it should be pointed out that metabolite formation rates did not always correlate with the rate of substrate depletion, suggesting that metabolites other than a simple hydroxylation may be formed by the CYP26 enzymes.

Based on the in vitro metabolism data, initial efforts focused on tazarotene, an acetylenic retinoid pro-drug which is hydrolyzed to tazarotenic acid upon topical administration and which is used to treat abnormal keratinocyte proliferation as well as adapalene, a naphthoic acid

containing retinoid that is generally used in the treatment of acne vulgaris (Brogden and Goa, 1997; Duvic, 1997; Madhu et al., 1997; Tang-Liu et al., 1999; Menter, 2000; Yu et al., 2003; Waugh et al., 2004; Attar et al., 2005; Alirezai et al., 2007; Irby et al., 2008; Talpur et al., 2009). Docking of tazarotenic acid in the active site of CYP26A1 and CYP26B1 identified a number of the same residues involved in orienting the compound in the active site as those important in binding retinoic acid. Residues such as Trp112, Phe222, Phe299, Thr304, Pro369 and Val370 (CYP26A1) and Trp65, Trp117, Thr121, Phe222, Phe295, Ser369, Val370 and Pro371 (CYP26B1) appear to be key in both delineating the steric boundaries of the active sites as well as in substrate binding (Gomaa et al., 2008; Karlsson et al., 2008; Gomaa et al., 2011a; Gomaa et al., 2011b; Saenz-Mendez et al., 2012). Perhaps more importantly, the ligand binding orientations resolved from the computational docking studies were supported by the results obtained from in vitro metabolite elucidation efforts which confirmed that tazarotenic acid is metabolized by CYP26A1 and CYP26B1 only on the benzothiopyranyl moiety of the molecule.

In order to verify the utility of the homology models with a second retinoid-like molecule as well as to assess the ability of CYP26 to metabolize compounds with sterically bulky functional groups, the metabolism of adapalene by CYP26A1, CYP26B1 and CYP26C1 was evaluated. As previously mentioned, the metabolism of many retinoids (as well as retinoic acid) occurs distal to the carboxylate moiety and as such, one can assume that the aim of including a sterically-hindering adamantyl group to the molecule was to block metabolic access to a energetically favorable O-demethylation pathway as well as to limit systemic exposure of adapalene after topical administration (Pierard et al., 2009). Indeed, in vitro metabolic incubations with adapalene and CYP26 identified a single site of oxidation presumed to be on the adamantyl ring. O-demethylation of adapalene was not observed. The in vitro evidence corroborated computational docking results with adapalene which suggested that the adamantyl ring would be the primary site of metabolism, with the methoxyl moiety unable to gain a metabolically favorable orientation to the heme iron. When a des-adamantyl version of

adapalene was computationally created and docked in the active site of the CYP26A1, CYP26B1 and CYP26C1 homology models, each model predicted the compound to be oriented in such a manner that O-demethylation would be the primary route of metabolism. Indeed, when this compound was synthesized and incubated with recombinant CYP26 membrane preparations, O-demethylation was the only metabolite observed, with no evidence of any other routes of metabolism. Taken as a whole, the data suggests that each of the CYP26 isoforms may be capable of accommodating sterically hindering moieties while metabolically switching to more favorable routes of metabolism, a fact which should be considered in the design of new retinoid therapeutics aimed at overcoming the pharmacokinetic shortfalls of *at*-RA.

To determine the overall contributions of the CYP26s to the metabolism of tazarotenic acid and adapalene, reaction phenotyping experiments were undertaken. Earlier reports have suggested that CYP2C8, FMO1 and FMO3 are primarily responsible for the sulfoxidation of tazarotenic acid, though these experiments were not carried out at clinically relevant concentrations of tazarotenic acid (Attar et al., 2003). There is no data currently available on the enzymes responsible for the metabolism of adapalene. At clinically relevant concentrations (100 nM), CYP26A1 and CYP26B1 were the two drug metabolizing enzymes which resulted in the greatest formation of tazarotenic acid sulfoxide and hydroxytazarotenic acid. Further, CYP26B1 and CYP26C1 showed the highest degree of adapalene hydroxylation, with CYP26A1 also playing a role. Additional drug metabolizing enzymes also were involved in the metabolism of tazarotenic acid (CYP2C8, CYP2C9, CYP2J2, CYP3A4, CYP3A5, CYP3A7 and aldehyde oxidase) and adapalene (CYP3A5, CYP2C8, CYP1A2, CYP3A4 and FMO5), though none to the extent of the CYP26s. As mRNA expression of CYP26A1, CYP26B1 and CYP26C1 in human skin cells has been previously reported, the possibility exists for CYP26 to play a role in the disposition of these compounds after topical administration (Loudig et al., 2000; Abu-Abed et al., 2002; Taimi et al., 2004). One caveat, however, is the lack of protein expression levels

for CYP26A1, CYP26B1 or CYP26C1 relative to other drug metabolizing enzymes in the skin, a piece of information that is critical to determining the overall contribution of the CYP26s to the metabolism of topically administered compounds.

After establishing the role of CYP26 in the metabolism of xenobiotic compounds, the potential for the enzymes to be involved in clinically-relevant drug interactions was explored. Taking advantage of the structural similarities between CYP26A1, CYP26B1 and CYP2C8, a set of known CYP2C8 inhibitors was used as the starting point for evaluating CYP26-mediated drug interactions. Using the recently developed tazarotenic acid sulfoxidation assay as a probe reaction of CYP26 activity in vitro, the inhibitory potency of known CYP26 and CYP2C8 inhibitors was measured. A comparison of IC_{50} values generated using tazarotenic acid versus 9-cis-retionic acid as the probe substrate indicated a statistically significant correlation between the two assays, though ultimately, the potential for differential inhibition profiles using the two assays cannot be ruled out. Of interest, more potent inhibition values were obtained with CYP26A1 when tazarotenic acid was the probe substrate and with CYP26B1 when 9-cis-retinoic acid was the substrate.

CYP2C8 is known to be involved in a number of clinically meaningful drug interactions with xenobiotics such as fluvoxamine, rosiglitazone, gemfibrozil, montelukast, rosiglitazone, pioglitazone, repaglidide, cerivastatin and loperamide (Backman et al., 2002; Niemi et al., 2003; Deng et al., 2005; Jaakkola et al., 2005; Niemi et al., 2006; Tornio et al., 2008; Karonen et al., 2010; Honkalammi et al., 2011). Furthermore, a significant amount of effort has gone into the characterization of the in vitro inhibition profile of CYP2C8 as well (Walsky et al., 2005; VandenBrink et al., 2011). When a panel of CYP2C8 inhibitors was screened for inhibition of CYP26A1 or CYP26B1, a number of potent and selective inhibitors were identified, including quercetin, fluconazole, benzbromarone, and zafirlukast for CYP26A1 and repaglinide for CYP26B1. The results suggest promising possibilities in terms of exploiting the active site

characteristics of each CYP26 isoform to identify new chemical matter that will result in selective chemical inhibition of one of the CYP26 isoforms. A comparison of the obtained CYP26A1 IC_{50} values with previously reported IC_{50} values for CYP2C8 revealed a statistically significant correlation ($r^2 = 0.849$), implying a potential overlap in the inhibitory pharmacophores of the two enzymes. Similar to what has been previously reported for compounds such as R115866, R116010 and ketoconazole, an in depth characterization of the spectral binding properties of clotrimazole revealed that the compound inhibits CYP26A1, CYP26B1 and CYP2C8 through type II heme-binding interactions (Thatcher et al., 2011). Computational docking experiments supported these findings, with the sp^2 nitrogen of clotrimazole's imidazole ring oriented within 3 Å of the heme iron in both homology models.

In order to translate the in vitro findings to potential in vivo outcomes, the well accepted approach of comparing in vitro inhibition potencies (IC_{50} or K_i) to free inhibitor concentrations in vivo ([I]) was utilized. In general, $[I]/K_i$ values of greater than 1 suggest the likely onset of a clinically significant drug interaction while any values between 0.1 and 1 imply that a drug interaction is possible (Bjornsson et al., 2003a; Bjornsson et al., 2003b; Kosugi et al., 2012). Using this approach, clotrimazole and fluconazole were identified as two potentially clinically relevant inhibitors of CYP26. The observed data suggests that fluconazole may have the potential to systemically inhibit CYP26 activity while the topical administration route of clotrimazole would most likely limit CYP26 drug interactions to the skin (Sawyer et al., 1975). Further, the data would seem to give credence to the role of CYP26 in previously observed drug interactions between fluconazole or clotrimazole and *at*-RA. For example, in at least one case study, co-administration of *at*-RA and fluconazole resulted in a 4-fold increase in the plasma exposure of *at*-RA, though the overall role of CYP26 in this interaction remains to be determined (Schwartz et al., 1995). In a second example, an increase in *at*-RA associated side effects were observed when *at*-RA was dosed with fluconazole and abated upon discontinuation of the

fluconazole regimen (Vanier et al., 2003). Pre-clinically, co-dosing of clotrimazole and *at*-RA to retinoic acid resistant cell lines resulted in the onset of cellular differentiation while co-administration to embryonic carcinoma cells resulted in the overall inhibition of *at*-RA metabolism (Williams and Napoli, 1987; Kizaki et al., 1996; Tiboni et al., 2009). As with the clinical data, the contributions of CYP26 to these drug interactions are worthy of additional consideration. Taken as a whole, the observed inhibition profiles of CYP26 in vivo suggest that the potential for meaningful CYP26-mediated drug interactions to occur in humans is a distinct possibility.

In conclusion, the research presented in this thesis details the first homology models of CYP26A1, CYP26B1 and CYP26C1 that are supported by metabolism data both from *at*-RA as well as xenobiotic substrates. In the process, the first known xenobiotic substrate of CYP26A1 and CYP26B1, tazarotenic acid, was identified. Subsequently, the catalytic pharmacophore of CYP26 was expanded to include other retinoids and retinoic acid receptor agonists and antagonists such as adapalene. In addition to the contributions of the enzymes to xenobiotic metabolism, their role in drug interactions was investigated with significant similarities to the inhibition profile of CYP2C8 being identified. Combined with the homology models, the data was used in an iterative fashion to compare the structural similarities and differences among the three CYP26 isoforms that lead to their catalytic and inhibitory properties and suggested the ability of the enzymes to bind larger, drug-like molecules in addition to their known pharmacophores. In its entirety, the data serves to increase the understanding of CYP26 ligand binding properties, information that should serve to further the pursuit of CYP26 as a drug target and expand the field of knowledge around its contributions to xenobiotic drug metabolism and drug interactions.

13. References

Abu-Abed S, MacLean G, Fraulob V, Chambon P, Petkovich M, and Dolle P (2002) Differential expression of the retinoic acid-metabolizing enzymes CYP26A1 and CYP26B1 during murine organogenesis. *Mechanisms of development* **110:**173-177.

Ahmad N and Mukhtar H (2004) Cytochrome P450: a target for drug development for skin diseases. *The Journal of investigative dermatology* **123:**417-425.

Al-Lazikani B, Jung J, Xiang Z, and Honig B (2001) Protein structure prediction. *Current opinion in chemical biology* **5:**51-56.

Alirezai M, George SA, Coutts I, Roseeuw DI, Hachem JP, Kerrouche N, Sidou F, and Soto P (2007) Daily treatment with adapalene gel 0.1% maintains initial improvement of acne vulgaris previously treated with oral lymecycline. *European journal of dermatology : EJD* **17:**45-51.

Altucci L, Leibowitz MD, Ogilvie KM, de Lera AR, and Gronemeyer H (2007) RAR and RXR modulation in cancer and metabolic disease. *Nature reviews Drug discovery* **6:**793-810.

Arimoto R (2006) Computational models for predicting interactions with cytochrome P450 enzyme. *Current topics in medicinal chemistry* **6:**1609-1618.

Asselineau D, Bernard BA, Bailly C, and Darmon M (1989) Retinoic acid improves epidermal morphogenesis. *Developmental biology* **133:**322-335.

Attar M, Dong D, Ling KH, and Tang-Liu DD (2003) Cytochrome P450 2C8 and flavin-containing monooxygenases are involved in the metabolism of tazarotenic acid in humans. *Drug metabolism and disposition: the biological fate of chemicals* **31:**476-481.

Attar M, Yu D, Ni J, Yu Z, Ling KH, and Tang-Liu DD (2005) Disposition and biotransformation of the acetylenic retinoid tazarotene in humans. *Journal of pharmaceutical sciences* **94:**2246-2255.

Backman JT, Kyrklund C, Neuvonen M, and Neuvonen PJ (2002) Gemfibrozil greatly increases plasma concentrations of cerivastatin. *Clinical pharmacology and therapeutics* **72:**685-691.

Berman HM, Westbrook J, Feng Z, Gilliland G, Bhat TN, Weissig H, Shindyalov IN, and Bourne PE (2000) The Protein Data Bank. *Nucleic acids research* **28:**235-242.

Bjornsson TD, Callaghan JT, Einolf HJ, Fischer V, Gan L, Grimm S, Kao J, King SP, Miwa G, Ni L, Kumar G, McLeod J, Obach RS, Roberts S, Roe A, Shah A, Snikeris F, Sullivan JT, Tweedie D, Vega JM, Walsh J, Wrighton SA, Pharmaceutical R, Manufacturers of America Drug Metabolism/Clinical Pharmacology Technical Working G, Evaluation FDACfD, and Research (2003a) The conduct of in vitro and in vivo drug-drug interaction studies: a Pharmaceutical Research and Manufacturers of America (PhRMA) perspective. *Drug metabolism and disposition: the biological fate of chemicals* **31:**815-832.

Bjornsson TD, Callaghan JT, Einolf HJ, Fischer V, Gan L, Grimm S, Kao J, King SP, Miwa G, Ni L, Kumar G, McLeod J, Obach SR, Roberts S, Roe A, Shah A, Snikeris F, Sullivan JT, Tweedie D, Vega JM, Walsh J, Wrighton SA, Pharmaceutical R, and Manufacturers of America Drug Metabolism/Clinical Pharmacology Technical Working G (2003b) The conduct of in vitro and in vivo drug-drug interaction studies: a PhRMA perspective. *Journal of clinical pharmacology* **43:**443-469.

Blobaum AL (2006) Mechanism-based inactivation and reversibility: is there a new trend in the inactivation of cytochrome p450 enzymes? *Drug metabolism and disposition: the biological fate of chemicals* **34:**1-7.

Blundell TL, Sibanda BL, Montalvao RW, Brewerton S, Chelliah V, Worth CL, Harmer NJ, Davies O, and Burke D (2006) Structural biology and bioinformatics in drug design: opportunities and challenges for target identification and lead discovery. *Philosophical transactions of the Royal Society of London Series B, Biological sciences* **361:**413-423.

Blundell TL, Sibanda BL, Sternberg MJ, and Thornton JM (1987) Knowledge-based prediction of protein structures and the design of novel molecules. *Nature* **326:**347-352.

Boulton DW, Walle UK, and Walle T (1998) Extensive binding of the bioflavonoid quercetin to human plasma proteins. *The Journal of pharmacy and pharmacology* **50:**243-249.

Brand N, Petkovich M, Krust A, Chambon P, de The H, Marchio A, Tiollais P, and Dejean A (1988) Identification of a second human retinoic acid receptor. *Nature* **332:**850-853.

Brogden RN and Goa KE (1997) Adapalene. A review of its pharmacological properties and clinical potential in the management of mild to moderate acne. *Drugs* **53:**511-519.

Brown GT, Cash BG, Blihoghe D, Johansson P, Alnabulsi A, and Murray GI (2014) The expression and prognostic significance of retinoic acid metabolising enzymes in colorectal cancer. *PloS one* **9:**e90776.

Browne WJ, North AC, Phillips DC, Brew K, Vanaman TC, and Hill RL (1969) A possible three-dimensional structure of bovine alpha-lactalbumin based on that of hen's egg-white lysozyme. *Journal of molecular biology* **42:**65-86.

Buttrick BR (2012) Characterization of selective and potent inhibitors of the human retinoic acid hydroxylases CYP26A1 and CYP26B1, in: *Pharmaceutics*, University of Washington, Seattle, WA.

Cavasotto CN and Phatak SS (2009) Homology modeling in drug discovery: current trends and applications. *Drug discovery today* **14:**676-683.

Chandraratna RA (1996) Tazarotene--first of a new generation of receptor-selective retinoids. *The British journal of dermatology* **135 Suppl 49:**18-25.

Charpentier B, Bernardon JM, Eustache J, Millois C, Martin B, Michel S, and Shroot B (1995) Synthesis, structure-affinity relationships, and biological activities of ligands binding to retinoic acid receptor subtypes. *Journal of medicinal chemistry* **38:**4993-5006.

Chen H, Fantel AG, and Juchau MR (2000a) Catalysis of the 4-hydroxylation of retinoic acids by cyp3a7 in human fetal hepatic tissues. *Drug metabolism and disposition: the biological fate of chemicals* **28:**1051-1057.

Chen H, Howald WN, and Juchau MR (2000b) Biosynthesis of all-trans-retinoic acid from all-trans-retinol: catalysis of all-trans-retinol oxidation by human P-450 cytochromes. *Drug metabolism and disposition: the biological fate of chemicals* **28:**315-322.

Clagett-Dame M and DeLuca HF (2002) The role of vitamin A in mammalian reproduction and embryonic development. *Annual review of nutrition* **22:**347-381.

Cosme J and Johnson EF (2000) Engineering microsomal cytochrome P450 2C5 to be a soluble, monomeric enzyme. Mutations that alter aggregation, phospholipid dependence of catalysis, and membrane binding. *The Journal of biological chemistry* **275:**2545-2553.

Cunningham TJ and Duester G (2015) Mechanisms of retinoic acid signalling and its roles in organ and limb development. *Nature reviews Molecular cell biology* **16:**110-123.

Czaplewski C, Rodziewicz-Motowidlo S, Dabal M, Liwo A, Ripoll DR, and Scheraga HA (2003) Molecular simulation study of cooperativity in hydrophobic association: clusters of four hydrophobic particles. *Biophysical chemistry* **105:**339-359.

Czaplewski C, Rodziewicz-Motowidlo S, Liwo A, Ripoll DR, Wawak RJ, and Scheraga HA (2000) Molecular simulation study of cooperativity in hydrophobic association. *Protein science : a publication of the Protein Society* **9:**1235-1245.

Daley-Yates PT, Kunka RL, Yin Y, Andrews SM, Callejas S, and Ng C (2004) Bioavailability of fluticasone propionate and mometasone furoate aqueous nasal sprays. *European journal of clinical pharmacology* **60:**265-268.

De Coster R, Wouters W, Van Ginckel R, End D, Krekels M, Coene MC, and Bowden C (1992) Experimental studies with liarozole (R 75,251): an antitumoral agent which inhibits retinoic acid breakdown. *The Journal of steroid biochemistry and molecular biology* **43:**197-201.

Deng LJ, Wang F, and Li HD (2005) Effect of gemfibrozil on the pharmacokinetics of pioglitazone. *European journal of clinical pharmacology* **61:**831-836.

Deshpande (2013) Evaluation of Topical Bioavailability of Clotrimazole Using DermatoPharmacoKinetic Method. *Int J Sci Inv Today* **2:**216-225.

di Masi A, Leboffe L, De Marinis E, Pagano F, Cicconi L, Rochette-Egly C, Lo-Coco F, Ascenzi P, and Nervi C (2015) Retinoic acid receptors: from molecular mechanisms to cancer therapy. *Molecular aspects of medicine* **41:**1-115.

DIFFERIN_(Adapalene)_Prescribing_Information.

Ding X and Kaminsky LS (2003) Human extrahepatic cytochromes P450: function in xenobiotic metabolism and tissue-selective chemical toxicity in the respiratory and gastrointestinal tracts. *Annual review of pharmacology and toxicology* **43:**149-173.

Duester G (2008) Retinoic acid synthesis and signaling during early organogenesis. *Cell* **134:**921-931.

Duvic M (1997) Tazarotene: a review of its pharmacological profile and potential for clinical use in psoriasis. *Expert opinion on investigational drugs* **6:**1537-1551.

Eksterowicz J, Rock DA, Rock BM, Wienkers LC, and Foti RS (2014) Characterization of the active site properties of CYP4F12. *Drug metabolism and disposition: the biological fate of chemicals* **42:**1698-1707.

Filppula AM, Laitila J, Neuvonen PJ, and Backman JT (2011) Reevaluation of the microsomal metabolism of montelukast: major contribution by CYP2C8 at clinically relevant concentrations. *Drug metabolism and disposition: the biological fate of chemicals* **39:**904-911.

Fiorella PD and Napoli JL (1991) Expression of cellular retinoic acid binding protein (CRABP) in Escherichia coli. Characterization and evidence that holo-CRABP is a substrate in retinoic acid metabolism. *The Journal of biological chemistry* **266:**16572-16579.

Foti RS and Fisher MB (2004) Impact of incubation conditions on bufuralol human clearance predictions: enzyme lability and nonspecific binding. *Drug metabolism and disposition: the biological fate of chemicals* **32:**295-304.

Foti RS, Honaker M, Nath A, Pearson JT, Buttrick B, Isoherranen N, and Atkins WM (2011) Catalytic versus inhibitory promiscuity in cytochrome P450s: implications for evolution of new function. *Biochemistry* **50:**2387-2393.

Foti RS, Isoherranen N, Zelter A, Dickmann LJ, Buttrick BR, Diaz P, and Douguet D (2016) Identification of Tazarotenic Acid as the First Xenobiotic Substrate of Human Retinoic Acid Hydroxylase CYP26A1 and CYP26B1. *J Pharm Exp Ther*.

Foti RS, Wienkers LC, and Wahlstrom JL (2010) Application of cytochrome P450 drug interaction screening in drug discovery. *Combinatorial chemistry & high throughput screening* **13:**145-158.

Friesner RA, Banks JL, Murphy RB, Halgren TA, Klicic JJ, Mainz DT, Repasky MP, Knoll EH, Shelley M, Perry JK, Shaw DE, Francis P, and Shenkin PS (2004) Glide: a new approach for rapid, accurate docking and scoring. 1. Method and assessment of docking accuracy. *Journal of medicinal chemistry* **47:**1739-1749.

Friesner RA, Murphy RB, Repasky MP, Frye LL, Greenwood JR, Halgren TA, Sanschagrin PC, and Mainz DT (2006) Extra precision glide: docking and scoring incorporating a model of hydrophobic enclosure for protein-ligand complexes. *Journal of medicinal chemistry* **49:**6177-6196.

Giguere V (1994) Retinoic acid receptors and cellular retinoid binding proteins: complex interplay in retinoid signaling. *Endocrine reviews* **15:**61-79.

Giguere V, Ong ES, Segui P, and Evans RM (1987) Identification of a receptor for the morphogen retinoic acid. *Nature* **330:**624-629.

Gleiter CH and Morike KE (2002) Clinical pharmacokinetics of candesartan. *Clinical pharmacokinetics* **41:**7-17.

Gomaa MS, Armstrong JL, Bobillon B, Veal GJ, Brancale A, Redfern CP, and Simons C (2008) Novel azolyl-(phenylmethyl)]aryl/heteroarylamines: potent CYP26 inhibitors and enhancers of all-trans retinoic acid activity in neuroblastoma cells. *Bioorganic & medicinal chemistry* **16:**8301-8313.

Gomaa MS, Bridgens CE, Aboraia AS, Veal GJ, Redfern CP, Brancale A, Armstrong JL, and Simons C (2011a) Small molecule inhibitors of retinoic acid 4-hydroxylase (CYP26): synthesis and biological evaluation of imidazole methyl 3-(4-(aryl-2-ylamino)phenyl)propanoates. *Journal of medicinal chemistry* **54:**2778-2791.

Gomaa MS, Bridgens CE, Veal GJ, Redfern CP, Brancale A, Armstrong JL, and Simons C (2011b) Synthesis and biological evaluation of 3-(1H-imidazol- and triazol-1-yl)-2,2-dimethyl-3-[4-(naphthalen-2-ylamino)phenyl]propyl derivatives as small molecule inhibitors of retinoic acid 4-hydroxylase (CYP26). *Journal of medicinal chemistry* **54:**6803-6811.

Gomaa MS, Yee SW, Milbourne CE, Barbera MC, Simons C, and Brancale A (2006) Homology model of human retinoic acid metabolising enzyme cytochrome P450 26A1 (CYP26A1): active site architecture and ligand binding. *Journal of enzyme inhibition and medicinal chemistry* **21:**361-369.

Goodman and Gilman (2006) *Goodman and Gilman's The Pharmacological Basis of Therapeutics*. McGraw-Hill Companies, Inc, USA.

Greer J (1990) Comparative modeling methods: application to the family of the mammalian serine proteases. *Proteins* **7:**317-334.

Gudas LJ and Wagner JA (2011) Retinoids regulate stem cell differentiation. *Journal of cellular physiology* **226:**322-330.

Guengerich FP (2005) Human Cytochrome P450 Enzymes, in: *Cytochrome P450: Structure, Mechanism, and Biochemistry* (Ortiz de Montellano PR ed), Kluwer Academic / Plenum, New York.

Guengerich FP (2006) Human Cytochrome P450 Enzymes, in: *Cytochrome P450: Structure, Mechanism, and Biochemistry* (Ortiz de Montellano PR ed), pp 377-574, Kluwer Academic / Plenum Publishers, New York.

Heise R, Mey J, Neis MM, Marquardt Y, Joussen S, Ott H, Wiederholt T, Kurschat P, Megahed M, Bickers DR, Merk HF, and Baron JM (2006) Skin Retinoid Concentrations Are Modulated by CYP26AI Expression Restricted to Basal Keratinocytes in Normal Human Skin and Differentiated 3D Skin Models. *The Journal of investigative dermatology* **126:**2473-2480.

Helvig C, Taimi M, Cameron D, Jones G, and Petkovich M (2011) Functional properties and substrate characterization of human CYP26A1, CYP26B1, and CYP26C1 expressed by recombinant baculovirus in insect cells. *Journal of pharmacological and toxicological methods* **64:**258-263.

Hillisch A, Pineda LF, and Hilgenfeld R (2004) Utility of homology models in the drug discovery process. *Drug discovery today* **9:**659-669.

Honkalammi J, Niemi M, Neuvonen PJ, and Backman JT (2011) Dose-dependent interaction between gemfibrozil and repaglinide in humans: strong inhibition of CYP2C8 with subtherapeutic gemfibrozil doses. *Drug metabolism and disposition: the biological fate of chemicals* **39:**1977-1986.

Hooft RW, Vriend G, Sander C, and Abola EE (1996) Errors in protein structures. *Nature* **381:**272.

http://www.drugbank.ca/ DrugBank: Open Data Drug and Drug Target Database.

Irby CE, Yentzer BA, and Feldman SR (2008) A review of adapalene in the treatment of acne vulgaris. *The Journal of adolescent health : official publication of the Society for Adolescent Medicine* **43:**421-424.

Iyanagi T and Mason HS (1973) Some properties of hepatic reduced nicotinamide adenine dinucleotide phosphate-cytochrome c reductase. *Biochemistry* **12:**2297-2308.

Jaakkola T, Backman JT, Neuvonen M, and Neuvonen PJ (2005) Effects of gemfibrozil, itraconazole, and their combination on the pharmacokinetics of pioglitazone. *Clinical pharmacology and therapeutics* **77:**404-414.

Jacobson MP, Pincus DL, Rapp CS, Day TJ, Honig B, Shaw DE, and Friesner RA (2004) A hierarchical approach to all-atom protein loop prediction. *Proteins* **55:**351-367.

John B and Sali A (2003) Comparative protein structure modeling by iterative alignment, model building and model assessment. *Nucleic acids research* **31:**3982-3992.

Jorgensen WL, Maxwell DS, and Tirado-Rives J (1996) Development and Testing of the OPLS All-Atom Force Field on Conformational Energetics and Properties of Organic Liquids. *Journal of the American Chemical Society* **118:**11225-11236.

Jorgensen WL and Tirado-Rives J (1988) The OPLS [optimized potentials for liquid simulations] potential functions for proteins, energy minimizations for crystals of cyclic peptides and crambin. *Journal of the American Chemical Society* **110:**1657-1666.

Jorgensen WL and Tirado-Rives J (2005) Potential energy functions for atomic-level simulations of water and organic and biomolecular systems. *Proceedings of the National Academy of Sciences of the United States of America* **102:**6665-6670.

Kaminski G, Duffy EM, Matsui T, and Jorgensen WL (1994) Free Energies of Hydration and Pure Liquid Properties of Hydrocarbons from the OPLS All-Atom Model. *The Journal of Physical Chemistry* **98:**13077-13082.

Karlsson M, Strid Å, Sirsjö A, and Eriksson LA (2008) Homology Models and Molecular Modeling of Human Retinoic Acid Metabolizing Enzymes Cytochrome P450 26A1 (CYP26A1) and P450 26B1 (CYP26B1). *Journal of Chemical Theory and Computation* **4:**1021-1027.

Karonen T, Filppula A, Laitila J, Niemi M, Neuvonen PJ, and Backman JT (2010) Gemfibrozil markedly increases the plasma concentrations of montelukast: a previously

unrecognized role for CYP2C8 in the metabolism of montelukast. *Clinical pharmacology and therapeutics* **88:**223-230.

Karonen T, Neuvonen PJ, and Backman JT (2011) The CYP2C8 inhibitor gemfibrozil does not affect the pharmacokinetics of zafirlukast. *European journal of clinical pharmacology* **67:**151-155.

Karonen T, Neuvonen PJ, and Backman JT (2012) CYP2C8 but not CYP3A4 is important in the pharmacokinetics of montelukast. *British journal of clinical pharmacology* **73:**257-267.

Kerdpin O, Elliot DJ, Boye SL, Birkett DJ, Yoovathaworn K, and Miners JO (2004) Differential contribution of active site residues in substrate recognition sites 1 and 5 to cytochrome P450 2C8 substrate selectivity and regioselectivity. *Biochemistry* **43:**7834-7842.

Khan FI, Wei DQ, Gu KR, Hassan MI, and Tabrez S (2016) Current updates on computer aided protein modeling and designing. *International journal of biological macromolecules* **85:**48-62.

Kizaki M, Ueno H, Yamazoe Y, Shimada M, Takayama N, Muto A, Matsushita H, Nakajima H, Morikawa M, Koeffler HP, and Ikeda Y (1996) Mechanisms of retinoid resistance in leukemic cells: possible role of cytochrome P450 and P-glycoprotein. *Blood* **87:**725-733.

Kosugi Y, Hirabayashi H, Igari T, Fujioka Y, Hara Y, Okuda T, and Moriwaki T (2012) Evaluation of cytochrome P450-mediated drug-drug interactions based on the strategies recommended by regulatory authorities. *Xenobiotica; the fate of foreign compounds in biological systems* **42:**127-138.

Krieger E, Koraimann G, and Vriend G (2002) Increasing the precision of comparative models with YASARA NOVA--a self-parameterizing force field. *Proteins* **47:**393-402.

Krieger E, Nabuurs SB, and Vriend G (2003) Homology Modeling, in: *Structural Bioinformatics* (Bourne PE and Weissig H eds), Wiley-Liss, Inc., New York.

Kuenzli S and Saurat JH (2001) Retinoids for the treatment of psoriasis: outlook for the future. *Current opinion in investigational drugs* **2:**625-630.

Lai XS, Yang LP, Li XT, Liu JP, Zhou ZW, and Zhou SF (2009) Human CYP2C8: structure, substrate specificity, inhibitor selectivity, inducers and polymorphisms. *Current drug metabolism* **10:**1009-1047.

Lazaridis T and Karplus M (1999) Discrimination of the native from misfolded protein models with an energy function including implicit solvation. *Journal of molecular biology* **288:**477-487.

Lee SJ, Perera L, Coulter SJ, Mohrenweiser HW, Jetten A, and Goldstein JA (2007) The discovery of new coding alleles of human CYP26A1 that are potentially defective in the metabolism of all-trans retinoic acid and their assessment in a recombinant cDNA expression system. *Pharmacogenetics and genomics* **17:**169-180.

Leo MA, Lasker JM, Raucy JL, Kim CI, Black M, and Lieber CS (1989) Metabolism of retinol and retinoic acid by human liver cytochrome P450IIC8. *Archives of biochemistry and biophysics* **269:**305-312.

Lesk AM and Chothia C (1986) The response of protein structures to amino-acid sequence changes. *Philos Trans R Soc Lond B Biol Sci* **317:**345-356.

Levin AA, Sturzenbecker LJ, Kazmer S, Bosakowski T, Huselton C, Allenby G, Speck J, Kratzeisen C, Rosenberger M, Lovey A, and et al. (1992) 9-cis retinoic acid stereoisomer binds and activates the nuclear receptor RXR alpha. *Nature* **355:**359-361.

Lewis DF (2002) Molecular modeling of human cytochrome P450-substrate interactions. *Drug metabolism reviews* **34:**55-67.

Liu H, Elstner M, Kaxiras E, Frauenheim T, Hermans J, and Yang W (2001) Quantum mechanics simulation of protein dynamics on long timescale. *Proteins* **44:**484-489.

Lopez-Rangel E and Van Allen MI (2005) Prenatal exposure to fluconazole: an identifiable dysmorphic phenotype. *Birth defects research Part A, Clinical and molecular teratology* **73:**919-923.

Lotan R (1980) Effects of vitamin A and its analogs (retinoids) on normal and neoplastic cells. *Biochimica et biophysica acta* **605:**33-91.

Loudig O, Babichuk C, White J, Abu-Abed S, Mueller C, and Petkovich M (2000) Cytochrome P450RAI(CYP26) promoter: a distinct composite retinoic acid response element underlies the complex regulation of retinoic acid metabolism. *Molecular endocrinology* **14:**1483-1497.

Lutz JD, Dixit V, Yeung CK, Dickmann LJ, Zelter A, Thatcher JE, Nelson WL, and Isoherranen N (2009) Expression and functional characterization of cytochrome P450 26A1, a retinoic acid hydroxylase. *Biochemical pharmacology* **77:**258-268.

Mackerell AD, Jr. (2004) Empirical force fields for biological macromolecules: overview and issues. *Journal of computational chemistry* **25:**1584-1604.

Maden M (2002) Retinoid signalling in the development of the central nervous system. *Nature reviews Neuroscience* **3:**843-853.

Madhu C, Duff S, Baumgarten V, Rix P, Small D, and Tang-Liu D (1997) Metabolic deesterification of tazarotene in human blood and rat and human liver microsomes. *Journal of pharmaceutical sciences* **86:**972-974.

Mangelsdorf DJ, Borgmeyer U, Heyman RA, Zhou JY, Ong ES, Oro AE, Kakizuka A, and Evans RM (1992) Characterization of three RXR genes that mediate the action of 9-cis retinoic acid. *Genes & development* **6:**329-344.

Marill J, Capron CC, Idres N, and Chabot GG (2002) Human cytochrome P450s involved in the metabolism of 9-cis- and 13-cis-retinoic acids. *Biochemical pharmacology* **63:**933-943.

Marill J, Cresteil T, Lanotte M, and Chabot GG (2000) Identification of human cytochrome P450s involved in the formation of all-trans-retinoic acid principal metabolites. *Mol Pharmacol* **58:**1341-1348.

Marill J, Idres N, Capron CC, Nguyen E, and Chabot GG (2003) Retinoic acid metabolism and mechanism of action: a review. *Current drug metabolism* **4:**1-10.

Mark M, Ghyselinck NB, and Chambon P (2006) Function of retinoid nuclear receptors: lessons from genetic and pharmacological dissections of the retinoic acid signaling pathway during mouse embryogenesis. *Annual review of pharmacology and toxicology* **46:**451-480.

Marti-Renom MA, Stuart AC, Fiser A, Sanchez R, Melo F, and Sali A (2000) Comparative protein structure modeling of genes and genomes. *Annual review of biophysics and biomolecular structure* **29:**291-325.

McCaffery P and Drager UC (2000) Regulation of retinoic acid signaling in the embryonic nervous system: a master differentiation factor. *Cytokine & growth factor reviews* **11:**233-249.

McDougle DR, Palaria A, Magnetta E, Meling DD, and Das A (2013) Functional studies of N-terminally modified CYP2J2 epoxygenase in model lipid bilayers. *Protein science : a publication of the Protein Society* **22:**964-979.

McSorley LC and Daly AK (2000) Identification of human cytochrome P450 isoforms that contribute to all-trans-retinoic acid 4-hydroxylation. *Biochemical pharmacology* **60:**517-526.

Melet A, Marques-Soares C, Schoch GA, Macherey AC, Jaouen M, Dansette PM, Sari MA, Johnson EF, and Mansuy D (2004) Analysis of human cytochrome P450 2C8 substrate specificity using a substrate pharmacophore and site-directed mutants. *Biochemistry* **43:**15379-15392.

Menegola E, Broccia ML, Di Renzo F, and Giavini E (2001) Antifungal triazoles induce malformations in vitro. *Reproductive toxicology* **15:**421-427.

Menter A (2000) Pharmacokinetics and safety of tazarotene. *Journal of the American Academy of Dermatology* **43:**S31-35.

Miller WH, Jr. (1998) The emerging role of retinoids and retinoic acid metabolism blocking agents in the treatment of cancer. *Cancer* **83:**1471-1482.

Moon YJ, Wang L, DiCenzo R, and Morris ME (2008) Quercetin pharmacokinetics in humans. *Biopharmaceutics & drug disposition* **29:**205-217.

Morris AL, MacArthur MW, Hutchinson EG, and Thornton JM (1992) Stereochemical quality of protein structure coordinates. *Proteins* **12:**345-364.

Muindi J, Frankel SR, Miller WH, Jr., Jakubowski A, Scheinberg DA, Young CW, Dmitrovsky E, and Warrell RP, Jr. (1992) Continuous treatment with all-trans retinoic acid causes a progressive reduction in plasma drug concentrations: implications for relapse and retinoid "resistance" in patients with acute promyelocytic leukemia. *Blood* **79:**299-303.

Murzin AG (2001) Progress in protein structure prediction. *Nature structural biology* **8:**110-112.

Nadin L and Murray M (1999) Participation of CYP2C8 in retinoic acid 4-hydroxylation in human hepatic microsomes. *Biochemical pharmacology* **58:**1201-1208.

Nath A, Zientek MA, Burke BJ, Jiang Y, and Atkins WM (2010) Quantifying and predicting the promiscuity and isoform specificity of small-molecule cytochrome P450 inhibitors. *Drug metabolism and disposition: the biological fate of chemicals* **38:**2195-2203.

Nayeem A, Sitkoff D, and Krystek S, Jr. (2006) A comparative study of available software for high-accuracy homology modeling: from sequence alignments to structural models. *Protein science : a publication of the Protein Society* **15:**808-824.

Nelson CH, Buttrick BR, and Isoherranen N (2013a) Therapeutic potential of the inhibition of the retinoic acid hydroxylases CYP26A1 and CYP26B1 by xenobiotics. *Current topics in medicinal chemistry* **13:**1402-1428.

Nelson CH, Lutz JD, and Isoherranen N (2013b) Cellular retinoic acid binding proteins (CRABPs) channel retinoic acid to CYP26A1. *The FASEB Journal* **27:**892.896.

Nelson DR (2006) Cytochrome P450 nomenclature, 2004. *Methods in molecular biology* **320:**1-10.

Niederreither K and Dolle P (2008) Retinoic acid in development: towards an integrated view. *Nature reviews Genetics* **9:**541-553.

Niemi M, Backman JT, Granfors M, Laitila J, Neuvonen M, and Neuvonen PJ (2003) Gemfibrozil considerably increases the plasma concentrations of rosiglitazone. *Diabetologia* **46:**1319-1323.

Niemi M, Tornio A, Pasanen MK, Fredrikson H, Neuvonen PJ, and Backman JT (2006) Itraconazole, gemfibrozil and their combination markedly raise the plasma concentrations of loperamide. *European journal of clinical pharmacology* **62:**463-472.

Njar VC (2002) Cytochrome p450 retinoic acid 4-hydroxylase inhibitors: potential agents for cancer therapy. *Mini reviews in medicinal chemistry* **2:**261-269.

Njar VC, Gediya L, Purushottamachar P, Chopra P, Vasaitis TS, Khandelwal A, Mehta J, Huynh C, Belosay A, and Patel J (2006) Retinoic acid metabolism blocking agents (RAMBAs) for treatment of cancer and dermatological diseases. *Bioorganic & medicinal chemistry* **14:**4323-4340.

Noy N (2000) Retinoid-binding proteins: mediators of retinoid action. *The Biochemical journal* **348 Pt 3:**481-495.

Obach RS, Baxter JG, Liston TE, Silber BM, Jones BC, MacIntyre F, Rance DJ, and Wastall P (1997) The prediction of human pharmacokinetic parameters from preclinical and in vitro metabolism data. *The Journal of pharmacology and experimental therapeutics* **283:**46-58.

Ortiz de Montellano PR and De Voss JJ (2002) Oxidizing species in the mechanism of cytochrome P450. *Natural product reports* **19:**477-493.

Osanai M and Lee GH (2011) Enhanced expression of retinoic acid-metabolizing enzyme CYP26A1 in sunlight-damaged human skin. *Medical molecular morphology* **44:**200-206.

Pawson BA, Ehmann CW, Itri LM, and Sherman MI (1982) Retinoids at the threshold: their biological significance and therapeutic potential. *Journal of medicinal chemistry* **25:**1269-1277.

Perola E, Walters WP, and Charifson PS (2004) A detailed comparison of current docking and scoring methods on systems of pharmaceutical relevance. *Proteins* **56:**235-249.

Petkovich M, Brand NJ, Krust A, and Chambon P (1987) A human retinoic acid receptor which belongs to the family of nuclear receptors. *Nature* **330:**444-450.

Pierard GE, Pierard-Franchimont C, Paquet P, and Quatresooz P (2009) Spotlight on adapalene. *Expert opinion on drug metabolism & toxicology* **5:**1565-1575.

Poulous TL and Johnson EF (2005) Structures of Cytochrome P450 Enzymes, in: *Cytochrome P450: Structure, Mechanism and Biochemistry* (Ortiz de Montellano PR ed), Kluwer Academic/Plenum Publishers, New York.

Purushottamachar P, Patel JB, Gediya LK, Clement OO, and Njar VC (2012) First chemical feature-based pharmacophore modeling of potent retinoidal retinoic acid metabolism blocking agents (RAMBAs): identification of novel RAMBA scaffolds. *European journal of medicinal chemistry* **47:**412-423.

Ransom J, Morgan PJ, McCaffery PJ, and Stoney PN (2014) The rhythm of retinoids in the brain. *Journal of neurochemistry* **129:**366-376.

Raverdeau M, Gely-Pernot A, Feret B, Dennefeld C, Benoit G, Davidson I, Chambon P, Mark M, and Ghyselinck NB (2012) Retinoic acid induces Sertoli cell paracrine signals for spermatogonia differentiation but cell autonomously drives spermatocyte meiosis. *Proceedings of the National Academy of Sciences of the United States of America* **109:**16582-16587.

Raverdeau M and Mills KH (2014) Modulation of T cell and innate immune responses by retinoic Acid. *Journal of immunology* **192:**2953-2958.

Ray WJ, Bain G, Yao M, and Gottlieb DI (1997) CYP26, a novel mammalian cytochrome P450, is induced by retinoic acid and defines a new family. *The Journal of biological chemistry* **272:**18702-18708.

Ren JH, Xiong XQ, Sha Y, Yan MC, Lin B, Wang J, Jing YK, Zhao DM, and Cheng MS (2008) Structure prediction and R115866 binding study of human CYP26A1: homology modelling, fold recognition, molecular docking and MD simulations. *Molecular Simulation* **34:**337-346.

Roos TC, Jugert FK, Merk HF, and Bickers DR (1998) Retinoid metabolism in the skin. *Pharmacological reviews* **50:**315-333.

Ross AC and Zolfaghari R (2011) Cytochrome P450s in the regulation of cellular retinoic acid metabolism. *Annual review of nutrition* **31:**65-87.

Ross SA, McCaffery PJ, Drager UC, and De Luca LM (2000) Retinoids in embryonal development. *Physiological reviews* **80:**1021-1054.

Rowbotham SE, Boddy AV, Redfern CP, Veal GJ, and Daly AK (2010) Relevance of nonsynonymous CYP2C8 polymorphisms to 13-cis retinoic acid and paclitaxel hydroxylation. *Drug metabolism and disposition: the biological fate of chemicals* **38:**1261-1266.

Saenz-Mendez P, Elmabsout AA, Savenstrand H, Awadalla MK, Strid A, Sirsjo A, and Eriksson LA (2012) Homology models of human all-trans retinoic acid metabolizing enzymes CYP26B1 and CYP26B1 spliced variant. *Journal of chemical information and modeling* **52:**2631-2637.

Sanchez R and Sali A (1997a) Advances in comparative protein-structure modelling. *Current opinion in structural biology* **7:**206-214.

Sanchez R and Sali A (1997b) Evaluation of comparative protein structure modeling by MODELLER-3. *Proteins* **Suppl 1:**50-58.

Saperstein S, Edgren RA, Lee GJ, Jung D, Fratis A, Kushinsky S, Mroszczak E, and Dorr A (1989) Bioequivalence of two oral contraceptive drugs containing norethindrone and ethinyl estradiol. *Contraception* **40:**581-590.

Sawyer PR, Brogden RN, Pinder RM, Speight TM, and Avery (1975) Clotrimazole: a review of its antifungal activity and therapeutic efficacy. *Drugs* **9:**424-447.

Saxena A, Sangwan RS, and Mishra S (2013) Fundamentals of homology modeling steps and comparison among important bioinformatics tools: An overview. *Science International* **1:**237.

Schenkman JB and Jansson I (1999) Interactions between cytochrome P450 and cytochrome b5. *Drug metabolism reviews* **31:**351-364.

Schenkman JB and Jansson I (2006) Spectral Analyses of Cytochromes P450, in: *Cytochrome P450 Protocols* (Phillips IR ed), Humana Press, Totowa, N.J.

Schoch GA, Yano JK, Sansen S, Dansette PM, Stout CD, and Johnson EF (2008) Determinants of cytochrome P450 2C8 substrate binding: structures of complexes with montelukast, troglitazone, felodipine, and 9-cis-retinoic acid. *The Journal of biological chemistry* **283:**17227-17237.

Schoch GA, Yano JK, Wester MR, Griffin KJ, Stout CD, and Johnson EF (2004) Structure of human microsomal cytochrome P450 2C8. Evidence for a peripheral fatty acid binding site. *The Journal of biological chemistry* **279:**9497-9503.

Schwartz EL, Hallam S, Gallagher RE, and Wiernik PH (1995) Inhibition of all-trans-retinoic acid metabolism by fluconazole in vitro and in patients with acute promyelocytic leukemia. *Biochemical pharmacology* **50:**923-928.

Sherman W, Beard HS, and Farid R (2006a) Use of an induced fit receptor structure in virtual screening. *Chemical biology & drug design* **67:**83-84.

Sherman W, Day T, Jacobson MP, Friesner RA, and Farid R (2006b) Novel procedure for modeling ligand/receptor induced fit effects. *Journal of medicinal chemistry* **49:**534-553.

Shimshoni JA, Roberts AG, Scian M, Topletz AR, Blankert SA, Halpert JR, Nelson WL, and Isoherranen N (2012) Stereoselective formation and metabolism of 4-hydroxy-retinoic

Acid enantiomers by cytochrome p450 enzymes. *The Journal of biological chemistry* **287:**42223-42232.

Sippl MJ (1995) Knowledge-based potentials for proteins. *Current opinion in structural biology* **5:**229-235.

Sloczynska K, Gunia-Krzyzak A, Zelaszczyk D, Waszkielewicz AM, and Marona H (2015) Skin metabolism established with the use of MetaSite for selected retinoids employed in topical and systemic treatment of various skin disorders and found in cosmeceuticals. *Acta biochimica Polonica* **62:**201-206.

Sonneveld E, van den Brink CE, van der Leede BM, Schulkes RK, Petkovich M, van der Burg B, and van der Saag PT (1998) Human retinoic acid (RA) 4-hydroxylase (CYP26) is highly specific for all-trans-RA and can be induced through RA receptors in human breast and colon carcinoma cells. *Cell growth & differentiation : the molecular biology journal of the American Association for Cancer Research* **9:**629-637.

Sporn MB and Roberts AB (1984) Role of retinoids in differentiation and carcinogenesis. *Journal of the National Cancer Institute* **73:**1381-1387.

Sun B, Song S, Hao CZ, Huang WX, Liu CC, Xie HL, Lin B, Cheng MS, and Zhao DM (2015) Molecular recognition of CYP26A1 binding pockets and structure-activity relationship studies for design of potent and selective retinoic acid metabolism blocking agents. *Journal of molecular graphics & modelling* **56:**10-19.

Taimi M, Helvig C, Wisniewski J, Ramshaw H, White J, Amad M, Korczak B, and Petkovich M (2004) A novel human cytochrome P450, CYP26C1, involved in metabolism of 9-cis and all-trans isomers of retinoic acid. *The Journal of biological chemistry* **279:**77-85.

Talpur R, Cox K, and Duvic M (2009) Efficacy and safety of topical tazarotene: a review. *Expert opinion on drug metabolism & toxicology* **5:**195-210.

Tang-Liu DD, Matsumoto RM, and Usansky JI (1999) Clinical pharmacokinetics and drug metabolism of tazarotene: a novel topical treatment for acne and psoriasis. *Clinical pharmacokinetics* **37:**273-287.

Tay S, Dickmann L, Dixit V, and Isoherranen N (2010) A comparison of the roles of peroxisome proliferator-activated receptor and retinoic acid receptor on CYP26 regulation. *Mol Pharmacol* **77:**218-227.

Thatcher JE, Buttrick B, Shaffer SA, Shimshoni JA, Goodlett DR, Nelson WL, and Isoherranen N (2011) Substrate specificity and ligand interactions of CYP26A1, the human liver retinoic acid hydroxylase. *Mol Pharmacol* **80:**228-239.

Thatcher JE and Isoherranen N (2009) The role of CYP26 enzymes in retinoic acid clearance. *Expert opinion on drug metabolism & toxicology* **5:**875-886.

Thatcher JE, Zelter A, and Isoherranen N (2010) The relative importance of CYP26A1 in hepatic clearance of all-trans retinoic acid. *Biochemical pharmacology* **80:**903-912.

Tiboni GM (1993) Second branchial arch anomalies induced by fluconazole, a bis-triazole antifungal agent, in cultured mouse embryos. *Research communications in chemical pathology and pharmacology* **79:**381-384.

Tiboni GM and Giampietro F (2005) Murine teratology of fluconazole: evaluation of developmental phase specificity and dose dependence. *Pediatric research* **58:**94-99.

Tiboni GM, Marotta F, and Carletti E (2009) Fluconazole alters CYP26 gene expression in mouse embryos. *Reproductive toxicology* **27:**199-202.

Topletz AR (2013) The Relative Importance of CYP26A1 and CYP26B1 in Mediating Retinoid Homeostasis: Studies on the Formation, Elimination and Biological Activity of All-trans-Retinoic Acid Metabolites, in: *Pharmaceutics*, University of Washington, Seattle, WA.

Topletz AR, Thatcher JE, Zelter A, Lutz JD, Tay S, Nelson WL, and Isoherranen N (2012) Comparison of the function and expression of CYP26A1 and CYP26B1, the two retinoic acid hydroxylases. *Biochemical pharmacology* **83:**149-163.

Topletz AR, Tripathy S, Foti RS, Shimshoni JA, Nelson WL, and Isoherranen N (2014) Induction of CYP26A1 by Metabolites of Retinoic Acid: Evidence that CYP26A1 is an Important Enzyme in the Elimination of Active Retinoids (Submitted). *Molecular Pharmacology*.

Tornio A, Niemi M, Neuvonen M, Laitila J, Kalliokoski A, Neuvonen PJ, and Backman JT (2008) The effect of gemfibrozil on repaglinide pharmacokinetics persists for at least 12 h after the dose: evidence for mechanism-based inhibition of CYP2C8 in vivo. *Clinical pharmacology and therapeutics* **84:**403-411.

Totah RA and Rettie AE (2005) Cytochrome P450 2C8: substrates, inhibitors, pharmacogenetics, and clinical relevance. *Clinical pharmacology and therapeutics* **77:**341-352.

Uchida S, Shimada K, Misaka S, Imai H, Katoh Y, Inui N, Takeuchi K, Ishizaki T, Yamada S, Ohashi K, Namiki N, and Watanabe H (2010) Benzbromarone pharmacokinetics and pharmacodynamics in different cytochrome P450 2C9 genotypes. *Drug metabolism and pharmacokinetics* **25:**605-610.

van der Leede BM, van den Brink CE, Pijnappel WW, Sonneveld E, van der Saag PT, and van der Burg B (1997) Autoinduction of retinoic acid metabolism to polar derivatives with decreased biological activity in retinoic acid-sensitive, but not in retinoic acid-resistant human breast cancer cells. *The Journal of biological chemistry* **272:**17921-17928.

VandenBrink BM, Foti RS, Rock DA, Wienkers LC, and Wahlstrom JL (2011) Evaluation of CYP2C8 inhibition in vitro: utility of montelukast as a selective CYP2C8 probe substrate. *Drug metabolism and disposition: the biological fate of chemicals* **39:**1546-1554.

Vanier KL, Mattiussi AJ, and Johnston DL (2003) Interaction of all-trans-retinoic acid with fluconazole in acute promyelocytic leukemia. *Journal of pediatric hematology/oncology* **25:**403-404.

Verfaille CJ, Borgers M, and van Steensel MA (2008) Retinoic acid metabolism blocking agents (RAMBAs): a new paradigm in the treatment of hyperkeratotic disorders. *Journal der*

Deutschen Dermatologischen Gesellschaft = Journal of the German Society of Dermatology : JDDG **6:**355-364.

Vermilion JL, Ballou DP, Massey V, and Coon MJ (1981) Separate roles for FMN and FAD in catalysis by liver microsomal NADPH-cytochrome P-450 reductase. *The Journal of biological chemistry* **256:**266-277.

Vermilion JL and Coon MJ (1978) Identification of the high and low potential flavins of liver microsomal NADPH-cytochrome P-450 reductase. *The Journal of biological chemistry* **253:**8812-8819.

Volkamer A, Kuhn D, Grombacher T, Rippmann F, and Rarey M (2012) Combining global and local measures for structure-based druggability predictions. *Journal of chemical information and modeling* **52:**360-372.

von Wachenfeldt C, Richardson TH, Cosme J, and Johnson EF (1997) Microsomal P450 2C3 is expressed as a soluble dimer in Escherichia coli following modification of its N-terminus. *Archives of biochemistry and biophysics* **339:**107-114.

Walsky RL, Gaman EA, and Obach RS (2005) Examination of 209 drugs for inhibition of cytochrome P450 2C8. *Journal of clinical pharmacology* **45:**68-78.

Walter-Sack I, de Vries JX, Ittensohn A, Kohlmeier M, and Weber E (1988) Benzbromarone disposition and uricosuric action; evidence for hydroxilation instead of debromination to benzarone. *Klinische Wochenschrift* **66:**160-166.

Wang F, Kwak HS, Elbuluk N, Kaczmarek AL, Hamilton T, Voorhees JJ, Fisher GJ, and Kang S (2009) Retinoic acid 4-hydroxylase inducibility and clinical response to isotretinoin in patients with acne. *Journal of the American Academy of Dermatology* **61:**252-258.

Wang Y, Zolfaghari R, and Ross AC (2002) Cloning of rat cytochrome P450RAI (CYP26) cDNA and regulation of its gene expression by all-trans-retinoic acid in vivo. *Archives of biochemistry and biophysics* **401:**235-243.

Waugh J, Noble S, and Scott LJ (2004) Adapalene: a review of its use in the treatment of acne vulgaris. *Drugs* **64:**1465-1478.

Weiner SJ, Kollman PA, Case DA, Singh UC, Ghio C, Alagona G, Profeta S, and Weiner P (1984) A new force field for molecular mechanical simulation of nucleic acids and proteins. *Journal of the American Chemical Society* **106:**765-784.

Westbrook J, Feng Z, Jain S, Bhat TN, Thanki N, Ravichandran V, Gilliland GL, Bluhm W, Weissig H, Greer DS, Bourne PE, and Berman HM (2002) The Protein Data Bank: unifying the archive. *Nucleic acids research* **30:**245-248.

White JA, Guo YD, Baetz K, Beckett-Jones B, Bonasoro J, Hsu KE, Dilworth FJ, Jones G, and Petkovich M (1996) Identification of the retinoic acid-inducible all-trans-retinoic acid 4-hydroxylase. *The Journal of biological chemistry* **271:**29922-29927.

White JA, Ramshaw H, Taimi M, Stangle W, Zhang A, Everingham S, Creighton S, Tam SP, Jones G, and Petkovich M (2000) Identification of the human cytochrome P450, P450RAI-2, which is predominantly expressed in the adult cerebellum and is responsible for all-trans-retinoic acid metabolism. *Proceedings of the National Academy of Sciences of the United States of America* **97:**6403-6408.

Williams JB and Napoli JL (1987) Inhibition of retinoic acid metabolism by imidazole antimycotics in F9 embryonal carcinoma cells. *Biochemical pharmacology* **36:**1386-1388.

Williams PA, Cosme J, Sridhar V, Johnson EF, and McRee DE (2000) Mammalian microsomal cytochrome P450 monooxygenase: structural adaptations for membrane binding and functional diversity. *Molecular cell* **5:**121-131.

Xi J and Yang Z (2008) Expression of RALDHs (ALDH1As) and CYP26s in human tissues and during the neural differentiation of P19 embryonal carcinoma stem cell. *Gene expression patterns : GEP* **8:**438-442.

Xiang Z (2006) Advances in homology protein structure modeling. *Current protein & peptide science* **7:**217-227.

Xu LZ, Sanchez R, Sali A, and Heintz N (1996) Ligand specificity of brain lipid-binding protein. *The Journal of biological chemistry* **271:**24711-24719.

Yamazaki H and Shimada T (1999) Effects of arachidonic acid, prostaglandins, retinol, retinoic acid and cholecalciferol on xenobiotic oxidations catalysed by human cytochrome P450 enzymes. *Xenobiotica; the fate of foreign compounds in biological systems* **29:**231-241.

Yu R, Wang J, Wang R, Lin Y, Hu Y, Wang Y, Shu M, and Lin Z (2015) Combined Pharmacophore Modeling, 3D-QSAR, Homology Modeling and Docking Studies on CYP11B1 Inhibitors. *Molecules* **20:**1014-1030.

Yu Z, Sefton J, Lew-Kaya D, Walker P, Yu D, and Tang-Liu DD (2003) Pharmacokinetics of tazarotene cream 0.1% after a single dose and after repeat topical applications at clinical or exaggerated application rates in patients with acne vulgaris or photodamaged skin. *Clinical pharmacokinetics* **42:**921-929.

Zanger UM and Schwab M (2013) Cytochrome P450 enzymes in drug metabolism: regulation of gene expression, enzyme activities, and impact of genetic variation. *Pharmacology & therapeutics* **138:**103-141.

Zhang QY, Dunbar D, and Kaminsky L (2000) Human cytochrome P-450 metabolism of retinals to retinoic acids. *Drug metabolism and disposition: the biological fate of chemicals* **28:**292-297.

Zhang Y (2008) Progress and challenges in protein structure prediction. *Current opinion in structural biology* **18:**342-348.

14. Vita

Robert S. Foti received his undergraduate degree in chemical biology from Stevens Institute of Technology (Hoboken, NJ) and a master's degree in chemistry from Lehigh University (Bethlehem, PA). From 1999 – 2005, Rob held a position in the Pharmacokinetics, Dynamics and Metabolism department at Pfizer (Groton, CT) where he worked on immunology and inflammation related discovery programs and subsequently on high-throughput screening assays for metabolic stability and drug interactions. Since 2005, Rob has worked in the Pharmacokinetics and Drug Metabolism group at Amgen (Seattle, WA; Cambridge, MA). Here he supports oncology, inflammation and neuroscience small molecule discovery through early development programs in addition to protein therapeutic discovery efforts within the same therapeutic areas.

The current research in Rob's lab focuses on the *in vitro* and *in silico* assessment of drug interactions and clearance mechanisms for both small molecules and protein therapeutics. Additional research interests include cytochrome P450 and UDP-glucuronosyltransferase enzymology, drug target characterization and enzymatic clearance mechanisms for protein therapeutics, resulting in over 30 peer-reviewed manuscripts and multiple invited reviews, book chapters and oral presentations. Externally, Rob is on the Editorial Board for Drug Metabolism and Disposition, is the current Secretary/Treasurer for the Drug Metabolism Division of ASPET, and is an active member of both ISSX and ACS while contributing as an *ad hoc* referee for multiple peer-reviewed journals.